Chemical Effect on Muonic Atom Formation through Muon Transfer Process in Hydrocarbon Molecules

（炭化水素分子系のミュオン転移過程によるミュオン原子形成における化学効果）

Makoto INAGAKI

A Thesis
Submitted to Graduate School of Science,
Osaka University

2018

Abstract

An atom is composed of a positively charged nucleus and negatively charged electrons. Since atoms are formed by electromagnetic interaction between the nucleus and electrons, even if one or both of them are changed to other particles having a positive and/or a negative charge, an atomic system can also be formed. Such an atomic system are called exotic atoms. Muonic and pionic atoms are well studied exotic atoms, which are atomic systems in which one electron is replaced with a muon or pion. As an interesting phenomenon, it is known that the chemical environment of muon or pion capturing atom affects the formation process of the muonic and pionic atoms. It is called chemical effect. Many studies have been done on chemical effects, and found valence electrons strongly influence on muon capture process. Most of studies deal with processes by which a muon or pion is captured directly by atoms. On the other hand, there are another muonic and pionic atoms formation process, which is called transfer processes. In transfer processes, a muon or pion firstly trapped by a hydrogen atom and form a muonic or pionic hydrogen atom. Due to the strong nuclear charge shielding effect by a negatively charged particle, muonic and pionic hydrogen atoms can diffuse freely like a neutron, and can move a muon or pion to other heavier atom. There are many unclear points about the chemical effect by transfer process.

The aim of this work is to clarify the chemical effect on muon transfer process, especially on muon transfer rate. For that purpose, the muon transfer processes in benzene and cyclohexane have been investigated whose chemical effects in the pion transfer process are observed in the previous study.

Experiments were carried out for two kinds of systems, gas and liquid. In the gas experiment, gas mixtures containing benzene or cyclohexane below atmospheric pressure were prepared as muon irradiation samples. In this experiment, the muon transfer rate becomes slow and it can be determined by observing intensities of the muonic X-ray originating only from the muon transfer process. In the liquid experiment, liquid mixtures of benzene or cyclohexane and carbon tetrachloride with various mixing ratios were prepared as the samples, which are the same system in which the chemical effect was previously observed on the pion transfer process. In this experiment, the muon transfer rates were determined using the model equation.

As a result, in the gas system, there was no difference in muon transfer rates between benzene and cyclohexane sample, on the other hand, the muon transfer rate to benzene was approximately 1.2 times the muon transfer rate to cyclohexane in the liquid system. It is known that the pion transfer rate to cyclohexane is approximately twice the pion

transfer rate to benzene in the liquid system. These differences can be explained by assuming that muonic and pionic hydrogen atoms in the excited state are more susceptible to molecular steric hindrance than those in the ground state. Muon transfers in the gas system occurred only from the ground state muonic hydrogen atoms. In the liquid system, muon transfer occurred from both ground and excited state muonic hydrogen atoms, and pion transfers occur only from excited state pionic hydrogen atoms. This indicates that excited state muonic and pionic hydrogen atoms play an important role in the chemical effects on the transfer processes in the hydrocarbon molecules.

Table of contents

1. General Introduction

1.1. Exotic Atoms

An atom is composed of a positively charged nucleus and a negatively charged electron. These are attracting each other by electromagnetic interaction and the electrons form atomic orbital around the nucleus. Even if one or both of the nuclei and electrons are replaced by particles having positive and/or negative charges, an atomic system can also be formed. Such atomic system is called exotic atom. As such atomic system consisting of non-nuclei and non-electrons, positronium composed of a positron and an electron, and muonium consisting of a positive muon and an electron are widely used in the research field of condensed matter physics.

Negatively charged particles can form a binding state with a nucleus in place of an electron and form an exotic atom. An atomic system composed of a nucleus, electrons and a negative muon is called muonic atom. Similar to a muonic atom, an atom consisting of a nucleus, electrons and a negative pion is called pionic atom. Table 1-1 shows the comparison of electrons, muons and pions, which compose muonic and pionic atoms. These exotic atoms can be formed simply by stopping muons or pions in a material. As a result, these are one of the well-studied exotic atoms. Since the 1950's, these have been used for research on the distribution of protons in nucleus and research on nucleon-nucleon interactions.[1,2] Recently, muonic hydrogen atoms were used for precise determination of the size of protons.[3,4] In addition, muonic atoms are applied to non-destructive elemental analysis by using high energy muonic X-rays emitted after muonic atom formation.[5–7]

Table 1-1 Comparison of electrons, muons and pions.

	Electron	**Negative muon**	**Negative pion**
Charge	−1	−1	−1
Mass	0.511 MeV/c^2 ≡ m_e	106 MeV/c^2 ~ 207 m_e	140 MeV/c^2 ~ 274 m_e
Lifetime	stable	2.2 μs	26 ns
Related interactions	coulomb interaction weak interaction	coulomb interaction weak interaction	coulomb interaction weak interaction strong interaction

The radius of atomic orbital and binding energy of the negative particles (muon or pion) with a certain principal quantum number n can be represented as follows using the Bohr model.

$$\mathrm{r_n} = \frac{n^2 m_e}{Z m_m} a_H$$

$$\mathrm{E_n} = -\frac{\mathrm{Z}^2 m_m}{n^2 m_e} I_H$$

Here, Z is the atomic number, m_e is the mass of an electron, m_m is the mass of a negative particle, a_H is the Bohr radius, and I_H is the first ionization energy of a hydrogen atom. In the case of the muonic atom, the mass of the muon is 207 times that of the electron, so the radius of the atomic muon orbital is approximately 1/200 of the electron and the binding energies are approximately 200 times that of the electron. Therefore, the energies of the characteristic X-rays that are emitted by the muon radiative transition between atomic muon levels are approximately 200 times those of the electron. For example, it becomes 75 keV with muon transition from 2p orbital to 1s orbital (K_α X-ray) of carbon atom. Such high energy X-rays has less influence of absorption by air and the material itself, hence it can be easily measured with a germanium semiconductor detector even if the source of X-rays exists deeply inside of the material. Therefore as mentioned above,

muonic X-rays can be utilized as a probe of non-destructive elemental analysis.

1.2. Atomic Capture Process of muon and pion

1.2.1. Direct Capture Process

The formation process of the muonic atom has still not been investigated completely, but from previous studies, the muon capture phenomena occur in the following process. When a free muon enters into a substance, it loses its kinetic energy due to scattering process with electrons in the substance. After slowing down, the muon is trapped by the Coulomb field of a nucleus, and the muon forms atomic muon orbital with a large principal quantum number. This process is called direct capture process. Since pion is a particle with similar mass to muon and strong interaction is not involved in the initial processes of the direct capture process, these processes of muon and pion are very similar to each other.

1.2.2. Transfer Process

When a muon is captured by a hydrogen atom, the only electron of the hydrogen atom is released, and an atomic system consisting only of the muon and the nucleus is formed. Due to the large mass of the muon, the muon exists very close to the atomic nucleus, and the muonic hydrogen atoms are very small atomic system. As a results, the charge of the nucleus is strongly shielded by the muon and muonic hydrogen atoms can be regarded as an electrically neutral particle with a size of 1/200 of the hydrogen atoms. Thus muonic hydrogen atoms behave like a neutron. Therefore, muonic hydrogen atoms can free from chemical bonds and move freely in the materials. When the muonic hydrogen atoms approach to nucleus of other atoms, the muon can be trapped deeper atomic muon orbital of other atom. As a results, the muon transfer to an atomic orbital with a larger binding energy of other atoms. This process is called muon transfer process.[8] The transfer process can be classified into two types, ‘internal transfer’ and ‘external transfer’. In the former process, muon is transferred intramolecularly to a neighboring atom to which a hydrogen

atom is bound without breaking chemical bond. In the latter process, muon is transferred to atoms of other molecules by breaking chemical bonds. In this thesis, "transfer" refers to ‘external transfer’ unless otherwise noted.

In the case of pion, the pion transfer process also occurs. However, there are little bit of difference in the pion transfer process. The pion transfer does not occur from the pionic ground (1s) state of pionic hydrogen atoms because they disappear immediately with an extremely short lifetime of less than 10^{-15} s by causing the reaction below:

$$\mathrm{p} + \pi^- \rightarrow \begin{cases} n + \gamma \ \ (40\%) \\ n + \pi^0 \ \ (60\%) \end{cases}$$

$$\pi^0 \rightarrow 2\gamma$$

This is in contrast to the lifetime of the ground state muonic hydrogen atoms being 2×10^{-6} s. By observing two 70 MeV gamma rays due to the collapse of π^0, neutral pion, it is possible to obtain information about the number of pion-capture by hydrogen atoms. Such information cannot be obtained in the case of a muon.

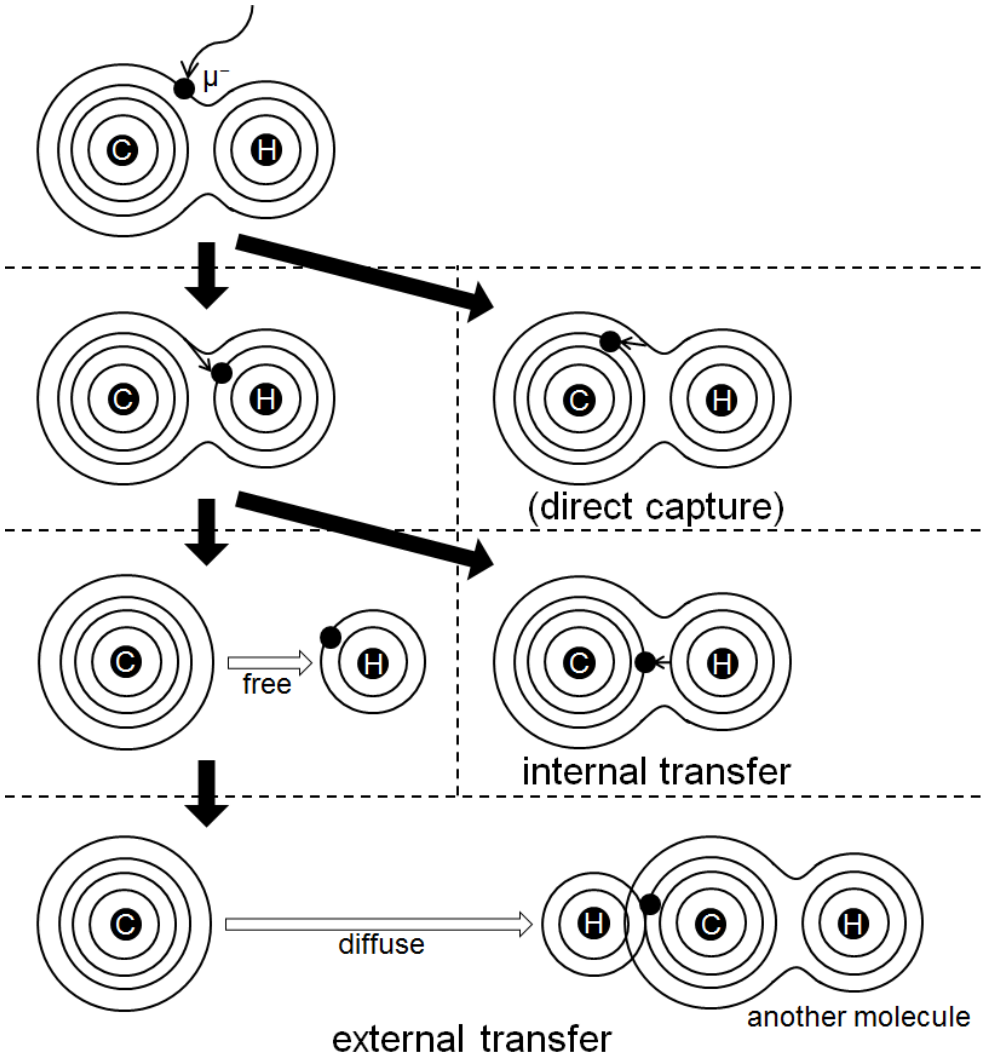

Fig. 1-1 Scheme of internal and external transfer processes in hydrocarbon molecules. "C" and "H" indicate carbon atom and hydrogen atom. Solid lines around atoms are molecular muon orbital (large mesomolecular orbital) and atomic muon orbital.

1.3. Cascade Process of Muon and Pion

The captured muon initially exists highly excited muon level, that is, has large principal quantum number (n) and large angular momentum quantum number (l). The muon immediately de-excites to muonic ground (1s) state. When the principal quantum number is large and the existence probability of the orbital electron is large around muon, the transition energy is given to the electron and the electron is released having energy corresponding to the difference between the transition energy and the binding energy of

electron. This process is called the Auger process, and the emitted electrons are called Auger electrons. When the principal quantum number becomes smaller and the surrounding electron density becomes low, photon emission transition becomes dominant. The characteristic X-rays emitted by muon transition are called muonic X-rays. The transition with X-ray emission is made according to the selection rule of angular momentum quantum number $\Delta l = \pm 1$. The sequential muon de-excitation process is called muon cascade process. The muon eventually reaches to muonic 1s orbital and keeps this state until the muon decays into an electron and two neutrinos by the individual lifetime, or is absorbed by the nucleus. The lifetime of this state varies depending on the element. For example, 2.2 μs for muonic hydrogen atoms, 2.0 μs for muonic carbon, 1.5 μs for muonic neon and 0.56 μs for muonic chlorine.[9]

Even in the case of pion, the pion de-excitation process is similar to muon cascade process, however there are difference in interaction between the pion and the nucleus. Due to the strong interaction between them, the pion is usually absorbed by the nucleus before it de-excites to 1s orbital.

In the direct capture process, the muon is captured at a high energy level with large principal quantum number. Because the muon can have large angular momentum quantum number at high energy level, the contribution of transitions with small Δn such as 3d→2p→1s become large at low energy level. On the other hand, in the transfer process, the muon once captured on the hydrogen atom and cascading down in the hydrogen atom, and then the muon transfer occurs. As a result, the muon is transferred to a low energy level with small principal quantum number. Since the muon cannot have large angular momentum quantum number at low energy level, the contribution of large Δn transition such as 3p→1s and 4p→1s increases.

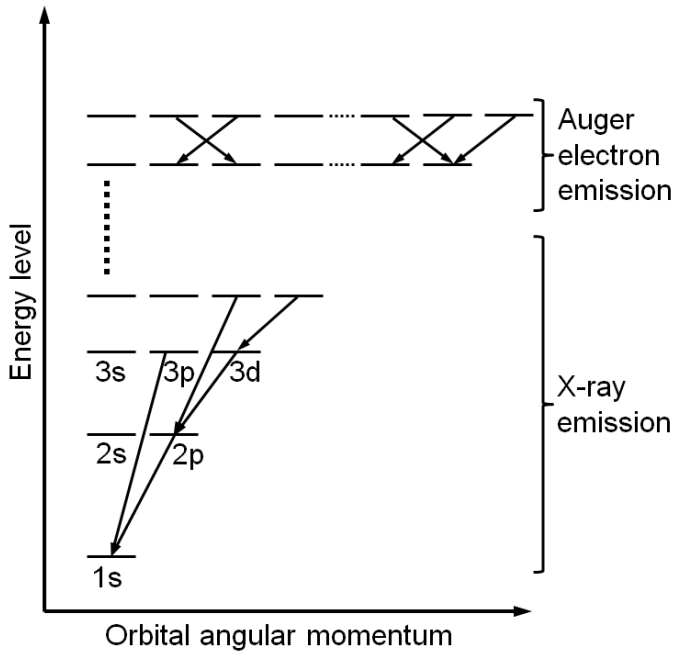

Fig. 1-2 Schematic view of the muon de-excitation path.

1.4. Previous Studies Related to This Work

1.4.1. Chemical Effect on Direct Capture Process

According to Fermi and Teller, when negative particle such as a muon or a pion is captured by an atom with an atomic number Z, the particle eventually locates far inward of the electron orbital, therefore the capture phenomenon is independent of the electronic state and depends only on nuclear charge Z. This is Fermi-Teller's Z-law.[10] According to the Z-law, the particle capture ratio per atom A(Z/Z ') of a $Z_kZ'_m$ type molecule can be expressed by the following formula.

$$A\left(\frac{Z}{Z'}\right) \equiv \frac{mW(Z)}{kW(Z')} = \frac{Z}{Z'}$$

Here, W(Z) is the capture rate to the Z atom. In many cases, the capture rate of the negative particles are not proportional to the atomic number, and most of experimental capture ratios are not expained by the Z-law as shown in Fig. 1-3.[11]

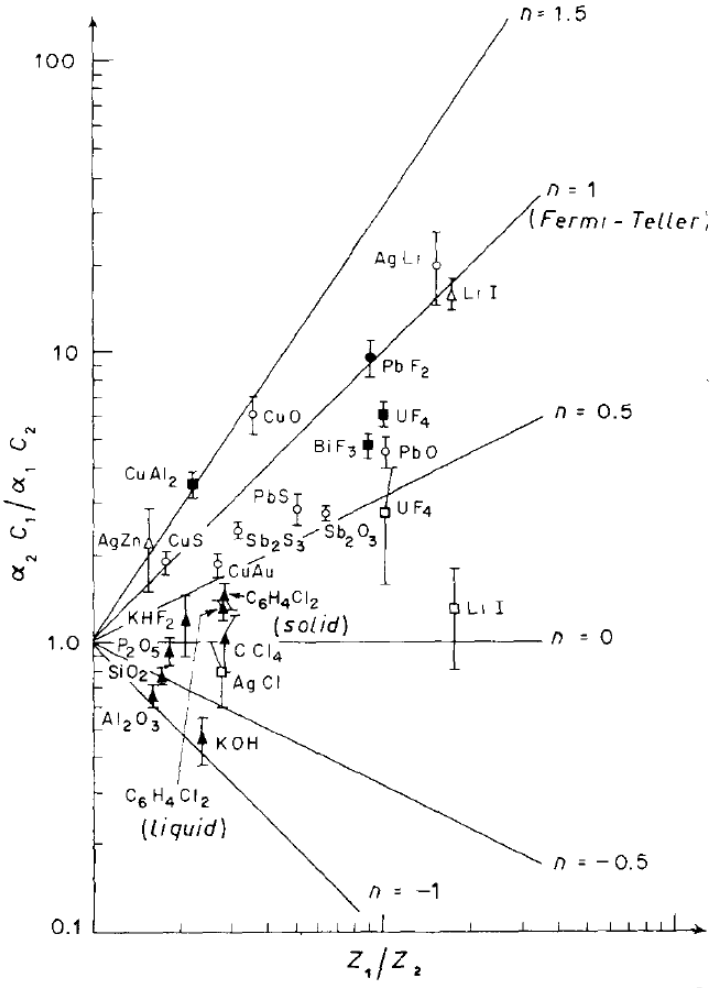

Fig. 1-3 The comparison between experimental muon capture ratios and the Z-law (taken from reference no. 11).

It is also known that the capture ratios A(Z/O) of the oxide molecules show smaller values than the Z-law prediction and it exhibits a periodicity such that it takes a minimum value with an alkali metal.[12] These facts indicate that the capture of muons and pions depends not only on the nuclear charge but also on the chemical environment of the muon capturing atom. Such phenomena are known as chemical effects. The muon capture ratios are different between substances composed of the same elements, it is the direct evidence that a chemical effect exists in muon and pion capture process.[13,14]

Many stuidies have been done so far to predict the capture ratios. Petrukhin and Suvorov revised the Z-law as follows.[15]

$$A\left(\frac{Z}{Z'}\right) = \frac{Z^{\frac{1}{3}} - 1}{Z'^{\frac{1}{3}} - 1}$$

Since the cross-sectional area of an atom is almost proportional to $Z^{1/3}$, this equation means that the capture of the particle depends on the cross-sectional area of the atom. Daniel adopted the shielding effect of the electronic cloud and revised it as follows.[16]

$$A\left(\frac{Z}{Z'}\right) = \frac{Z^{\frac{1}{3}} ln(0.57Z)}{Z'^{\frac{1}{3}} ln(0.57Z')}$$

In some case, these expressions reproduce the experimental values better than the Z-law, but the periodicity by atomic number cannot be reproduced. Daniel revised it by considering the size of the electronic cloud as follows.[17]

$$A\left(\frac{Z}{Z'}\right) = \frac{Z^{\frac{1}{3}} ln(0.57Z) \cdot R(Z')}{Z'^{\frac{1}{3}} ln(0.57Z') \cdot R(Z)}$$

Where R(Z) is the radius of the Z atom. In this formula, the periodicity of the experiment values can be reproduced to some extent. However, the muon and pion capture processes are still not completely understood, and capture ratios cannot be predicted only from the molecular formula.

1.4.2. Chemical Effect on Transfer Process

For the transfer process, many pion capturing experiments are conducted in the gas phase system. In the gas mixture system of H_2 + Z, Petrukhin and Suvorov expressed the capture rate W_H to hydrogen atoms as follows.[15]

$$W_H = \frac{1}{1 + S_H C_Z} \frac{1}{1 + \Lambda_Z C_Z}$$

Here, S_H is the stopping power ratio of a Z atom to a hydrogen atom, Λ_Z is a parameter corresponding to the rate constant for the pion transfer from pionic hydrogen atoms to Z atoms, and C_Z is atomic ratio of gas mixture (n_Z / n_H). This equation indicates the probability of pion nuclear capture by hydrogen atoms, that is, the probability that a pion is captured by hydrogen atoms and not transferred to Z atoms. The parameters of S_H and

Λ_Z were determined as follows from systematic studies of gas mixtures at a pressure of 40 atm.[15]

$$S_H = (7.1 \pm 0.1)(Z^{\frac{1}{3}} - 1)$$

$$\Lambda_Z = S_H C_Z^{\frac{1}{3}}$$

Here, Z is the atomic number of Z atom. This model can explain pion capture ratio in hydrogen atom for various mixture gas system. However, in this formula, contributions of chemical effects are not included. Contrary to direct capture process, the studies on chemical effects on the transfer process are very limited.

The difference in pion capture ratios by the sample temperature was reported for H_2O and NH_3. Horváth *et al.* performed pion irradiation experiment for H_2O and NH_3 samples with various temperature condition. They found the number of pions captured by hydrogen atoms and not transferred to other atoms in the supercritical state was larger than that in the solid state, and the number increased with the temperature rise in the liquid state.[18] This results suggest that the rate of pion transfer from pionic hydrogen atoms to oxygen or nitrogen atoms become lower with temperature rise. They also conducted the pion transfer experiments using selectively partial deuterated methanol. Because the π^0 particle production reactions in pionic deuterium atoms are strongly suppressed, the hydrogen atom which capture the pion in the molecule can be distingished. As a result, they found that the number of capture changed with temperature change only in the case of the hydrogen atom of a hydroxy group.[19] This is because the hydrogen bond strength changes with temperature and the pion capture ratio to the hydrogen atom has changed due to the change in the electron density around the hydrogen atom.

Shinohara *et al.* measured the pion transfer rates in the two component mixture liquid systems with benzene or cyclohexane and carbon tetrachloride.[20] From the experiments with variaus mixing ratio, they found that the transfer rate to carbon atoms of benzene is approximately twice the rate to carbon atoms of cyclohexane. They conclude that the steric hindrance affected the pion transfer rate to carbon atoms. Because two hydrogen

atoms bonded to the carbon atom of cyclohexane while one hydrogen atoms bonded to the carbon atom of benzene, the exisitence of hydrogen atoms binding with carbon atom may prevent pionic hydrogen atoms from approaching carbon atoms.

1.5. Aim of This Work

As mentioned above, the chemical effect have been known in muon and pion capture processes. Although the details of the chemical effect have still not been fully investigated, there are many studies on the chemical effect in muon and pion capture processes, and especially, the direct capture processes are undergoing systematic understanding. On the other hand, in the transfer process there are few observations on chemical effects. The chemical effects have been known in pion transfer process, on the othe hand, there are no report in muon transfer procese due to difficulty in experimental measureing of muon capture phenomena in hydrogen atoms.

The muon and pion capture processes are influenced by the chemical environment. Using these property, the chemical environment of muon and pion capturing atoms can be investigated by observing muon and pion capture phenomena. The chemical effect on the transfer process can be a probe for the properties of hydrogen atom itself and its containing molecules. In fact, the strength of hydrogen bonding was sucessfully investigated by the pion transfer process. If the influence of molecular structure on the transfer process is systematically clarified, the chemical effect on the transfer process can be a tool to explore the structure of the molecule. Additionally, in applying elemental analysis using muonic X-ray to organic matter, it is indispensable to understand the chemical effect on the transfer process in order to know the capture rate to each element through the transfer process.

The aim of this work is to clarify the chemical effect on the muon transfer process, especially the effect of molecular structure on muon transfer rate. In this work, I forcused on the transfer proceses in benzene and cyclohexane molecules whose chemical effects on the pion transfer process have been observed in the previous study. Because there is

no information obtained from the gamma rays due to the collapse of the π^0 unlike pion transfer process, the new method for investigation of muon transfer phenomena was applied in this work. For this purpose, the following two experiments were conducted.

The first experiment was conducted by using benzene and cyclohexane in a low density gaseous condition to investigate the chemical effect on the muon transfer process in a low density condition. In this experiment, the muon transfer rate was investigated by observing the muonic X-rays derived only from the muon transfer process that can be observed even after 1 μs from muon injection due to the slow muon transfer rate. In this condition, the muon transfer occurs after muon cascading and reaching muonic 1s state in muonic hydrogen atoms. Such an experiment using a pion is impossible, because of the extremely short lifetime of pionic hydrogen atoms in the ground state.

The second experiment was carried out by using the mixtures of benzene or cyclohexane and carbon tetrachloride to examine the chemical effect on the muon transfer process in a high dense liquid condition. The experimental system is the same as the previous study where the chemical effect on the pion transfer process was observed. In high density liquid sample, since muon transfer rate is very high, it is difficult to distinguish muonic X-rays originating from the muon transfer and the direct capture processes. As a result, unlike low density sample, it is a difficult to obtain the muon transfer rate from muonic X-ray intensity directly. Therefore, in this work, precise experiments were carried out while changing the mixing ratio of liquids, and the muon transfer rate were analyzed by using a model.

2. Experimental

2.1. Experiment of Gas System

2.1.1. Outline

The aim of this experiment is to investigate the chemical effect on the muon transfer process in low density condition by using benzene and cyclohexane in gaseous state. In this experiment, to determine muon transfer rate, muonic X-rays originating only from muon transfer were measured. Because muon tranfer rate is is low at low density sample, the muonic X-ray signal originated from muon transfer and muon direct capture processes can be distinguished each other easily from time structure. The sample of benzene or cyclohexane and neon gases mixed into hydrogen gas (96.8%) were prepared for muon irradiation. In this condition, most of the muons are firstly captured by hydrogen atoms and then transfers to benzene, cyclohexane and neon atoms. Since the number of muon captures due to the muon transfer is proportional to the muon transfer rate, by comparing the X-ray intensity ratio of carbon and neon between samples, the muon transfer rate to carbon atoms of benzene and cyclohexane can be compared based on the transfer rate to neon. In this experiemnt, the sample gas is very small density, low momentum muon beam is essential. In addition, such a low momentum muon beam can not be identified by trigger counters due to strong contribution of muon stop in the counters. In this way, pulsed muon beam is suitable for this experiment.

2.1.2. Accelerator Facility, J-PARC MUSE

The muon irradiation experiment was conducted at the accelerator facility J-PARC (Japan Proton Accelerator Research Complex) in Tokai-mura, Naka-gun, Ibaraki Prefecture. The whole arrangement of J-PARC is shown in Fig. 2-1. In J-PARC, protons accelerated to 400 MeV at LINAC are introduced to synchrotron and further accelerated to 3 GeV. Most of the protons are transported to MLF (Materials and Life Science Experimental Facility) and remainings are sent to 50 GeV synchrotron. The 3 GeV protons transported to the MLF are impinged to the graphite made pion production target,

and produced pions. The protons passed through the target are sent to the neutron production target constructed in the down stream of pion production target. In the pion production target, various secondary particles including electrons, neutrons, pions and so on are generated by a nuclear reaction. The pions are collected by the magnet system and guided to the superconducting solenoid. In the solenoid magnet, the pions are converted to the muons by the pion decay reaction as shown below.

$$\pi^- \rightarrow \mu^- + \overline{\nu_\mu}$$

The generated muons are transported to the D1 or D2 experimental area using dipole and quadrupole magnet system and selected their momentum. Electrons having the same momentum were removed by electric and magnetic fields of Wien filter. The whole facility of muon generation and transportation is called MUSE (Muon Science Establishment), and the beamline used for the experiment is called D-Line. The arrangement of the pion generation target (muon target) and D-Line are shown in Fig. 2-2.

The time structure of produced muon beam becomes the same as that of the proton. Since a synchrotron is used to accelerate protons, the MUSE provides a pulsed muon beam that supply a large number of muons at once. The operation cycle of MUSE is 25 Hz with double bunched stracture. A schematic diagram of the time structure of the beam is shown in Fig. 2-3.

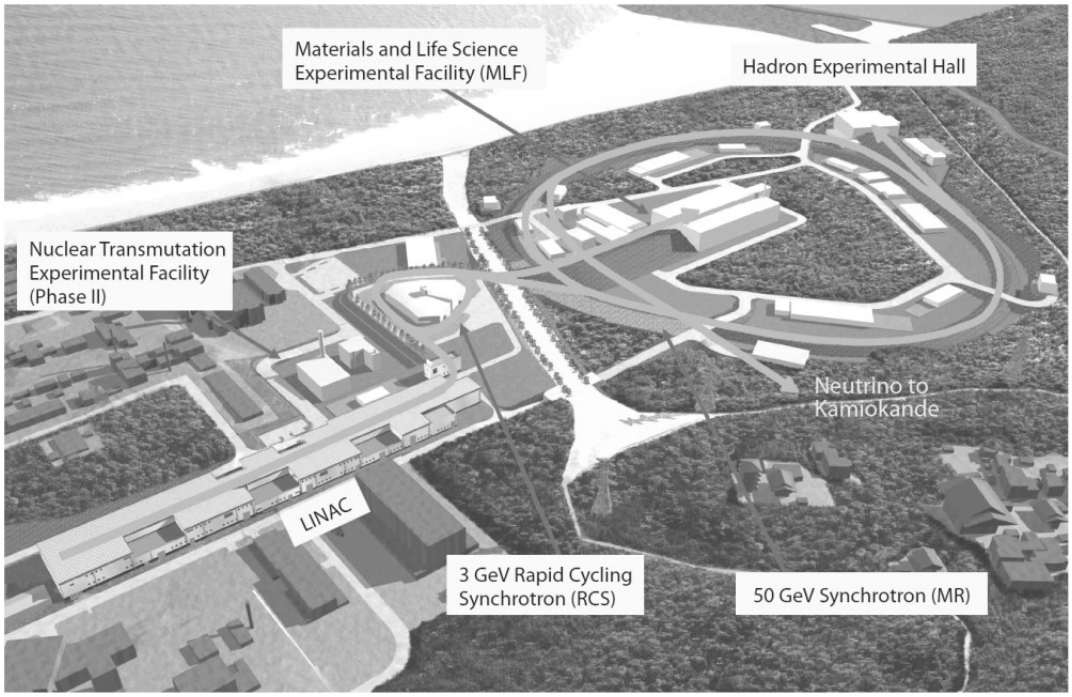

Fig. 2-1 Configuration of J-PARC (taken from reference no. 21).

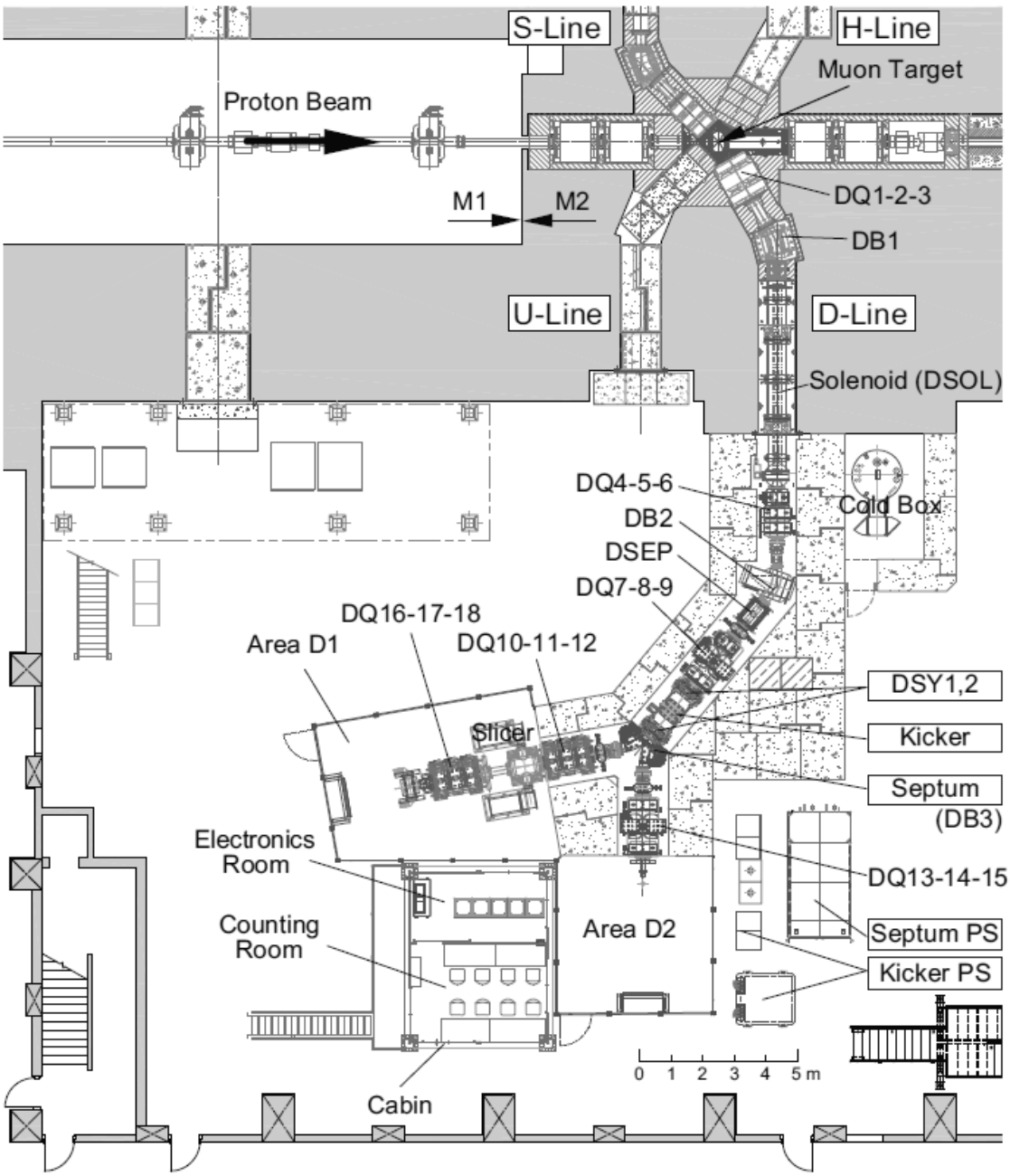

Fig. 2-2 Layout of the MUSE D-Line in the MLF (taken from reference no. 22). μSR spectrometer was installed instead of DQ16-17-18 at the time of the experiment.

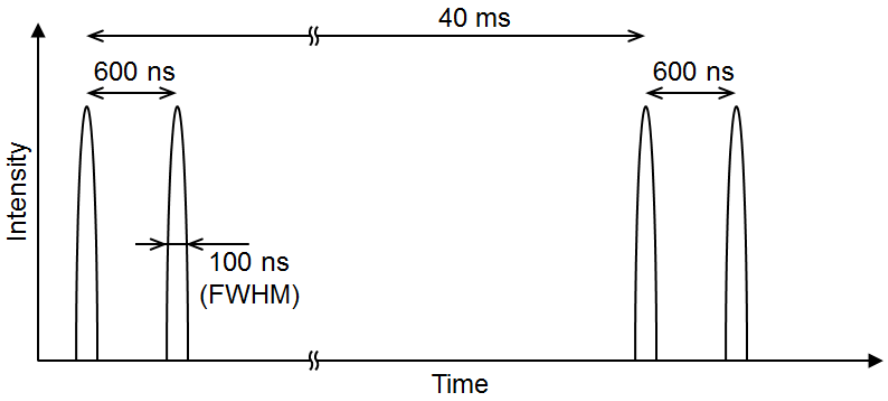

Fig. 2-3 Schematic diagram of time structure of pulsed muon beam.

2.1.3. Experimental Setup

The experiment setup was installed in the D1 experimental area. It consists of gas chamber, liquid benzene / cyclohexane containers, pressure gauge, gas handling line and germanium semiconductor detector. The gas chamber is made of aluminum and has a cylindrical shape with an inner diameter of 140 mm, a length of 300 mm, and an inner volume of approximately 4.6 L. There are four windows in the chamber. One is in the axial direction and is a polyimide film window with a diameter of 45 mm and a thickness of 50 μm. From here the sample was irradiated with muon beam. The remaining three are in the radial direction and are made of aluminum with a diameter of 60 mm and a thickness of 100 μm. X-rays are measured from here. A gas piping made of stainless steel is connected to the downstream side of the beam. Schematic views of the setup and the gas handling line are shown in Fig. 2-4 and Fig. 2-5, picture of the setup is shown in Fig. 2-6, and details of pressure gauge and germanium semiconductor detector are shown in Table 2-1 and Table 2-2.

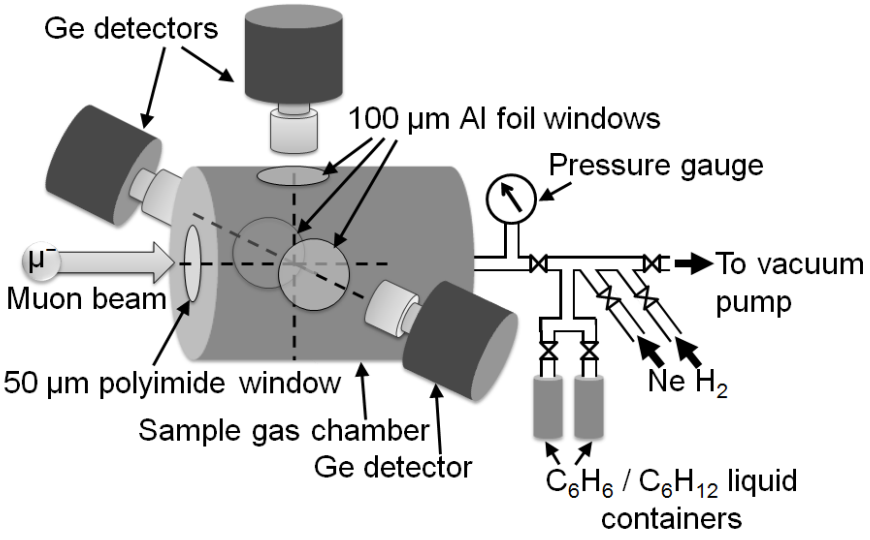

Fig. 2-4 Schematic view of the experimental setup.

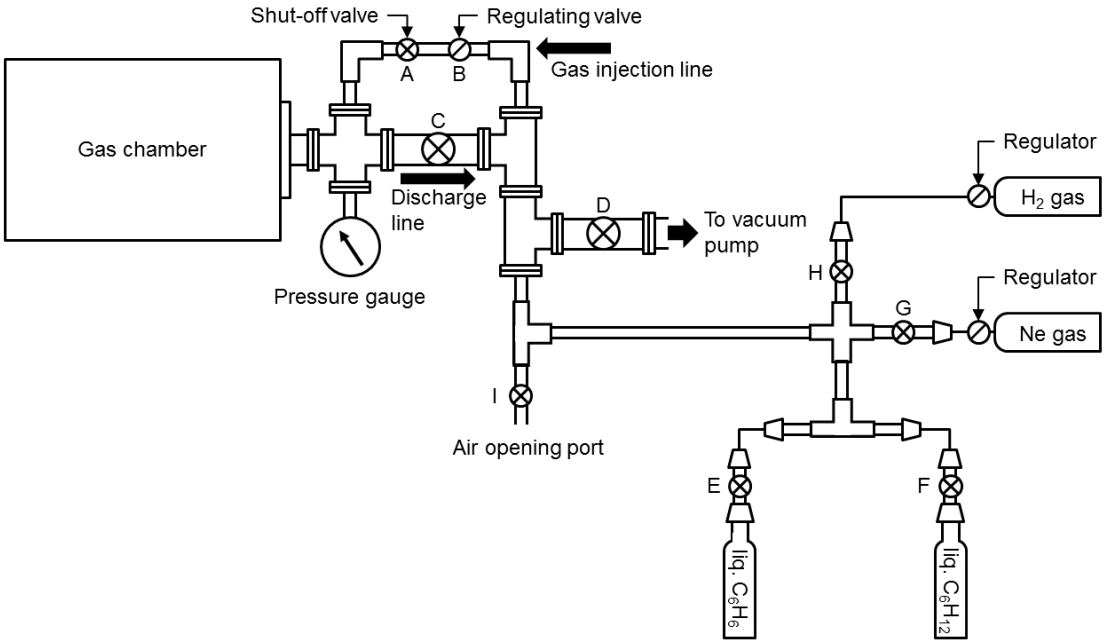

Fig. 2-5 Schematic view of the gas handling line.

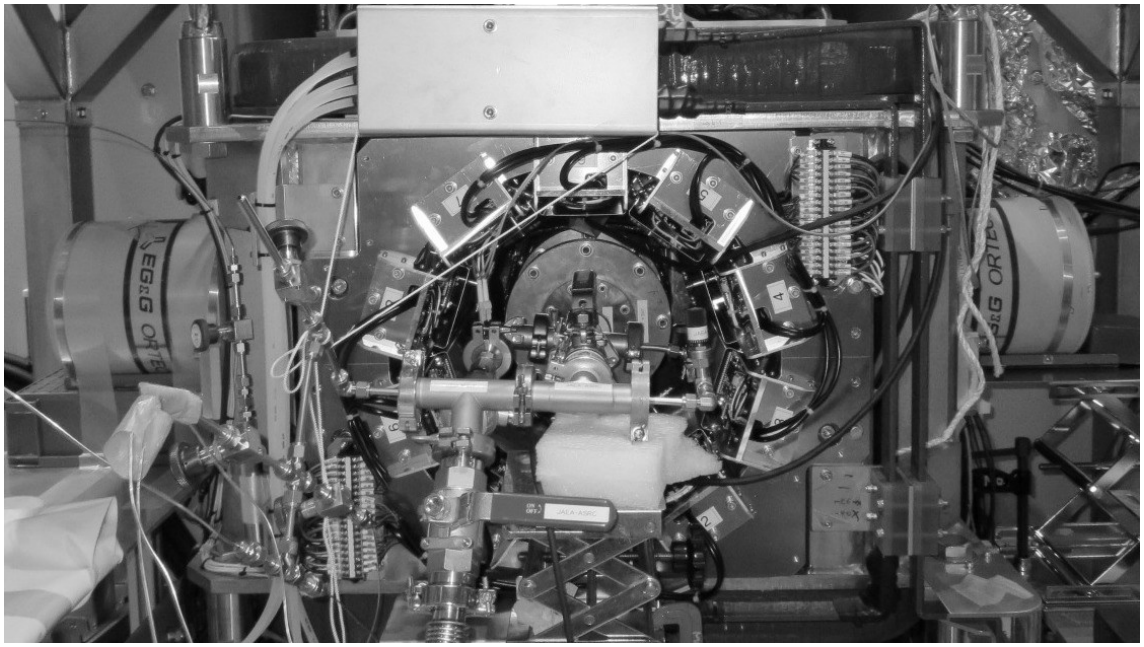

Fig. 2-6 Picture of the experimental setup viewed from the beam downstream. The sample gas chamber was located on center of the picture. The device surrounding the chamber is μSR spectrometer that was not used in the experiment. Two germanium detectors were located on left and right side of the picture. The other germanium detector was located on the upside of the chamber, but not reflected in the picture.

Table 2-1 Specification of the pressure sensor.

Manufacturer	VALCOM
Model	VHG-A6-100kPa(abs)T-4
Type	Diaphragm type absolute pressure sensor
Pressure port material	SUS316L
Diaphragm material	NW6022
Pressure range	0–100 kPa abs.
Output	4–20 mA
Power-supply voltage	DC 24 V

Table 2-2 Specification of the germanium detectors.

Detector name		**LEPS**	**Loax**	**Ge-K**
Manufacturer		CANBERRA	ORTEC	ORTEC
Model		GL0515R	Loax 36300 /15-P-S	GLP-16195 /10-P-S
Germanium crystal	**diameter**	25.2 mm	35.9 mm	16.0 mm
	thickness	15.0 mm	14.0 mm	10.0 mm
Cryostat window	**material**	Beryllium	Beryllium	Beryllium
	thickness	0.15 mm	0.5 mm	0.127 mm

2.1.4. Measurement System

For obtaining the spectrum by the germanium semiconductor detector, a circuit as shown in Fig. 2-7 was used. The signal output from the germanium semiconductor detector is branched into two and sent to an amplifier with high energy precision (spectroscopy amplifier) and an amplifier with good time response (timing amplifier). In addition, a gate signal having a width of a fixed time is generated from the arrival signal of the muon pulse supplied from the accelerator (beam signal) and is supplied to the discriminator. The discriminator passes only signals over a certain intensity within a certain time from the beam signal among the signals from the timing amplifier. This signal is sent to TDC (Time-to-Digital Converter), converts the time difference from the beam signal into a numerical value, and obtains the time spectrum (time versus count histogram). Further, a gate signal is generated from this signal and supplied to ADC (Analog-to-Digital Converter). The ADC operates only while the gate signal is supplied , converts the amplitude of the signal sent from the spectroscopy amplifier to a numerical value, and obtains an energy spectrum (energy versus count histogram). By doing this, it is possible to record only the signal synchronized with the muon pulse and reduce the noise. Also, time information and energy information were recorded at the same time, and these were recorded as list data associated one-to-one. By using the list data, it is possible

to analyze the energy spectrum of only a certain time domain as described later.

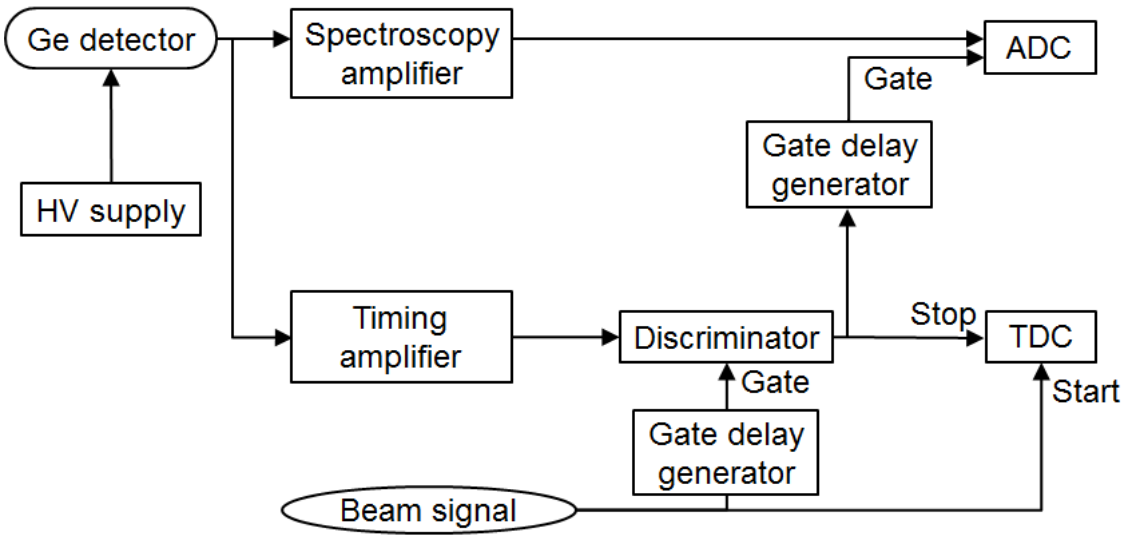

Fig. 2-7 Scheme of the electronic circuit for taking the data of measurements.

2.1.5. Sample Preparation

Preparation of a mixed gas of C_6H_6 (0.2 kPa) + Ne (3.0 kPa) + H_2 (96.8 kPa) as a sample was carried out in the following procedure.

1) Liquid benzene was placed in a container and connected to a gas handling line.
2) Valves E, F and I in Fig. 2-5 were closed, all the other valves were opened, and the whole was evacuated.
3) The entire container containing benzene was immersed in liquid nitrogen, and benzene was solidified.
4) Valve E was opened and evacuated the container.
5) Valve E was closed and benzene returned to normal temperature.
6) Repeat steps 3 to 5 several times to remove air dissolved in benzene.
7) Valve E was closed and benzene was returned to room temperature, and all valves were closed to stop evacuation.
8) Open valves A and E, slightly open valve B while watching the pressure gauge,

slowly put benzene to the desired pressure (0.2 kPa), and close valve B.

9) Valves A and E were closed, valve D was opened and the line was evacuated, and valve D was closed.
10) Operate the Ne cylinder regulator, set the appropriate secondary pressure, open the valves A and G, open the valve B slightly while watching the pressure gauge, put Ne in the target pressure (3.0 kPa), and valve B was closed.
11) Valves A and G were closed, valve D was opened and the line was evacuated, and valve D was closed.
12) Operate the H_2 cylinder regulator, set the appropriate secondary pressure, open the valves A and H, open the valve B slightly while watching the pressure gauge, put H_2 in the target pressure (total pressure 100.0 kPa), and the valves A, B and H were closed.

The other samples were also prepared by the similer operation. In principle, benzene and cyclohexane can be used as a gas up to approximatelly 10 kPa, which is the vapor pressure at room temperature. Benzene and cyclohexane can not be treated strictly as an ideal gas, but since the pressure used is an extremely low pressure, it was treated as an ideal gas.

2.1.6. Measurement

In the J-PARC MLF MUSE D2 experiment area, muon beam irradiation experiment was conducted from April 24 to April 26, 2014. The momentum of muon beam used was 19 MeV/c. The measured samples and measurement times are shown in Table 2-3.

Table 2-3 Samples and irradiation times.

Sample name	**Composition**	**Irradiation time**
Benzene sample	C_6H_6 (0.2 kPa)+Ne (3.0 kPa)+H_2 (96.8 kPa)	9.5 h
Cyclohexane sample	C_6H_{12} (0.2 kPa)+Ne (3.0 kPa)+H_2 (96.8 kPa)	9.1 h
Blank sample	Ne (3.0 kPa)+H_2 (97.0 kPa)	3.7 h

2.2. Experiment of Liquid System

2.2.1. Outline

The aim of this experiment is to investigate the chemical effect on the muon transfer process in high density materials by using the liquid state benzene and cyclohexane. The liquid mixtures of benzene or cyclohexane and carbon tetrachloride in which a chemical effect on the pion transfer process was observed in the previous study were used as a sample. In this experiment, it is impossible to extract muonic X-rays originating only from muon transfer, because the muon transfer rate is very fast unlike the gas system. Therefore, experiments are carried out while changing the mixing ratio, and the muon transfer rate was analyzed using the model.

2.2.2. Accelerator Facility, RCNP MuSIC

Experiments were conducted at muon facility MuSIC, RCNP (Research Center for Nuclear Physics), Osaka University. The layout of the entire RCNP is shown in Fig. 2-8.

Protons accelerated to 140 MeV with AVF cyclotron are introduced to the ring cyclotron and further accelerated to 400 MeV. The protons are transferred to graphite made pion production target. In RCNP-MuSIC, all proton beams are consumed by thick pion production target unlike other muon facilities including J-PARC MUSE. The pion generated by the pion production target is captured by a superconducting solenoid installed to surround the target and guided to the beam line. The muon generated by the decay of the pion is guided to the beam exit after separation of the momentum by the

electromagnet and separation of electrons by the Wien filter. The beam line used in the experiment is called M1 beam line. The arrangement of the pion production target and the M1 beam line is shown in Fig. 2-9.

Since the cyclotron is used for the acceleration of protons, the supplied muon beam is a DC beam in which muons are delivered one by one.

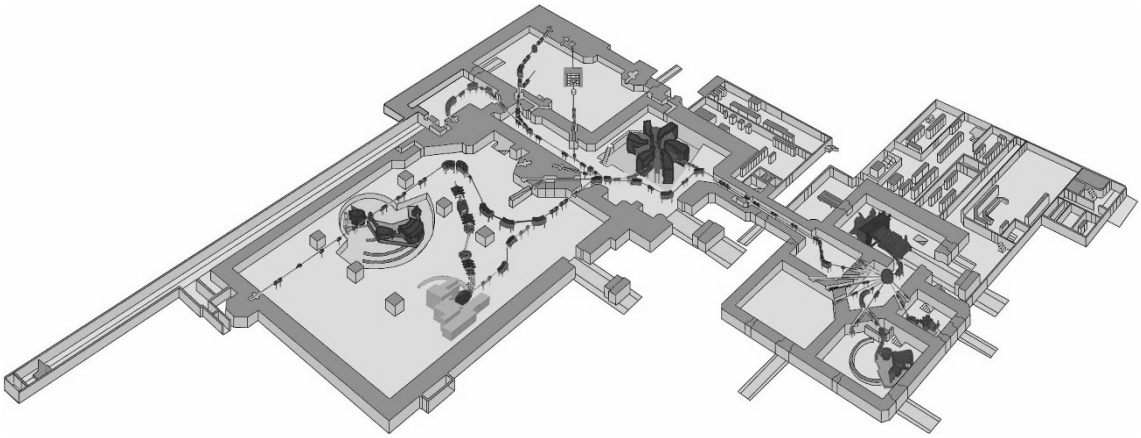

Fig. 2-8 Configuration of RCNP (taken from reference no. 23).

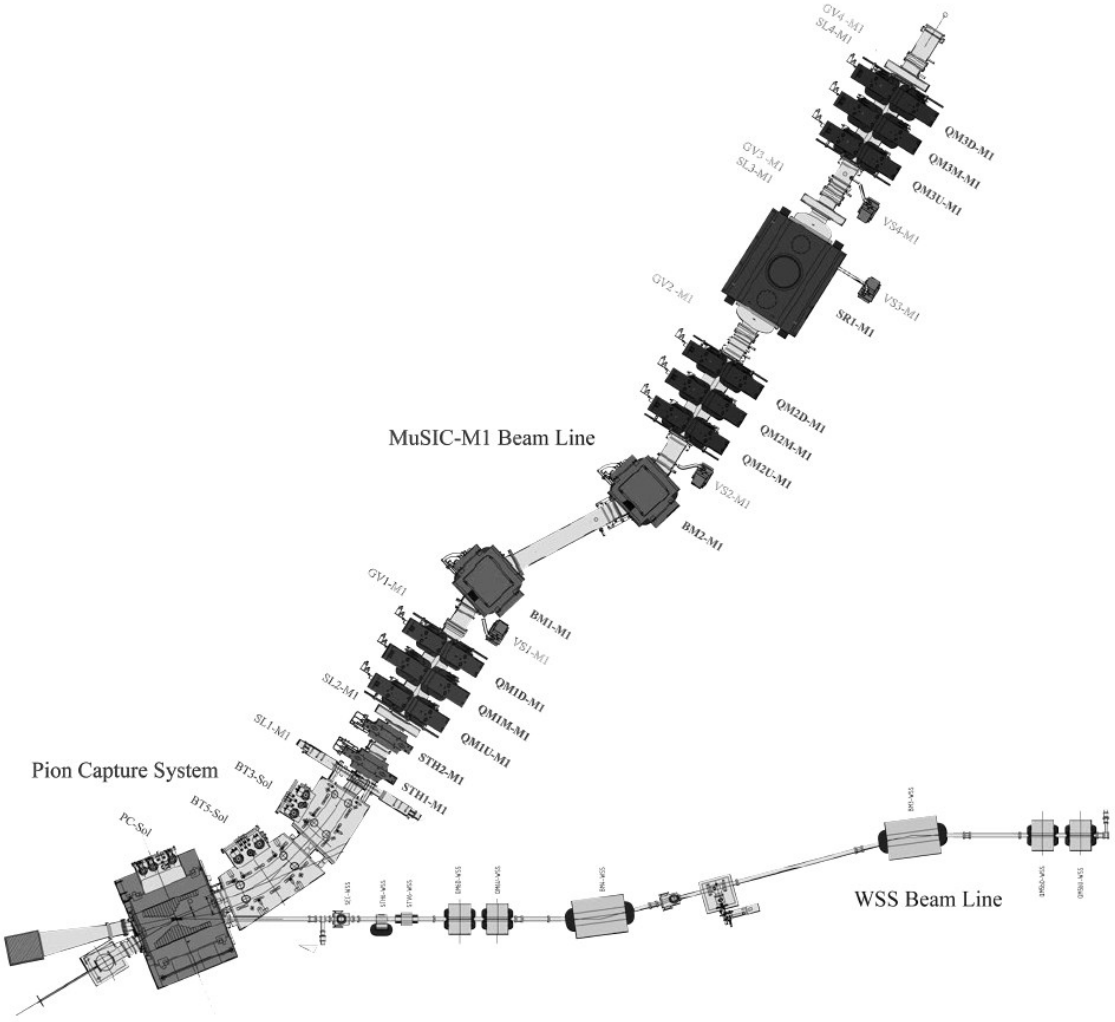

Fig. 2-9 Layout of the MuSIC M1 beam line in the RCNP (taken from reference no. 24).

2.2.3. Experimental Setup

The experimental setup consists of plastic scintillators, a degrader, a sample liquid holder, and germanium semiconductor detectors. The sample liquid holder has a rectangular parallelepiped shape, made of aluminum, having an inner volume of approximatelly 25 mL and a window thickness of 0.3 mm. The frame and the window were bonded by welding. Two plastic scintillators were installed upstream of the sample and the incidence of the muon was detected. Photomultipliers were used to detect light from the scintillators. In addition, an aluminum plate with a thickness of 0.2 mm was installed as a degrader, and the incident muon was decelerated, and adjusted so that the

muon stopped at the center of the sample. The muon stopping ranges were calculated using the software package SRIM, which is based on a Monte Carlo simulation method.[25] Schematic views of experimental setup and sample liquid holder are shown in Fig. 2-10 and Fig. 2-11, and pictures of experiment setup and sample liquid holder are shown in Fig. 2-12 and Fig. 2-13. Details of the photomultiplier, plastic scintillator and germanium semiconductor detectors are shown in Table 2-4, Table 2-5 and Table 2-6.

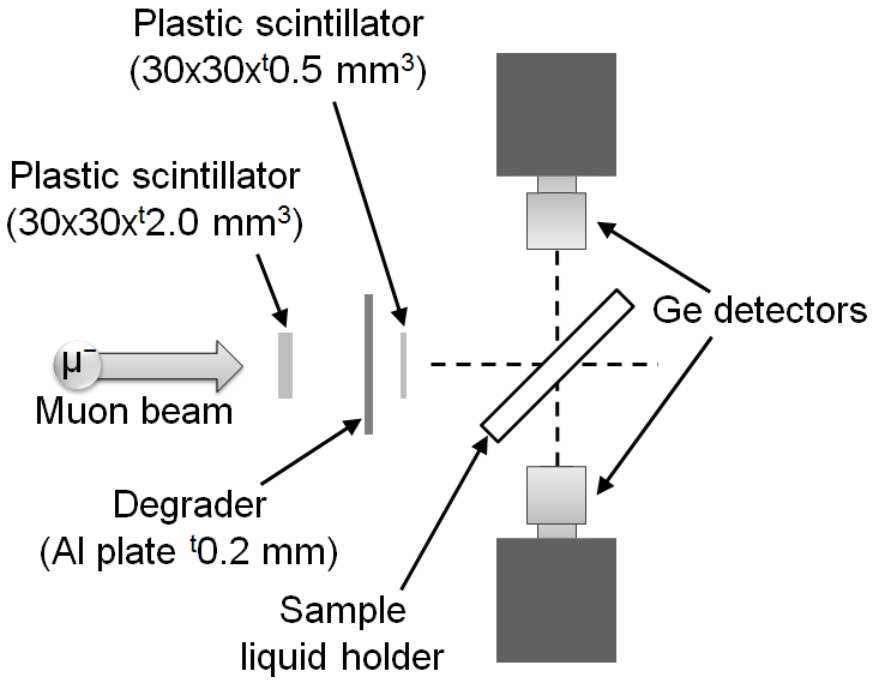

Fig. 2-10 Schematic view of the experimental setup.

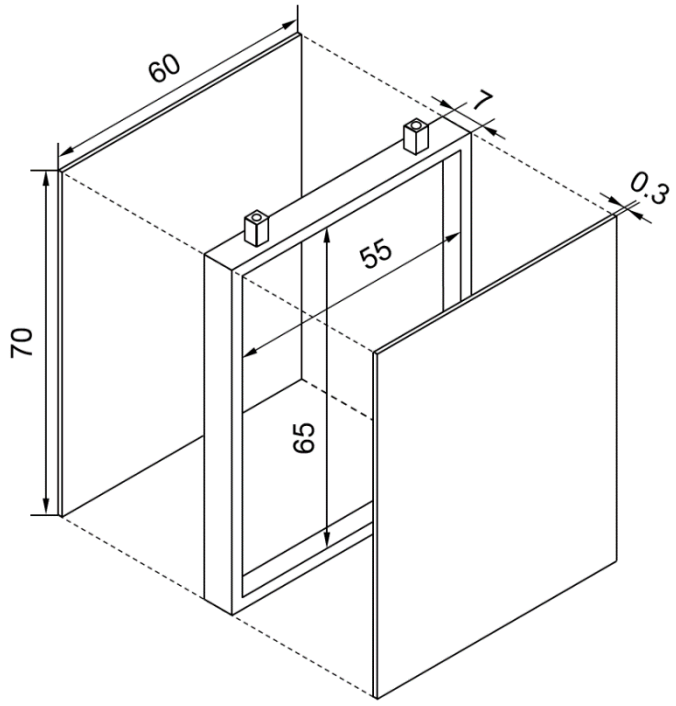

Fig. 2-11 Schematic view of the sample liquid holder. Injection ports of 1.5 mm in diameter are on the upper side of the frame. Dimensions are shown in millimeters.

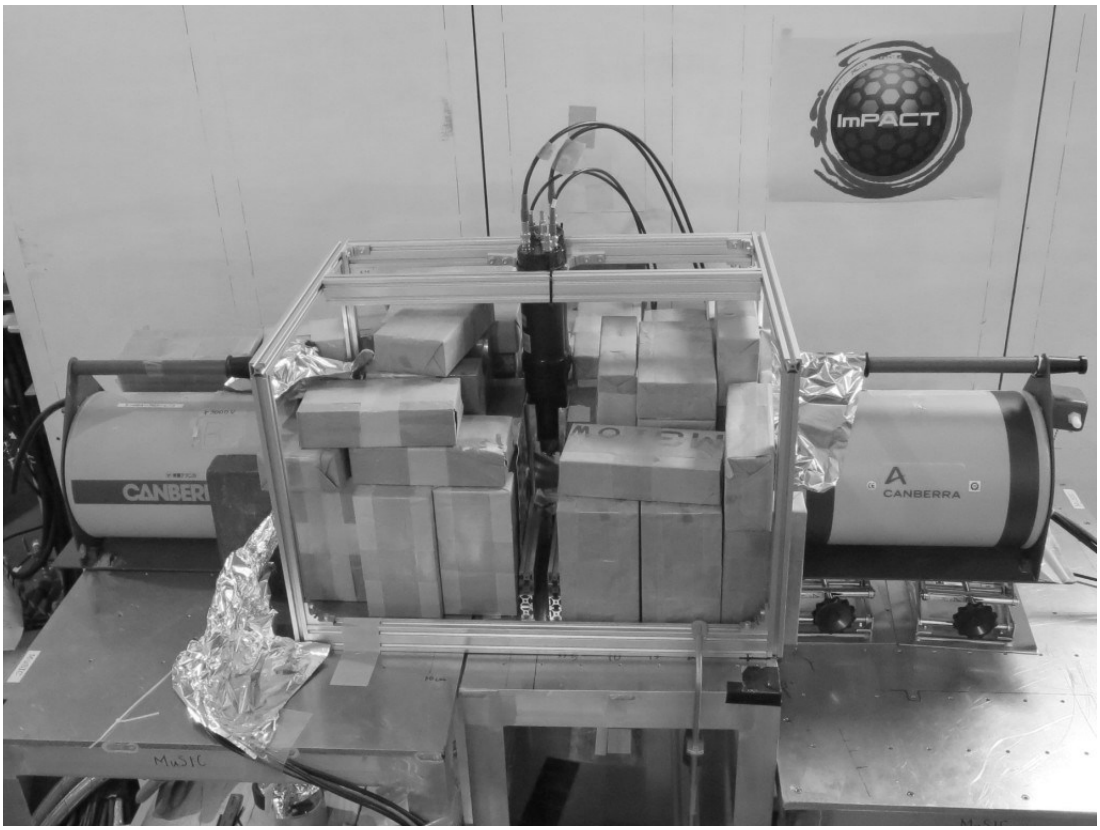

Fig. 2-12 Picture of the experimental setup viewed from the beam downstream. The blocks that were stacked in the center are paraffin blocks for neutron shielding. Inside of them, lead blocks for gamma ray shielding were stacked. The liquid sample holder and photomultipliers were located between the blocks on the center of the picture.

Fig. 2-13 Picture of the sample liquid holder used in the experiment.

Table 2-4 Specification of the photomultiplier.

Manufacturer	Hamamatsu Photonics
Assembly model	H7195
PMT model	R329-02
Photocathode area size	46 mm in diameter
Wavelength	300 nm – 650 nm
Gain	3.0×10^6 (typ.)
Dark current	10 nA (typ.)
Rise time	2.7 ns (typ.)
Transit time	40 ns (typ.)
Transit time spread	1.1 ns (typ.)

Table 2-5 Specification of the plastic scintillator.

Supplier	OHYO KOKEN KOGYO
Model	NE102A
Polymer base	Polyvinyl toluene
Density	1.032 g/cm^3
Light output	65% Anthracene
Wavelength of maximum emission	423 nm
Decay time	2.4 ns

Table 2-6 Specification of the germanium detectors.

Detector name		**Ge-T**	**Ge-B**
Manufacturer		CANBERRA	CANBERRA
Model		BE2020	BE3830
Germanium	**diameter**	51.5 mm	69.5 mm
Crystal	**thickness**	20.8 mm	30.0 mm
Cryostat	**material**	Carbon composite	Carbon composite
window	**thickness**	0.6 mm	0.6 mm

2.2.4. Measurement System

For the detection of the muon incident by the plastic scintillator, a circuit as shown in Fig. 2-14 was used. Coincidence was taken with upstream and downstream scintillators, and it was judged that a muon was incident when it detect at the same time. For obtaining the spectrum by the germanium semiconductor detector, a circuit as shown in Fig. 2-15 was used. The signal output from the germanium semiconductor detector is branched into two and sent to an amplifier with high energy precision (spectroscopy amplifier) and an amplifier with good time response (timing amplifier). Timing amplifier signals are discriminated by the discriminator below a certain intensity, the timing is adjusted by a gate delay generator, and sent to TAC / SCA. The TAC / SCA converts the time difference between this signal and the signal from the scintillator into signal amplitude and sends it to the ADC. From here, the time spectrum is obtained. Also, a gate signal is generated from this signal and sent to the linear gate. The linear gate sends a signal sent from the spectroscopy amplifier to the ADC only while the gate signal is being supplied. From here, the energy spectrum is obtained. By doing like this, it is possible to record only the signal synchronized with the incidence of the muon and reduce the noise. Also, record the time information and energy information at the same time, it is recorded as a list data associated one-to-one.

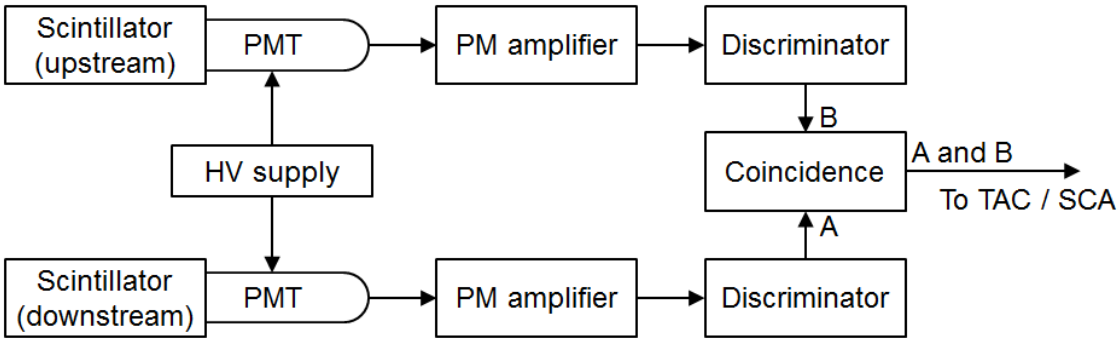

Fig. 2-14 Scheme of the electronic circuit for scintillators.

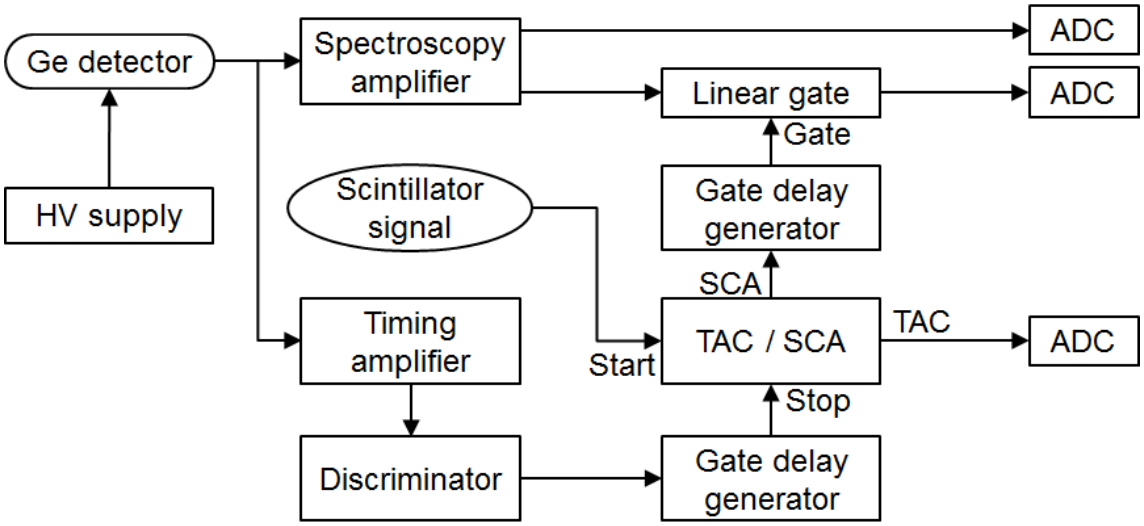

Fig. 2-15 Scheme of the electronic circuit for germanium detectors.

2.2.5. Sample Preparation

The prepared samples are shown in Table 2-7. The mixed sample was mixed while weighing with an electronic balance and adjusted so that the molar ratio was a predetermined mixing ratio. Distilled water was used for background measurement. Mixed weights are shown in Table 2-8. The reagents used are shown in Table 2-9.

Table 2-7 List of samples.

Sample name	Composition
C_6H_6+CCl_4 (70%) sample	C_6H_6 (30.0%) + CCl_4 (70.0%)
C_6H_6+CCl_4 (30%) sample	C_6H_6 (70.0%) + CCl_4 (30.0%)
C_6H_6+CCl_4 (15%) sample	C_6H_6 (85.0%) + CCl_4 (15.0%)
C_6H_{12}+CCl_4 (70%) sample	C_6H_{12} (30.0%) + CCl_4 (70.0%)
C_6H_{12}+CCl_4 (30%) sample	C_6H_{12} (70.0%) + CCl_4 (30.0%)
C_6H_{12}+CCl_4 (15%) sample	C_6H_{12} (85.0%) + CCl_4 (15.0%)
CCl_4 sample	CCl_4 (100%)
C_6H_6 sample	C_6H_6 (100%)
C_6H_{12} sample	C_6H_{12} (100%)
H_2O sample	Distillated water (100%)

Table 2-8 Mixed weight of samples.

Sample name	C_6H_6 / g	C_6H_{12} / g	CCl_4 / g
C_6H_6+CCl_4 (70%) sample	12.3870		56.9126
C_6H_6+CCl_4 (30%) sample	29.8990		25.2209
C_6H_6+CCl_4 (15%) sample	36.7699		12.7739
C_6H_{12}+CCl_4 (70%) sample		12.5857	53.6715
C_6H_{12}+CCl_4 (30%) sample		28.1064	22.0233
C_6H_{12}+CCl_4 (15%) sample		33.5931	10.8338

Table 2-9 Reagents used for samples.

	Supplier	Grade	Purity
C_6H_6	Sigma-Aldrich	for HPLC	≥ 99.9%
C_6H_{12}	Sigma-Aldrich	for HPLC	≥ 99.9%
CCl_4	Wako	Super Special Grade	99.8%

2.2.6. Measurement

At the M1 beamline of RCNP-MuSIC, muon beam irradiation experiments were conducted from June 17 to June 18, 2017. The momentum of muon beam used was 50 MeV/c. The measured samples and measurement times are as shown in Table 2-10.

Table 2-10 Samples and irradiation times.

Sample name	**Irradiation time**
C_6H_6+CCl_4 (70%) sample	1.8 h
C_6H_6+CCl_4 (30%) sample	2.8 h
C_6H_6+CCl_4 (15%) sample	2.9 h
C_6H_{12}+CCl_4 (70%) sample	1.7 h
C_6H_{12}+CCl_4 (30%) sample	3.0 h
C_6H_{12}+CCl_4 (15%) sample	4.0 h
CCl_4 sample	1.5 h
C_6H_6 sample	0.6 h
C_6H_{12} sample	0.6 h
H_2O sample	1.3 h

2.3. Analysis

2.3.1. Detection Efficiency

Detection efficiency of germanium semiconductor detector was calculated by Monte Carlo simulation code EGS5,[26] based on data measured with standard source. Sample self-absorption differs depending on the sample, so it was calculated taking into account self-absorption for each sample. The detection efficiency in gas system experiment is shown in Fig. 2-16, the detection efficiency in liquid system experiment is shown in Fig. 2-17. The detection efficiency of Ge-K detector in the gas system experiment became small because the germanium crystal of the detector is small and the distance to the sample was long due to placement restrictions.

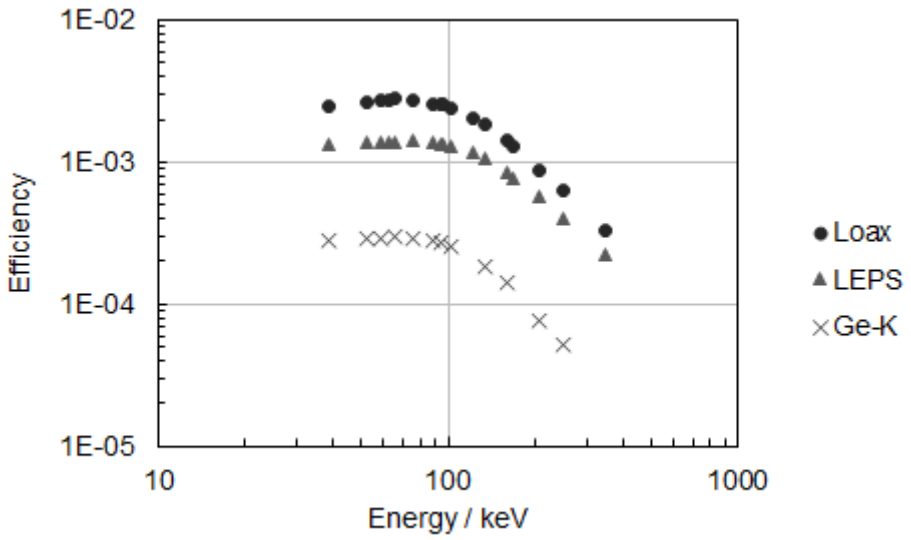

Fig. 2-16 Efficiency of the germanium detectors in the experiment of gas system. The values in this figure do not consider self-absorption by samples.

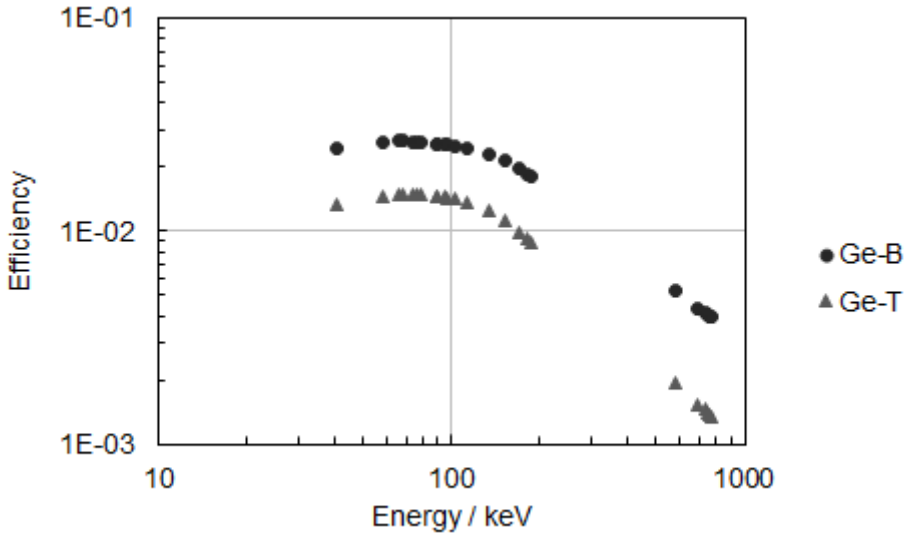

Fig. 2-17 Efficiency of the germanium detectors in the experiment of liquid system. The values in this figure do not consider self-absorption by samples.

2.3.2. Analysis using List Mode Measurement

The data measured with the germanium semiconductor detector was recorded as data in the form of a list in which the time when X-rays were detected and the energy of X-rays were related one-to-one. Therefore, it is possible to analyze the energy spectrum of only data at specific timing. In the gas system experiment, the data were analyzed the time domain in the vicinity of the muon pulse (prompt) and the time domain delayed from the muon pulse (delayed). The X-rays in delayed spectrum is derived only from the muon transfer, and muon transfer can be investigated by analyzing delayed spectrum. The scheme of this analysis is shown in Fig. 2-18.

In gas system experiment, the first half of the first pulse was fitted with a Gaussian function and the center ±3σ was taken as the area of the first prompt. The area of the second prompt is the area of the first prompt + 600 ns. Between the first and second prompt, and from the end of the second prompt to 8.8 μs later were taken as the area of delayed. The areas of prompt and delayed are shown in Fig. 2-19 and Fig. 2-20.

In liquid system experiment, prompt and delayed cannot be separated because muon transfer rate is very high, so the analysis divided into prompt and delayed was not conducted.

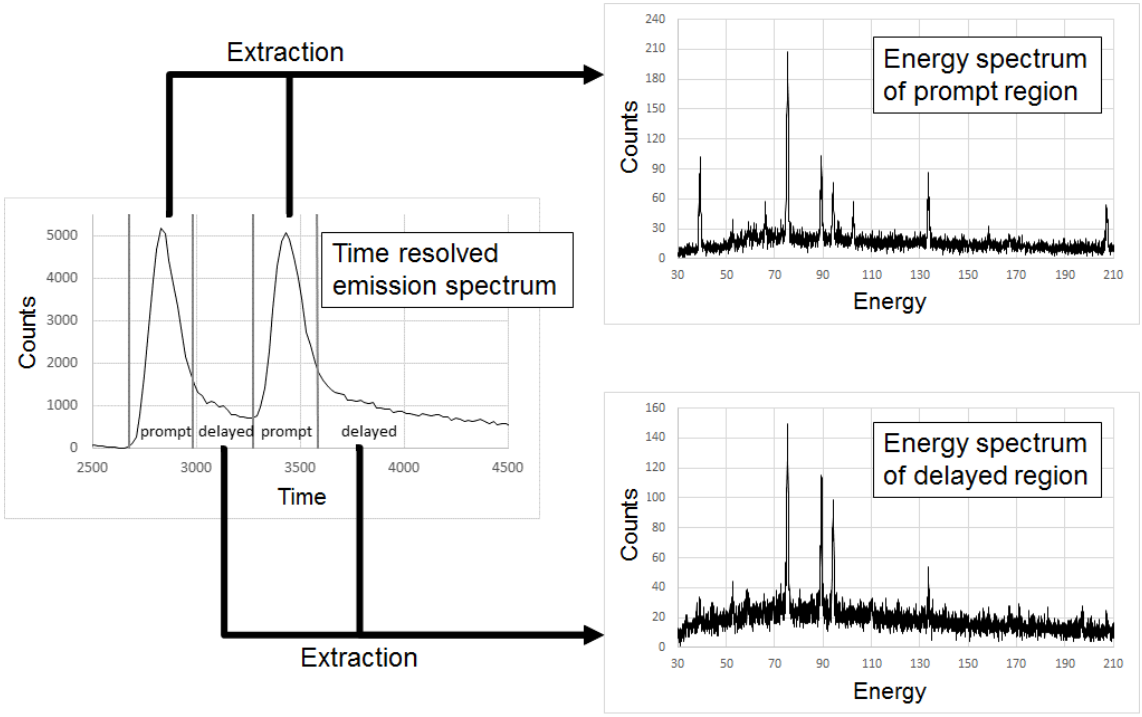

Fig. 2-18 Scheme of the extraction of prompt and delayed regions and reconstruction of energy spectrum

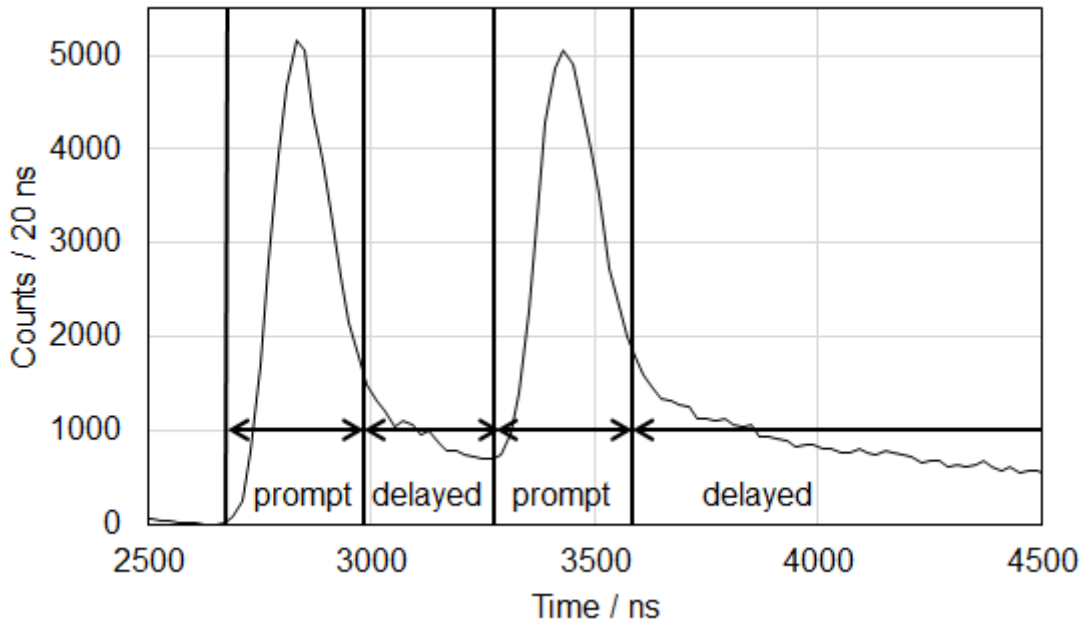

Fig. 2-19 Time resolved emission spectrum between beam signal and X-ray detection in the gas system experiment (expansion of prompt part).

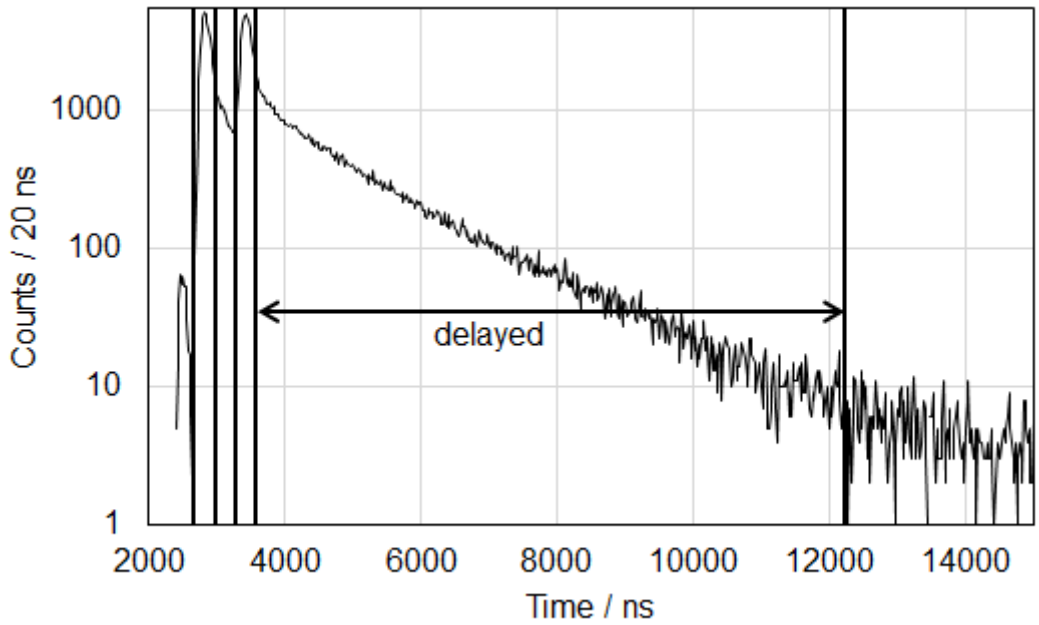

Fig. 2-20 Time resolved emission spectrum between beam signal and X-ray detection in the gas system experiment (all part).

3. Results

3.1. Results I: Experiment of Gas System

3.1.1. Spectra and Peak Identification

The X-ray spectra measured by a Loax detector in Benzene sample (C_6H_6 + Ne + H_2), Cyclohexane sample (C_6H_{12} + Ne + H_2) and Blank sample (Ne + H_2) are shown in Fig. 3-1 to Fig. 3-12. μZ (n-n′) represents muonic X-ray due to the transition from the principal quantum number n to n′ at the Z atom. For example, μC (2-1) indicates the K_α of muonic X-ray of carbon.

X-rays of carbon Lyman series, neon Lyman and Balmer series derived from samples were detected. The neon Lyman series except for μNe (2-1) were not detected due to low intensity of the peaks and low detection efficiency at high energy. The X-ray of aluminum is derived from the sample gas chamber. The X-rays of carbon, nitrogen and oxgen in Blank sample, and nitrogen and oxgen in Benzene sample and Cyclohexane sample are thought to originate from the polyimide window upstream of the sample gas chamber. These peaks almost disappear in delayed spectra, but they remain slightly. Therefore, using the X-ray intensity ratio of carbon to oxgen in the Blank sample, the components derived from polyimide were subtracted from the carbon X-rays of Benzene sample and Cyclohexane sample (for details, see the next section).

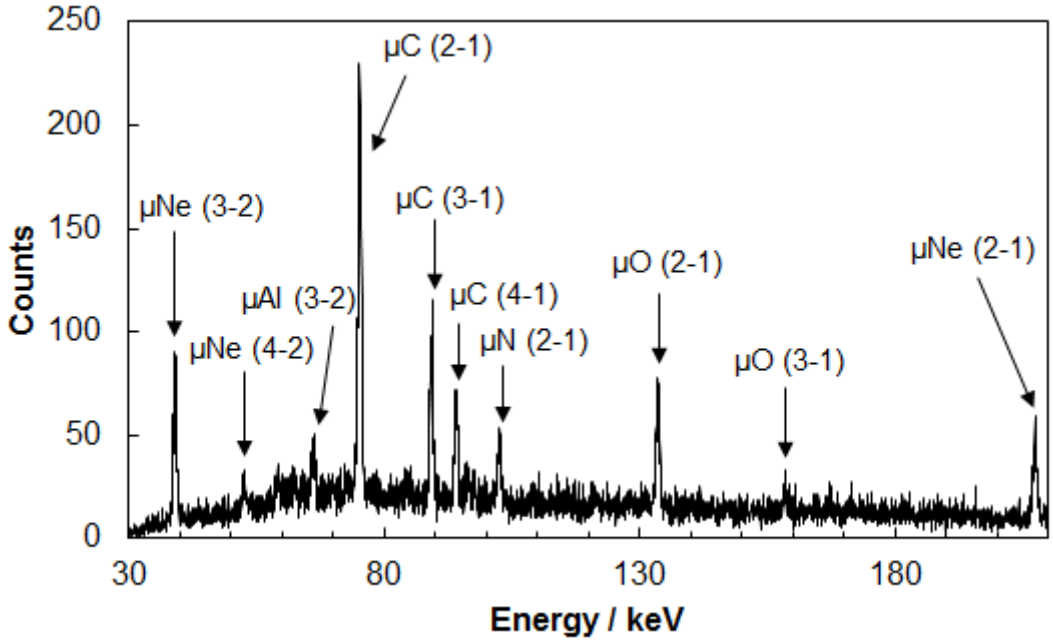

Fig. 3-1 Prompt spectrum of Benzene sample (30–210 keV).

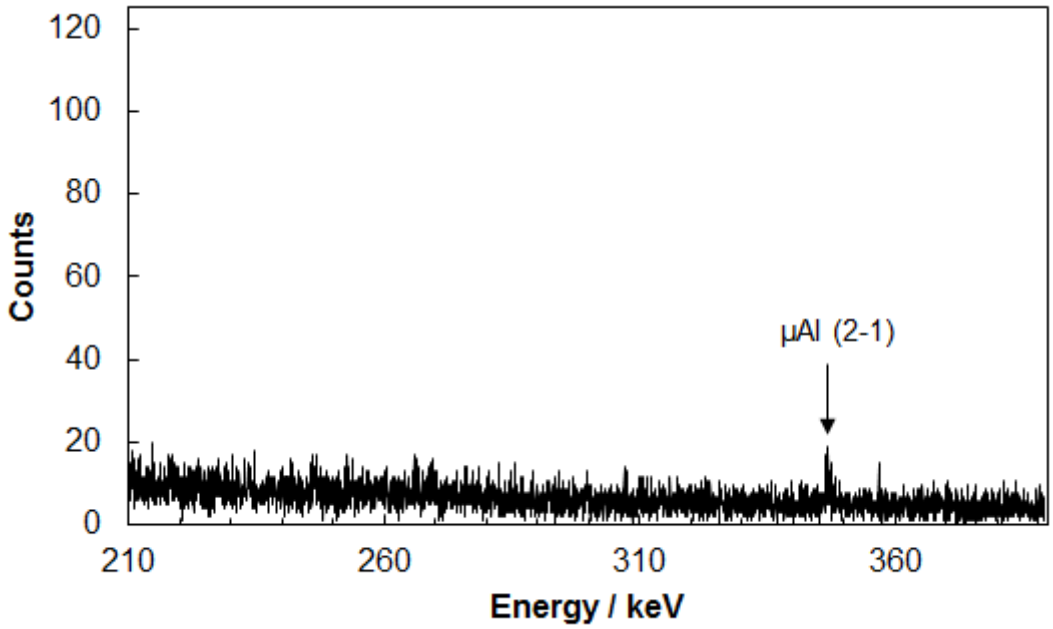

Fig. 3-2 Prompt spectrum of Benzene sample (210–390keV).

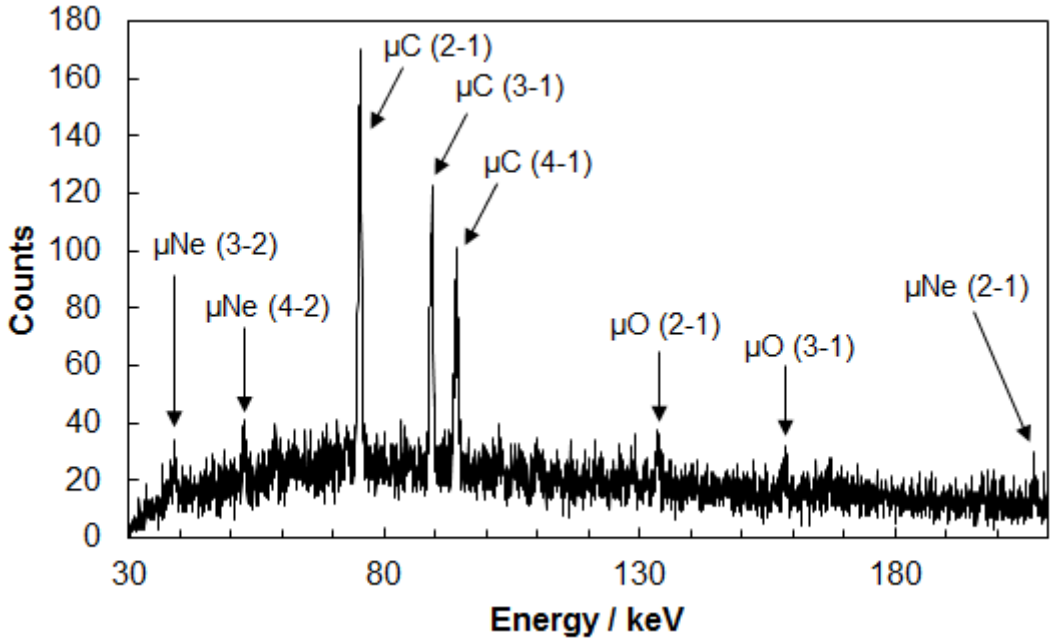

Fig. 3-3 Delayed spectrum of Benzene sample (30–210 keV).

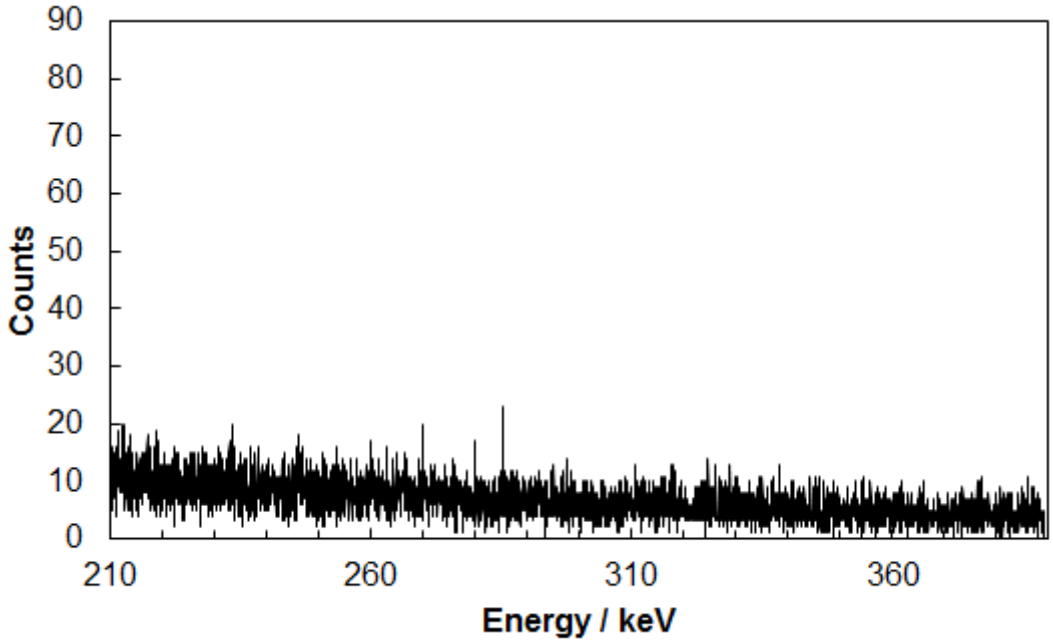

Fig. 3-4 Delayed spectrum of Benzene sample (210–390keV).

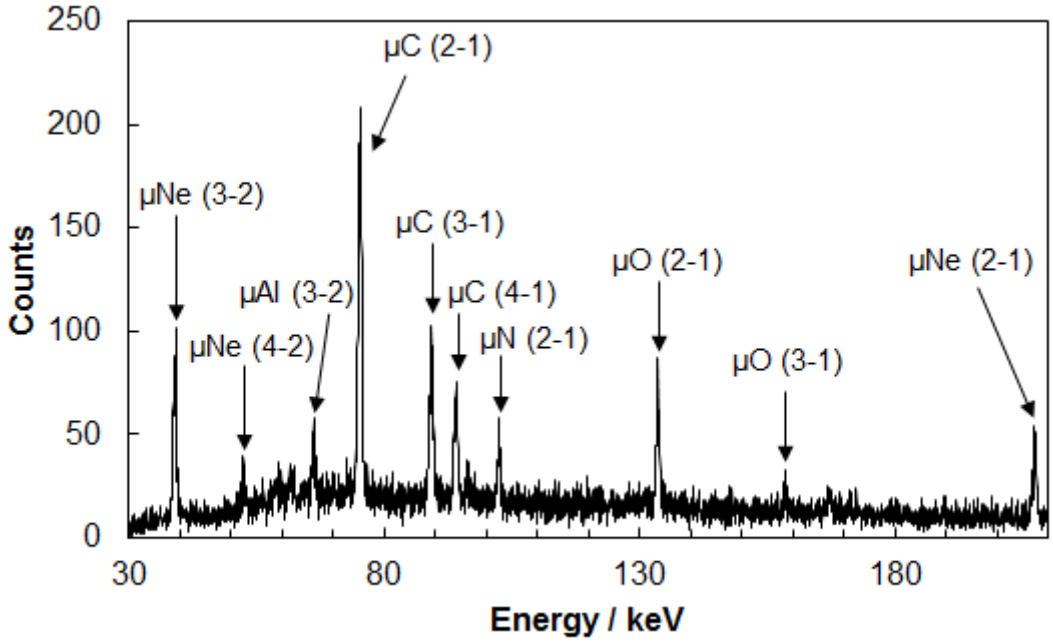

Fig. 3-5 Prompt spectrum of Cyclohexane sample (30–210 keV).

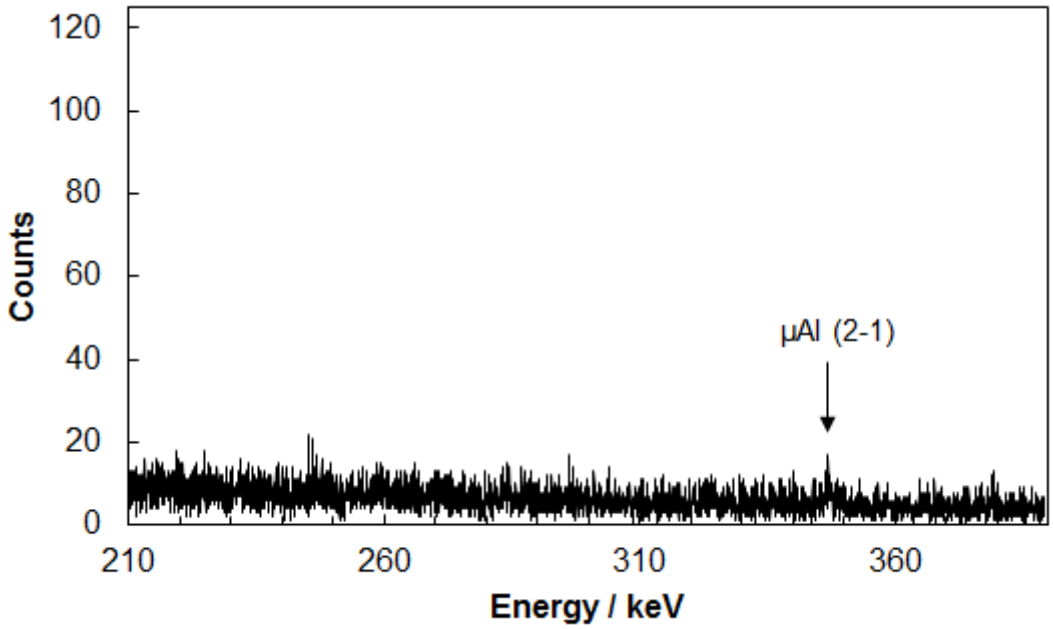

Fig. 3-6 Prompt spectrum of Cyclohexane sample (210–390keV).

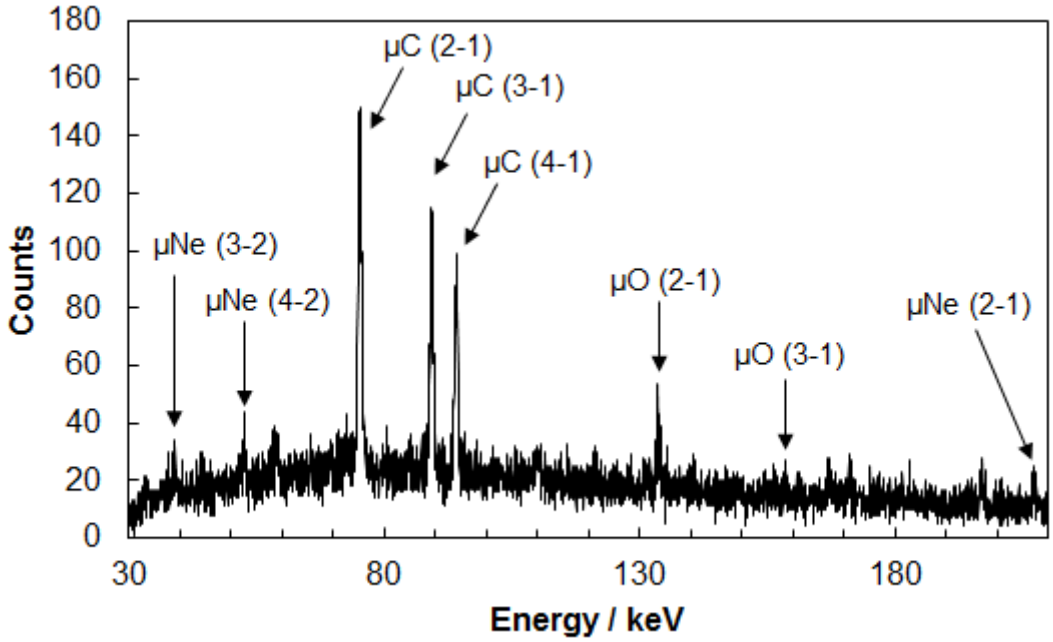

Fig. 3-7 Delayed spectrum of Cyclohexane sample (30–210 keV).

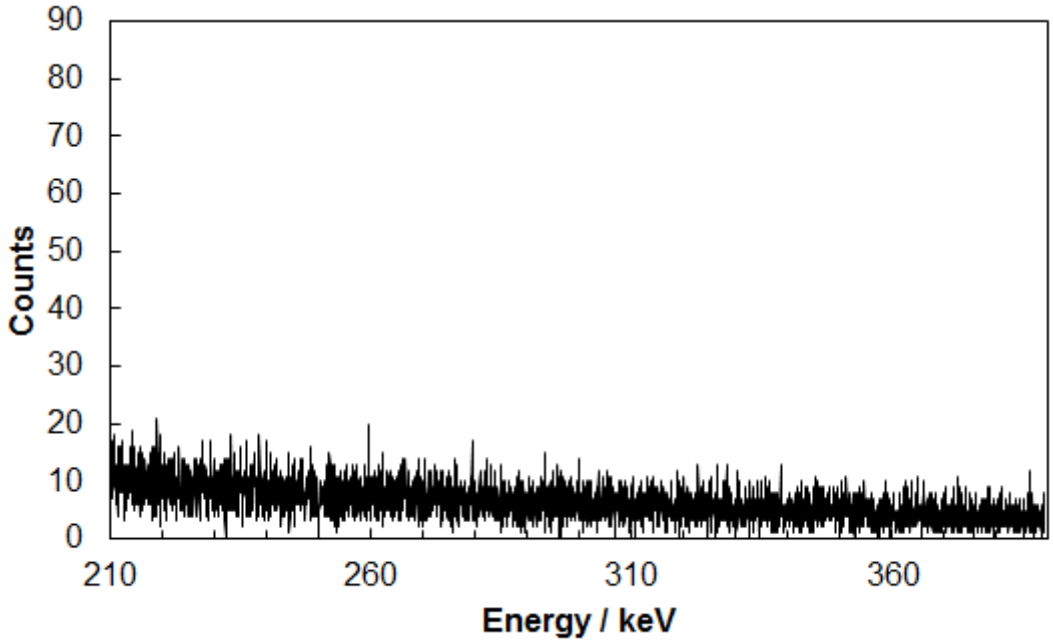

Fig. 3-8 Delayed spectrum of Cyclohexane sample (210–390keV).

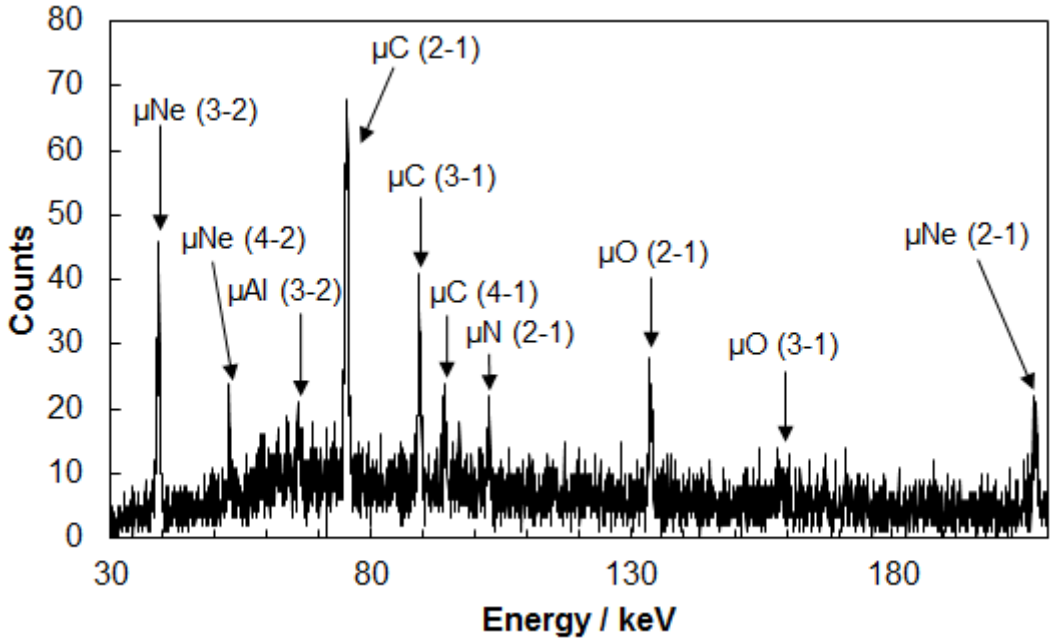

Fig. 3-9 Prompt spectrum of Blank sample (30–210 keV).

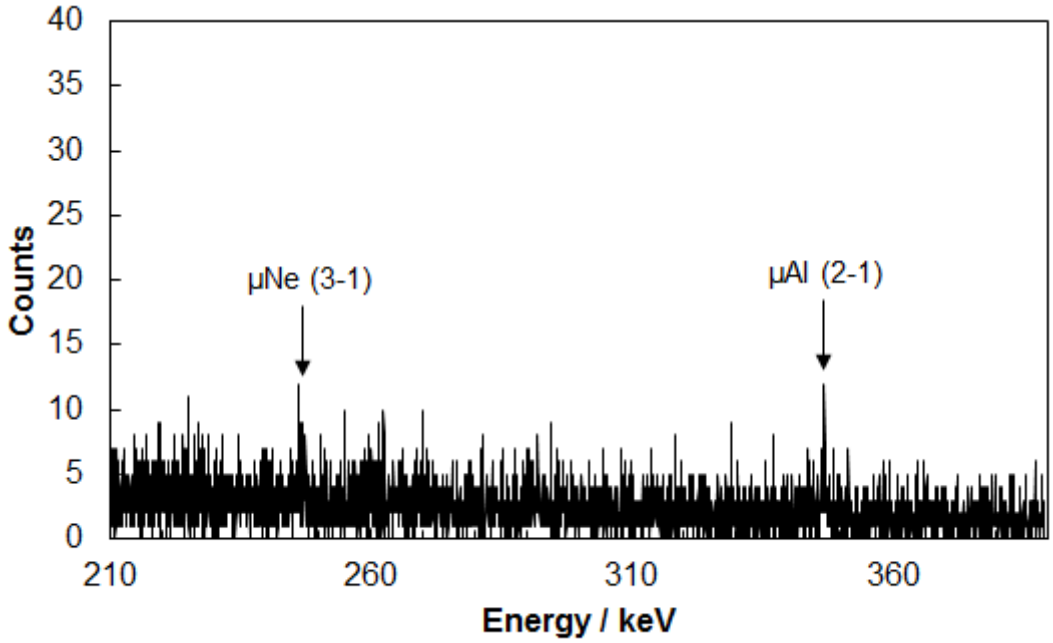

Fig. 3-10 Prompt spectrum of Blank sample (210–390keV).

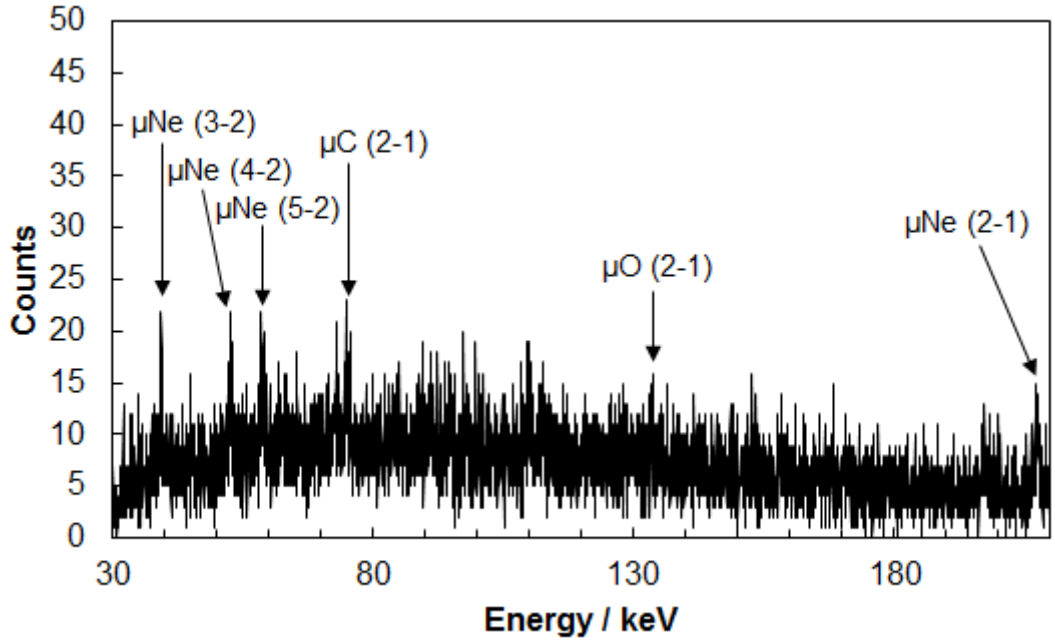

Fig. 3-11 Delayed spectrum of Blank sample (30–210 keV).

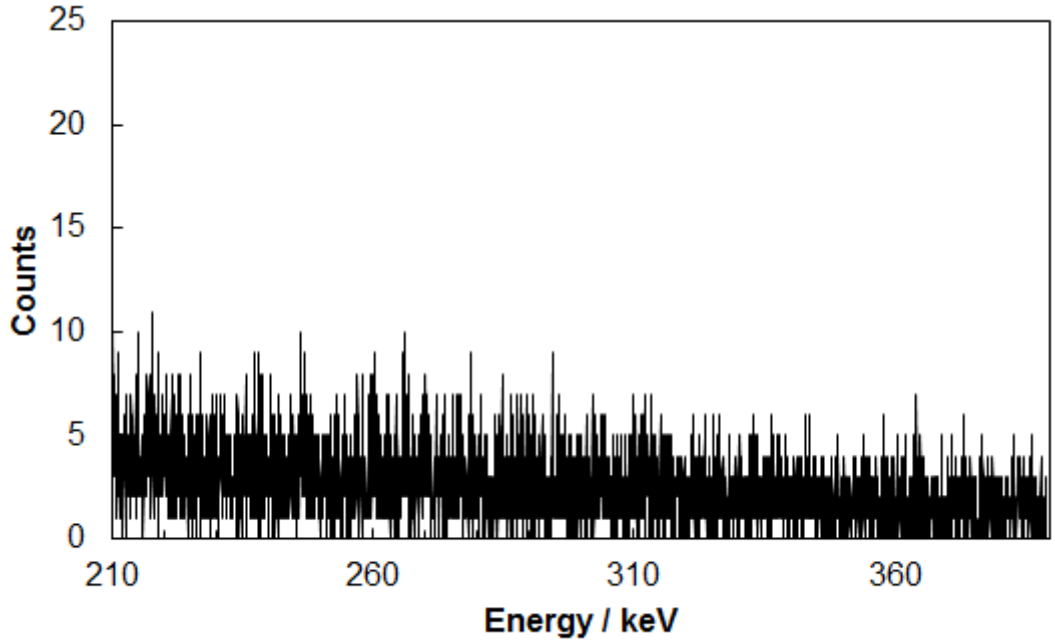

Fig. 3-12 Delayed spectrum of Blank sample (30–210 keV).

3.1.2. X-ray Intensity of Each Peak

For the prompt spectrum and the delayed spectrum of each sample, the X-ray intensities of carbon Lyman series, neon Lyman series, neon Balmer series and oxygen Lyman series were analyzed. Also, using the intensity ratio of the carbon Lyman series to the oxygen Lyman series in the Blank sample not containing hydrocarbons, the components derived from the polyimide contained in the carbon Lyman series of Benzene sample and Cyclohexane sample were subtracted, and the intensity of the Lyman series of carbon (μC HC) was determined.

$$\mu C\ \ HC = \mu C\ \ \text{Lyman} - \mu O\ \ \text{Lyman} \times \frac{\mu C\ \ \text{Lyman}\ \ (\text{Blank sample})}{\mu O\ \ \text{Lyman}\ \ (\text{Blank sample})}$$

The intensity ratio of carbon to oxygen used for the prompt spectrum was determined from the prompt spectrum of the Blank sample, and that for the delayed spectrum was determined from the delayed spectrum of the Blank sample.

The analysis results are shown in Table 3-1 to Table 3-6. In the tables, "μNe All" means the sum of all neon Lyman and Balmer series (neon Lyman series except for μNe (2-1) were not detected). For the prompt component, many of the components derived from polyimide occupied the X-ray of carbon, which was 63% for the LEPS detector and 90% for the Loax detector. As for the Ge-K detector, the components derived from polyimide were not detected because the distance was far from the chamber. For the delayed component, the components derived from polyimide in the X-ray of carbon were 6% for the LEPS detector and 11% for the Loax detector. For the Ge-K detector, the detection efficiency was low and the data amount were poor, and almost no X-ray of neon in the delayed component was detected.

Table 3-1 Muonic X-ray intensities in prompt spectrum of Benzene sample.

	Emission rate / min^{-1}		
	LEPS	**Loax**	**Ge-K**
μNe (3-2)	11.0 ± 0.7	8.1 ± 0.5	17.5 ± 1.9
μNe (4-2)	2.2 ± 0.4	1.6 ± 0.2	2.0 ± 1.1
μNe (5-2)	1.6 ± 0.4	1.0 ± 0.4	n.d.
sum μNe Balmer	14.9 ± 0.9	10.7 ± 0.7	19.4 ± 2.2
μAl (3-2)	2.7 ± 0.4	1.7 ± 0.3	5.3 ± 1.4
μC (2-1)	23.4 ± 1.3	18.3 ± 1.0	10.2 ± 1.5
μC (3-1)	9.9 ± 0.7	8.0 ± 0.5	4.1 ± 1.1
μC (4-1)	7.6 ± 0.6	5.3 ± 0.4	n.d.
sum μC Lyman	40.8 ± 1.6	31.7 ± 1.2	14.3 ± 1.9
μN (2-1)	3.5 ± 0.5	3.5 ± 0.3	n.d.
μO (2-1)	10.8 ± 0.9	8.4 ± 0.6	n.d.
μO (3-1)	3.0 ± 0.8	2.6 ± 0.4	n.d.
μO (4-1)	2.6 ± 0.6	1.7 ± 0.5	n.d.
sum μO Lyman	16.4 ± 1.3	12.6 ± 0.9	—
μNe (2-1)	19.5 ± 1.5	13.0 ± 1.0	16.8 ± 3.4
μC HC	13.2 ± 4.4	3.9 ± 3.9	14.3 ± 1.9
μNe All	34.4 ± 1.8	23.7 ± 1.2	36.2 ± 4.1
μC HC / μNe Balmer	0.89 ± 0.30	0.36 ± 0.36	0.74 ± 0.13
μC HC / μNe (2-1)	0.68 ± 0.23	0.30 ± 0.30	0.85 ± 0.21
μC HC / μNe All	0.38 ± 0.13	0.16 ± 0.16	0.39 ± 0.07

Table 3-2 Muonic X-ray intensities in delayed spectrum of Benzene sample.

	Emission rate / min^{-1}		
	LEPS	**Loax**	**Ge-K**
μNe (3-2)	0.9 ± 0.3	2.4 ± 0.3	n.d.
μNe (4-2)	1.2 ± 0.4	1.2 ± 0.2	n.d.
μNe (5-2)	1.8 ± 0.4	0.9 ± 0.4	n.d.
sum μNe Balmer	3.9 ± 0.7	4.5 ± 0.6	—
μAl (3-2)	n.d.	n.d.	n.d.
μC (2-1)	15.4 ± 1.0	12.6 ± 0.7	18.1 ± 2.0
μC (3-1)	13.0 ± 0.9	8.7 ± 0.6	8.4 ± 1.4
μC (4-1)	9.8 ± 0.7	7.7 ± 0.5	7.3 ± 1.3
sum μC Lyman	38.3 ± 1.5	29.0 ± 1.1	26.6 ± 2.4
μN (2-1)	1.4 ± 0.4	0.7 ± 0.3	n.d.
μO (2-1)	2.7 ± 0.6	1.5 ± 0.4	n.d.
μO (3-1)	2.2 ± 0.7	1.7 ± 0.5	n.d.
μO (4-1)	1.7 ± 0.6	1.9 ± 0.5	n.d.
sum μO Lyman	6.5 ± 1.1	5.1 ± 0.8	—
μNe (2-1)	3.4 ± 0.9	3.6 ± 0.7	n.d.
μC HC	36.1 ± 1.5	26.0 ± 1.2	26.6 ± 2.4
μNe All	7.3 ± 1.1	8.1 ± 0.9	n.d.
μC HC / μNe Balmer	9.23 ± 1.61	5.74 ± 0.75	—
μC HC / μNe (2-1)	10.58 ± 2.84	7.23 ± 1.53	—
μC HC / μNe All	4.93 ± 0.78	3.20 ± 0.39	—

Table 3-3 Muonic X-ray intensities in prompt spectrum of Cyclohexane sample.

	Emission rate / min^{-1}		
	LEPS	**Loax**	**Ge-K**
μNe (3-2)	11.1 ± 0.7	8.6 ± 0.5	15.3 ± 1.9
μNe (4-2)	1.7 ± 0.4	1.4 ± 0.2	3.9 ± 1.1
μNe (5-2)	1.2 ± 0.5	1.6 ± 0.4	n.d.
sum μNe Balmer	14.0 ± 1.0	11.6 ± 0.7	19.2 ± 2.2
μAl (3-2)	2.5 ± 0.4	2.1 ± 0.3	3.6 ± 1.4
μC (2-1)	22.8 ± 1.3	18.7 ± 1.0	8.9 ± 1.5
μC (3-1)	10.9 ± 0.8	8.0 ± 0.5	4.7 ± 1.2
μC (4-1)	8.1 ± 0.7	5.7 ± 0.4	1.2 ± 1.0
sum μC Lyman	41.8 ± 1.7	32.4 ± 1.2	13.5 ± 1.9
μN (2-1)	4.2 ± 0.5	2.8 ± 0.3	n.d.
μO (2-1)	10.6 ± 0.9	8.6 ± 0.6	n.d.
μO (3-1)	2.1 ± 0.8	2.2 ± 0.4	n.d.
μO (4-1)	2.0 ± 0.6	2.7 ± 0.5	n.d.
sum μO Lyman	14.6 ± 1.3	13.5 ± 0.9	—
μNe (2-1)	21.0 ± 1.6	13.3 ± 1.1	9.7 ± 3.2
μC HC	17.2 ± 4.1	2.7 ± 4.1	13.5 ± 1.9
μNe All	33.4 ± 1.8	23.8 ± 1.2	27.6 ± 3.7
μC HC / μNe Balmer	1.23 ± 0.31	0.23 ± 0.35	0.71 ± 0.13
μC HC / μNe (2-1)	0.82 ± 0.21	0.20 ± 0.31	1.40 ± 0.50
μC HC / μNe All	0.49 ± 0.12	0.11 ± 0.16	0.47 ± 0.09

Table 3-4 Muonic X-ray intensities in delayed spectrum of Cyclohexane sample.

	Emission rate / min^{-1}		
	LEPS	**Loax**	**Ge-K**
μNe (3-2)	1.4 ± 0.4	1.7 ± 0.3	2.8 ± 1.6
μNe (4-2)	2.3 ± 0.4	1.5 ± 0.3	n.d.
μNe (5-2)	1.9 ± 0.4	1.5 ± 0.4	n.d.
sum μNe Balmer	5.7 ± 0.7	4.7 ± 0.6	2.8 ± 1.6
μAl (3-2)	n.d.	n.d.	n.d.
μC (2-1)	15.4 ± 1.0	12.8 ± 0.7	17.7 ± 2.0
μC (3-1)	11.5 ± 0.8	8.8 ± 0.6	9.9 ± 1.5
μC (4-1)	9.1 ± 0.7	7.6 ± 0.5	9.0 ± 1.3
sum μC Lyman	36.0 ± 1.4	29.2 ± 1.1	27.6 ± 2.5
μN (2-1)	0.4 ± 0.4	n.d.	n.d.
μO (2-1)	2.7 ± 0.6	2.6 ± 0.5	n.d.
μO (3-1)	2.8 ± 0.7	0.5 ± 0.4	n.d.
μO (4-1)	1.3 ± 0.6	2.2 ± 0.5	n.d.
sum μO Lyman	6.8 ± 1.1	5.2 ± 0.8	—
μNe (2-1)	3.7 ± 0.9	3.1 ± 0.7	n.d.
μC HC	33.8 ± 1.5	26.1 ± 1.2	27.6 ± 2.5
μNe All	8.9 ± 1.1	7.4 ± 0.9	2.8 ± 1.6
μC HC / μNe Balmer	5.96 ± 0.77	5.51 ± 0.70	9.80 ± 5.66
μC HC / μNe (2-1)	9.14 ± 2.30	8.55 ± 2.11	—
μC HC / μNe All	3.61 ± 0.47	3.35 ± 0.43	9.80 ± 5.66

Table 3-5 Muonic X-ray intensities in prompt spectrum of Blank sample.

	Emission rate / min^{-1}		
	LEPS	**Loax**	**Ge-K**
μNe (3-2)	12.1 ± 1.0	8.5 ± 0.7	16.4 ± 2.7
μNe (4-2)	1.4 ± 0.6	1.7 ± 0.4	3.1 ± 1.8
μNe (5-2)	1.0 ± 0.7	1.2 ± 0.6	n.d.
sum μNe Balmer	14.5 ± 1.3	11.4 ± 1.0	19.5 ± 3.3
μAl (3-2)	2.2 ± 0.6	1.2 ± 0.4	n.d.
μC (2-1)	16.6 ± 1.3	14.0 ± 0.9	3.0 ± 1.9
μC (3-1)	6.7 ± 0.9	6.0 ± 0.6	n.d.
μC (4-1)	2.2 ± 0.7	2.4 ± 0.4	n.d.
sum μC Lyman	25.5 ± 1.7	22.5 ± 1.2	3.0 ± 1.9
μN (2-1)	3.3 ± 0.7	2.3 ± 0.4	n.d.
μO (2-1)	10.0 ± 1.2	6.7 ± 0.8	n.d.
μO (3-1)	3.8 ± 1.2	2.6 ± 0.7	n.d.
μO (4-1)	1.3 ± 0.9	0.9 ± 0.7	n.d.
sum μO Lyman	15.1 ± 1.9	10.2 ± 1.2	
μNe (2-1)	21.4 ± 2.1	16.1 ± 1.6	23.5 ± 5.6
μC Lyman / μO (2-1)	1.69 ± 0.24	2.21 ± 0.29	—

Table 3-6 Muonic X-ray intensities in delayed spectrum of Blank sample.

	Emission rate / min^{-1}		
	LEPS	**Loax**	**Ge-K**
μNe (3-2)	2.4 ± 0.6	2.4 ± 0.5	n.d.
μNe (4-2)	2.3 ± 0.6	2.2 ± 0.4	n.d.
μNe (5-2)	2.2 ± 0.7	1.6 ± 0.6	n.d.
sum μNe Balmer	6.9 ± 1.1	6.3 ± 0.9	—
μAl (3-2)	0.8 ± 0.5	n.d.	n.d.
μC (2-1)	1.0 ± 0.6	1.3 ± 0.4	n.d.
μC (3-1)	0.0 ± 0.6	1.0 ± 0.4	n.d.
μC (4-1)	0.0 ± 0.6	0.6 ± 0.4	3.9 ± 1.7
sum μC Lyman	1.0 ± 1.1	2.9 ± 0.7	—
μN (2-1)	1.6 ± 0.7	n.d.	n.d.
μO (2-1)	1.1 ± 0.9	0.9 ± 0.7	n.d.
μO (3-1)	1.0 ± 1.2	1.9 ± 0.7	n.d.
μO (4-1)	1.0 ± 0.9	2.0 ± 0.7	n.d.
sum μO Lyman	3.1 ± 1.7	4.8 ± 1.2	—
μNe (2-1)	7.4 ± 1.6	8.0 ± 1.3	1.5 ± 4.8
μC Lyman / μO (2-1)	0.33 ± 0.39	0.59 ± 0.21	—

3.1.3. X-ray Structure

The value obtained by normalizing the X-ray intensity of each transition of carbon with the intensity of μC (2-1). The values in the prompt spectrum are shown in Table 3-7 and Table 3-8, and the values in the delayed spectrum are shown in Table 3-9 and Table 3-10. Because there are too many polyimide-derived components in the X-ray of carbon in the prompt spectra by the LEPS detector and the Loax detector, only the values by the Ge-K detector are shown. In the delayed spectrum, the components derived from polyimide in the X-ray of carbon are not large in each detector, but the values by the Ge-K detector are not shown because the data amount is poor.

In the prompt spectrum, the transitions of μC (3-1) and μC (4-1) in the Cyclohexane sample became stronger compared to the Benzene sample. As the proportion of muon transfer increases, the transition with large Δn increases, this indicate that the muon transfer to the carbon atom in the Cyclohexane sample occurs more frequently than the Benzene sample. This is consistent with the fact that the total amount of muon transfer in the Cyclohexane sample is larger than that in the Benzene sample because the number of hydrogen atoms of cyclohexane molecules is larger than that of benzene molecules.

In the delayed spectrum, the difference between the samples coincided within the error range. This is consistent with the fact that all muonic X-rays in the delayed spectrum are derived only from the muon transfer. In the delayed spectrum, μC (4-1) was strongly observed, but μC (5-1) was not observed. This indicate that the muonic hydrogen atoms transfer its muon to n = 4 level of carbon.

Table 3-7 Muonic carbon X-ray structure normalized by μC (2-1) intensity in prompt spectrum of Benzene sample.

	Ge-K
μC (3-1) / (2-1)	0.40 ± 0.13
μC (4-1) / (2-1)	**—**

Table 3-8 Muonic carbon X-ray structure normalized by μC (2-1) intensity in prompt spectrum of Cyclohexane sample.

	Ge-K
μC (3-1) / (2-1)	0.53 ± 0.16
μC (4-1) / (2-1)	0.14 ± 0.11

Table 3-9 Muonic carbon X-ray structure normalized by μC (2-1) intensity in delayed spectrum of Benzene sample.

	LEPS	Loax	Average
μC (3-1) / (2-1)	0.84 ± 0.08	0.70 ± 0.06	0.75 ± 0.05
μC (4-1) / (2-1)	0.64 ± 0.06	0.61 ± 0.05	0.62 ± 0.04

Table 3-10 Muonic carbon X-ray structure normalized by μC (2-1) intensity in delayed spectrum of Cyclohexane sample.

	LEPS	Loax	Average
μC (3-1) / (2-1)	0.75 ± 0.07	0.69 ± 0.06	0.71 ± 0.05
μC (4-1) / (2-1)	0.59 ± 0.06	0.59 ± 0.05	0.59 ± 0.04

3.1.4. X-ray Intensity Ratio

Ratio of X-ray intensity of carbon derived from hydrocarbons to X-ray intensity of neon. This is a value that reflects the ratio of the number of muon captures to carbon and neon. The values in the prompt spectrum are shown in Table 3-11 and Table 3-12, and the values in the delayed spectrum are shown in Table 3-13 and Table 3-14. In the tables, "μNe Balmer" means the sum of neon Balmer series, and "μNe Lyman" means the sum of neon Lyman series (neon Lyman series except for μNe (2-1) were not detected). In the prompt spectrum by the Loax detector, the component derived from polyimide occupying the X-ray of carbon is 90% and the error of the corrected value is very large, so only the values by the LEPS detector and the Ge-K detector are shown. In the delayed spectrum

by the Ge-K detector, the data amount was poor and almost no neon X-rays were detected, so only the values by the LEPS detector and the Loax detector are shown.

In the results of prompt spectrum, some values of cyclohexane sample were slightly higher than that of benzene sample, but almost of the differences between samples are within the errors.

In the results of delayed spectrum, The values of μC HC / μNe Balmer and μC HC / μNe All by the LEPS detector show a difference exceeding slightly the error between samples, but the difference between the samples falls within the error range in the averaged value with the Loax detector. This is considered to be due to poor data amount by the LEPS detector. The difference of μC HC / μNe Lyman did not exceed the error between samples.

Table 3-11 Muonic X-ray intensity ratio of carbon to neon in prompt spectrum of Benzene sample.

	LEPS	**Ge-K**	**Average**
μC HC / μNe Balmer	0.89 ± 0.30	0.74 ± 0.13	0.76 ± 0.12
μC HC / μNe Lyman	0.68 ± 0.23	0.85 ± 0.21	0.77 ± 0.15
μC HC / μNe All	0.38 ± 0.13	0.39 ± 0.07	0.39 ± 0.06

Table 3-12 Muonic X-ray intensity ratio of carbon to neon in prompt spectrum of Cyclohexane sample.

	LEPS	**Ge-K**	**Average**
μC HC / μNe Balmer	1.23 ± 0.31	0.71 ± 0.13	0.78 ± 0.12
μC HC / μNe Lyman	0.82 ± 0.21	1.40 ± 0.50	0.90 ± 0.19
μC HC / μNe All	0.49 ± 0.12	0.47 ± 0.09	0.48 ± 0.07

Table 3-13 Muonic X-ray intensity ratio of carbon to neon in delayed spectrum of Benzene sample.

	LEPS	Loax	Average
μC HC / μNe Balmer	9.2 ± 1.6	5.7 ± 0.7	6.4 ± 0.7
μC HC / μNe Lyman	10.6 ± 2.8	7.2 ± 1.5	8.0 ± 1.3
μC HC / μNe All	4.9 ± 0.8	3.2 ± 0.4	3.5 ± 0.4

Table 3-14 Muonic X-ray intensity ratio of carbon to neon in delayed spectrum of Cyclohexane sample.

	LEPS	Loax	Average
μC HC / μNe Balmer	6.0 ± 0.8	5.5 ± 0.7	5.7 ± 0.5
μC HC / μNe Lyman	9.1 ± 2.3	8.6 ± 2.1	8.8 ± 1.6
μC HC / μNe All	3.6 ± 0.5	3.4 ± 0.4	3.5 ± 0.3

3.2. Results II: Experiment of Liquid System

3.2.1. Spectra and Peak Identification

The spectra of C_6H_{12}+CCl_4 (30%) sample, C_6H_6+CCl_4 (15%) sample, C_6H_{12}+CCl_4 (15%) sample, C_6H_{12}+CCl_4 (15%) sample, C_6H_6 sample, C_6H_{12} sample, CCl_4 sample, and H_2O sample measured by the Ge-T detector are shown in Fig. 3-13 to Fig. 3-42. μZ (n-n') represents the muonic X-ray of the Z atom and eZ (n-n') represents the electronic X-ray of the Z atom.

X-rays of carbon and chlorine derived from samples were measured with high accuracy in each sample. X-rays of aluminum are derived from a sample liquid holder, and X-rays of tin are derived from a tin plate used for shielding. X-rays of slightly observed oxygen and nitrogen are derived from air. In the H_2O sample for background evaluation, X-rays of μAl (4-2) were observed at the same energy as μC (3-1) although the intensity was small. Therefore, using the intensity ratio of μAl (3-2) and μAl (4-2) in the H_2O sample, the intensity of μC (3-1) in other samples was corrected. In the energy

range of carbon and chlorine X-rays, no other peaks disturbing them were observed.

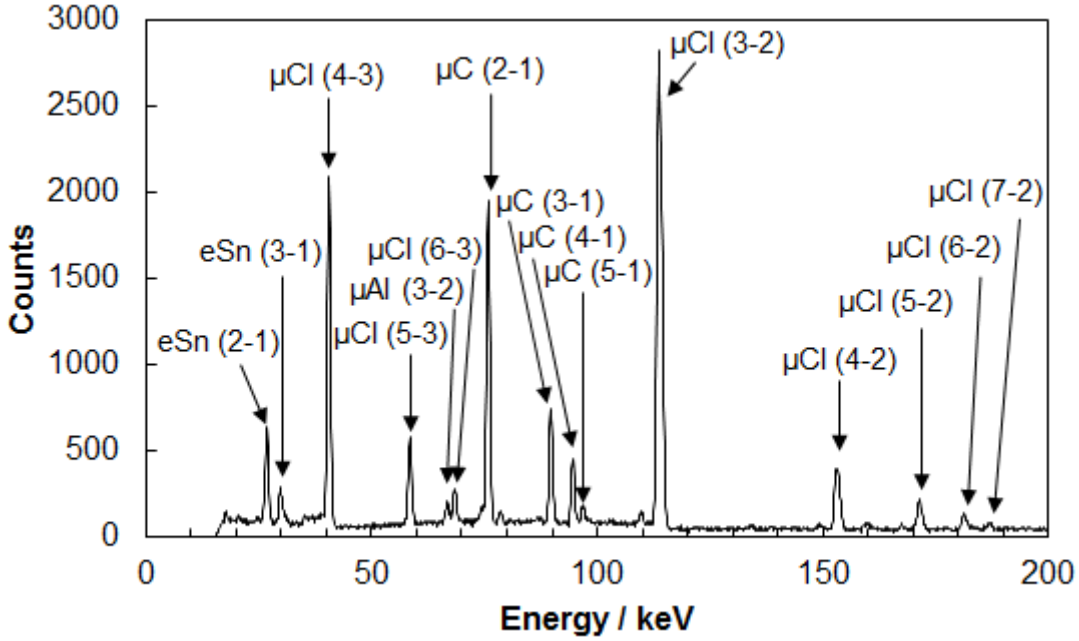

Fig. 3-13 X-ray spectrum of C_6H_6+CCl_4 (70%) sample (0–200 keV).

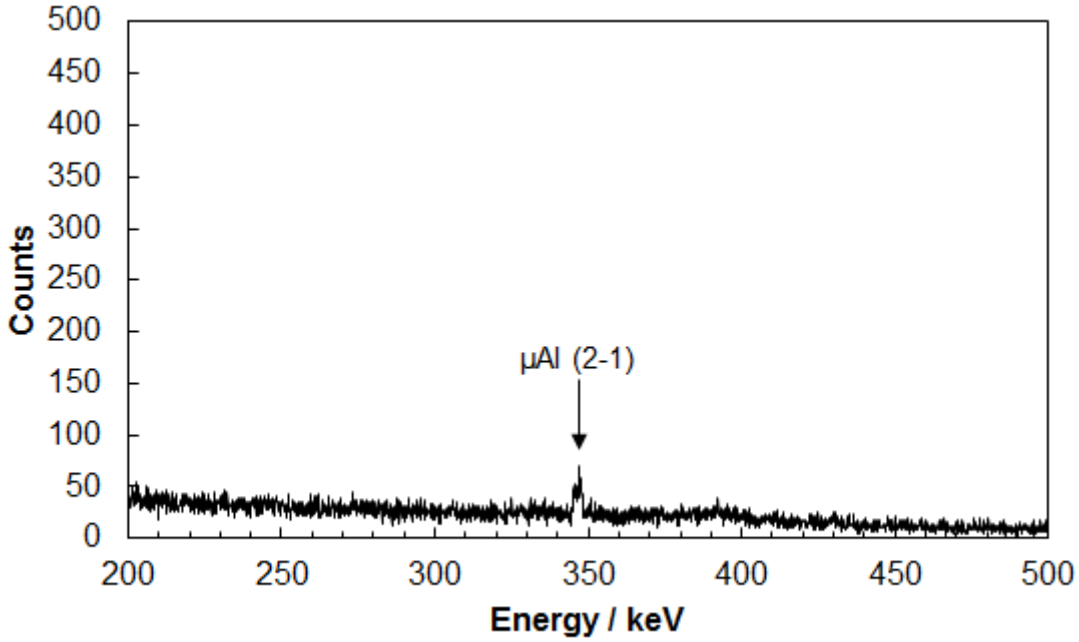

Fig. 3-14 X-ray spectrum of C_6H_6+CCl_4 (70%) sample (200–500 keV).

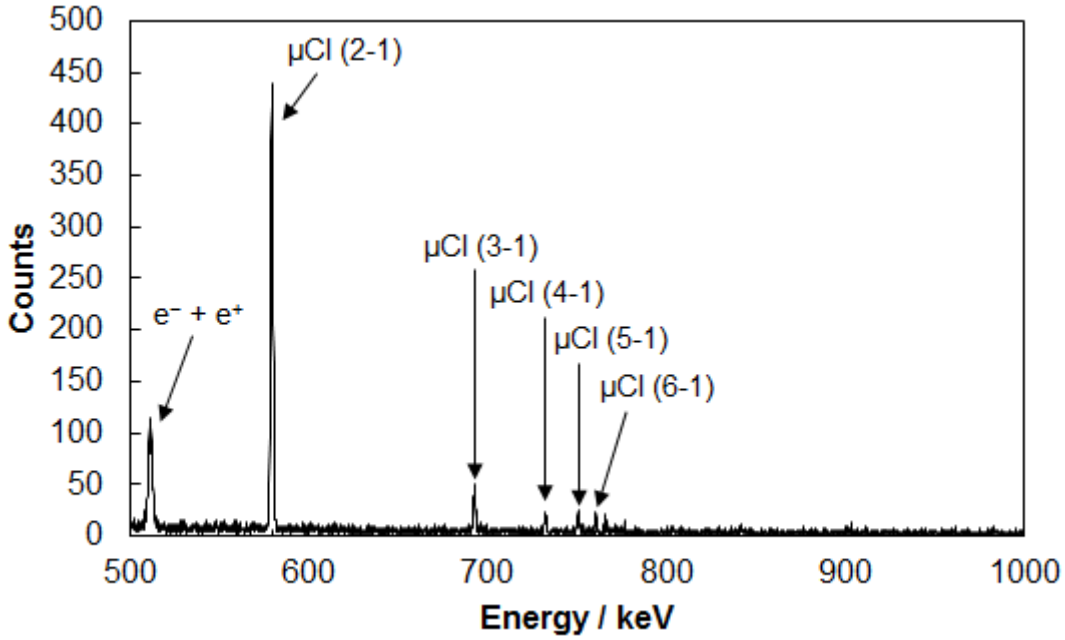

Fig. 3-15 X-ray spectrum of C_6H_6+CCl_4 (70%) sample (500–1000 keV).

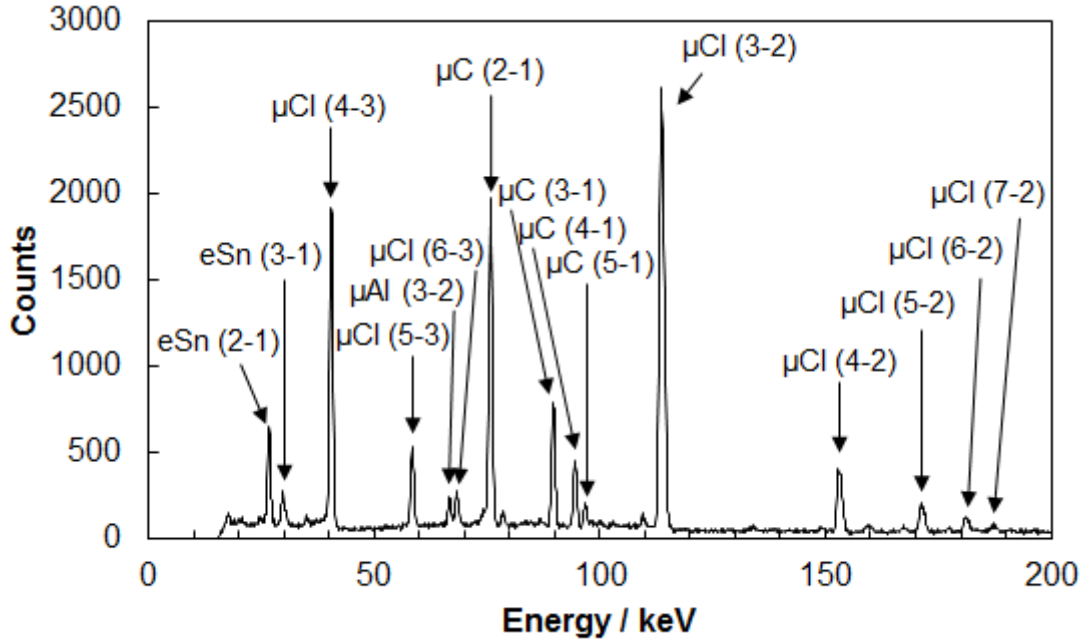

Fig. 3-16 X-ray spectrum of C_6H_{12}+CCl_4 (70%) sample (0–200 keV).

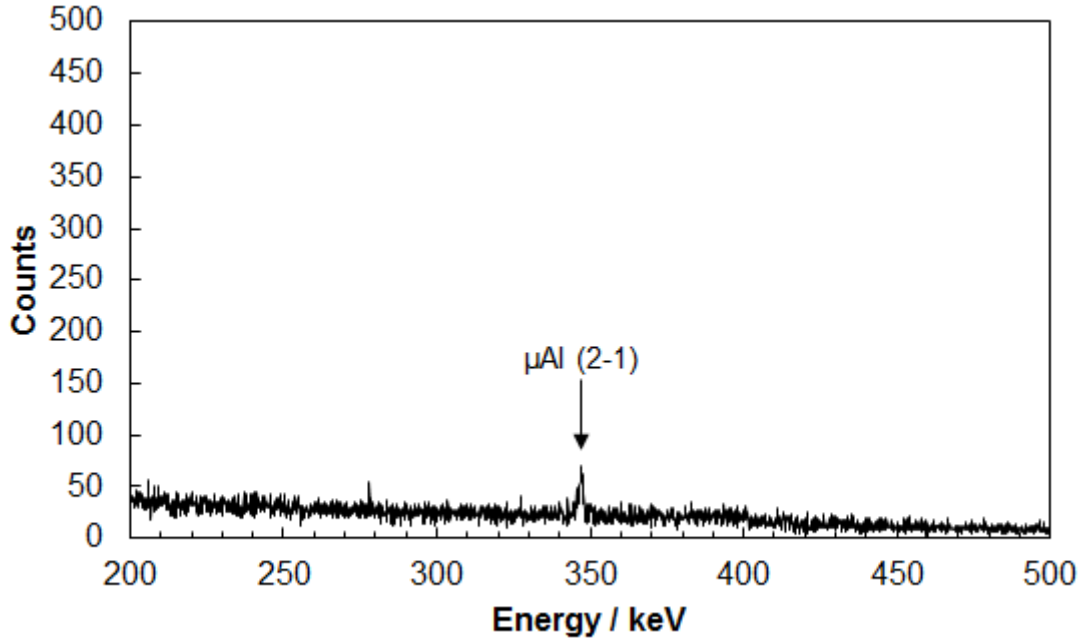

Fig. 3-17 X-ray spectrum of C_6H_{12}+CCl_4 (70%) sample (200–500 keV).

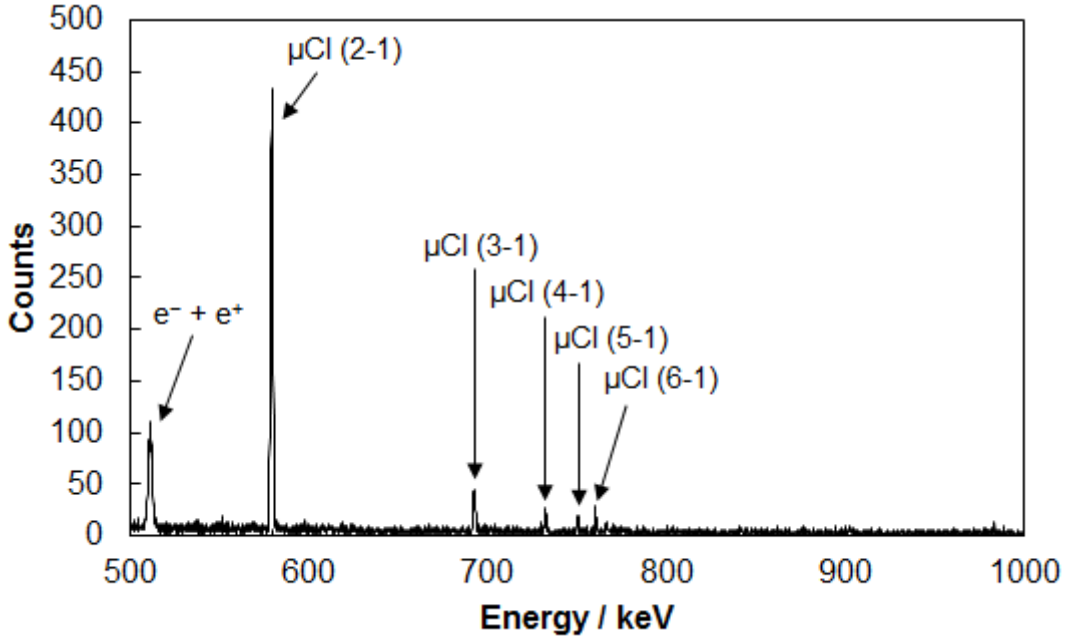

Fig. 3-18 X-ray spectrum of C_6H_{12}+CCl_4 (70%) sample (500–1000 keV).

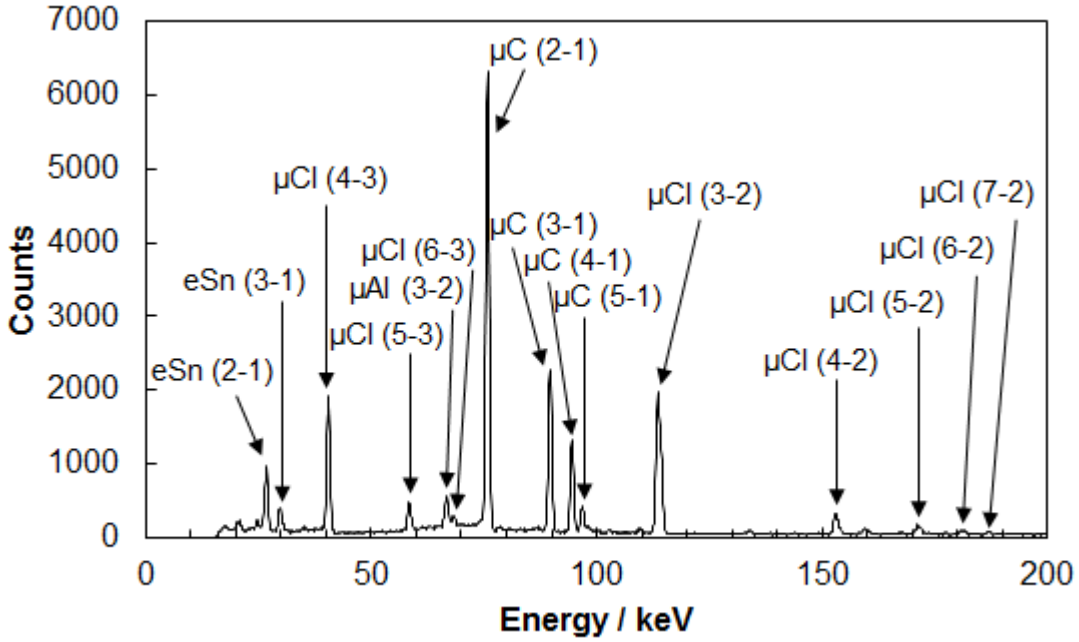

Fig. 3-19 X-ray spectrum of C_6H_6+CCl_4 (30%) sample (0–200 keV).

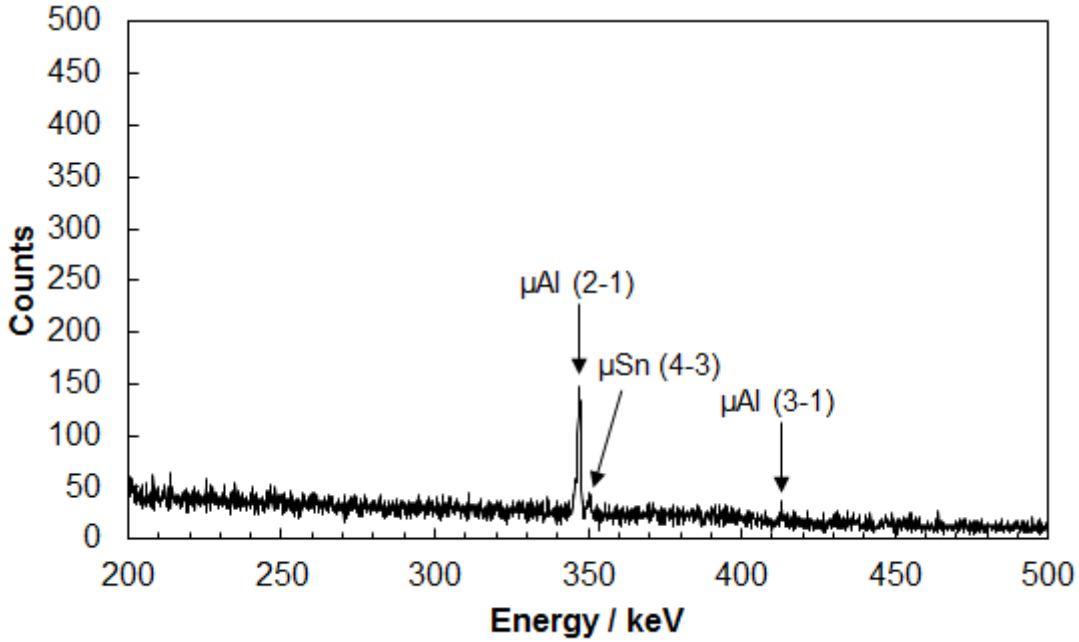

Fig. 3-20 X-ray spectrum of C_6H_6+CCl_4 (30%) sample (200–500 keV).

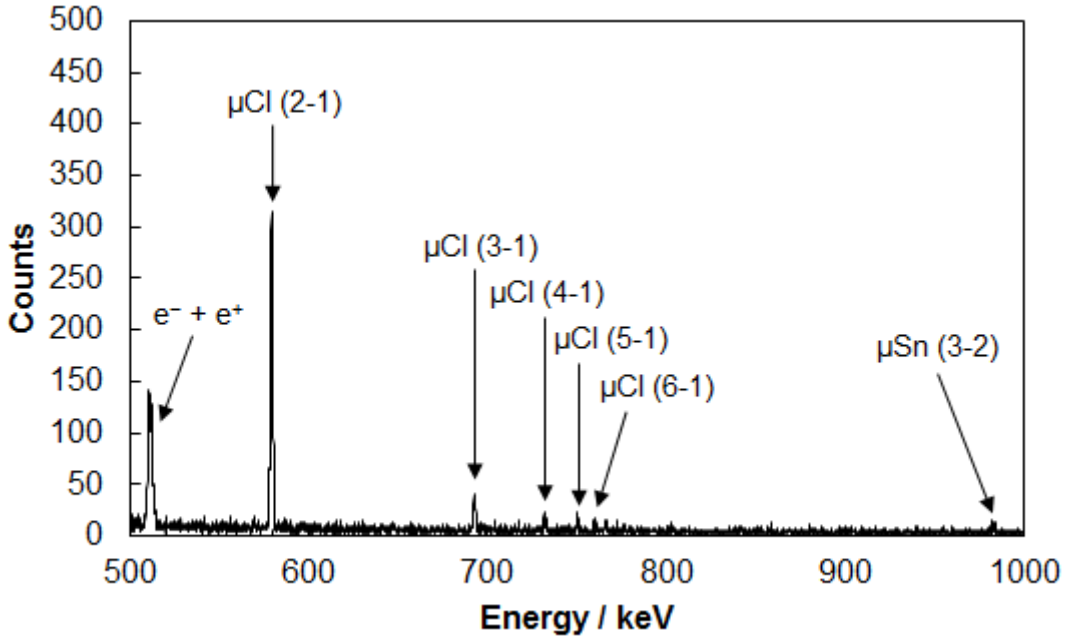

Fig. 3-21 X-ray spectrum of C_6H_6+CCl_4 (30%) sample (500–1000 keV).

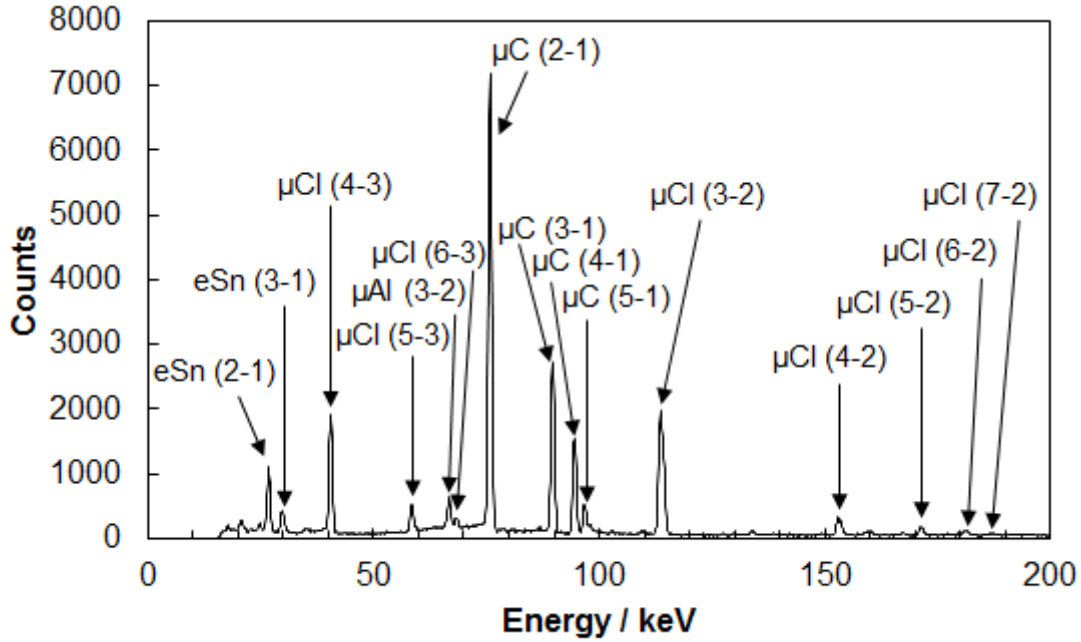

Fig. 3-22 X-ray spectrum of C_6H_{12}+CCl_4 (30%) sample (0–200 keV).

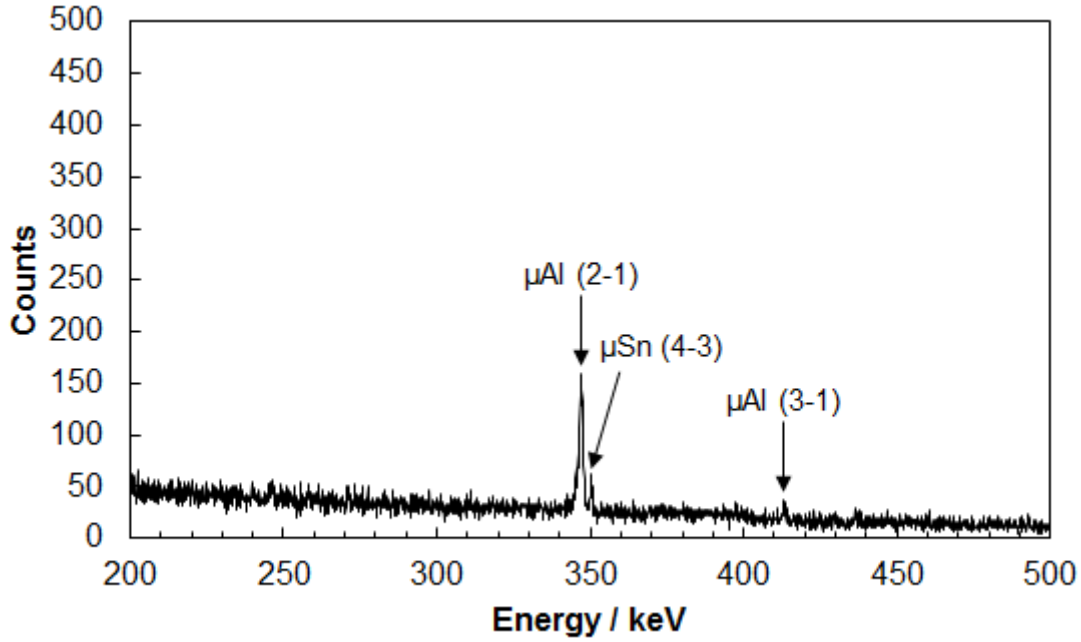

Fig. 3-23 X-ray spectrum of C_6H_{12}+CCl_4 (30%) sample (200–500 keV).

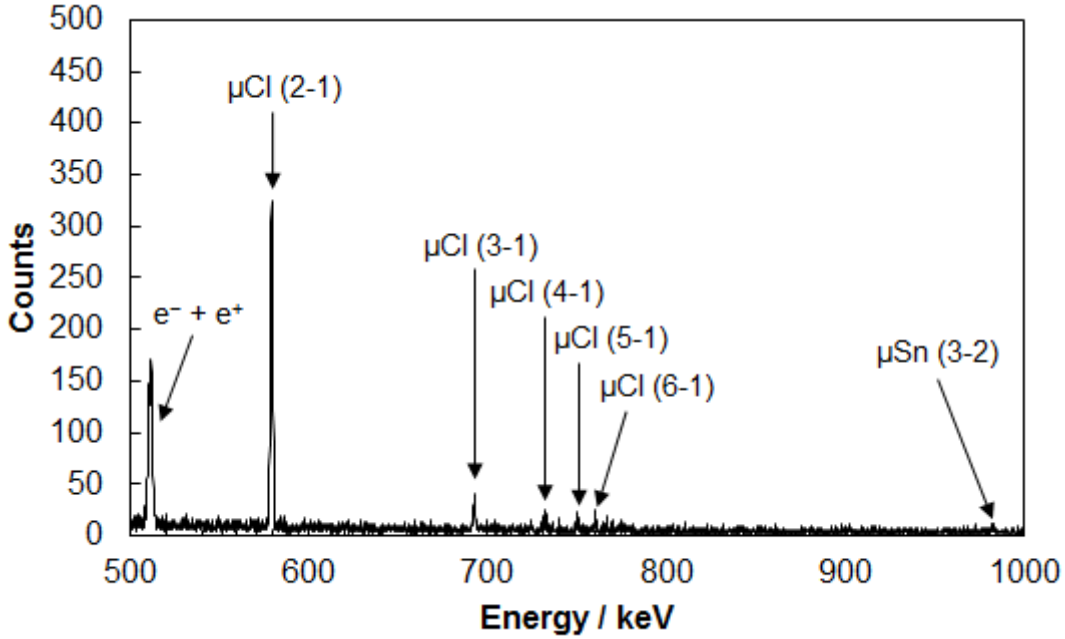

Fig. 3-24 X-ray spectrum of C_6H_{12}+CCl_4 (30%) sample (500–1000 keV).

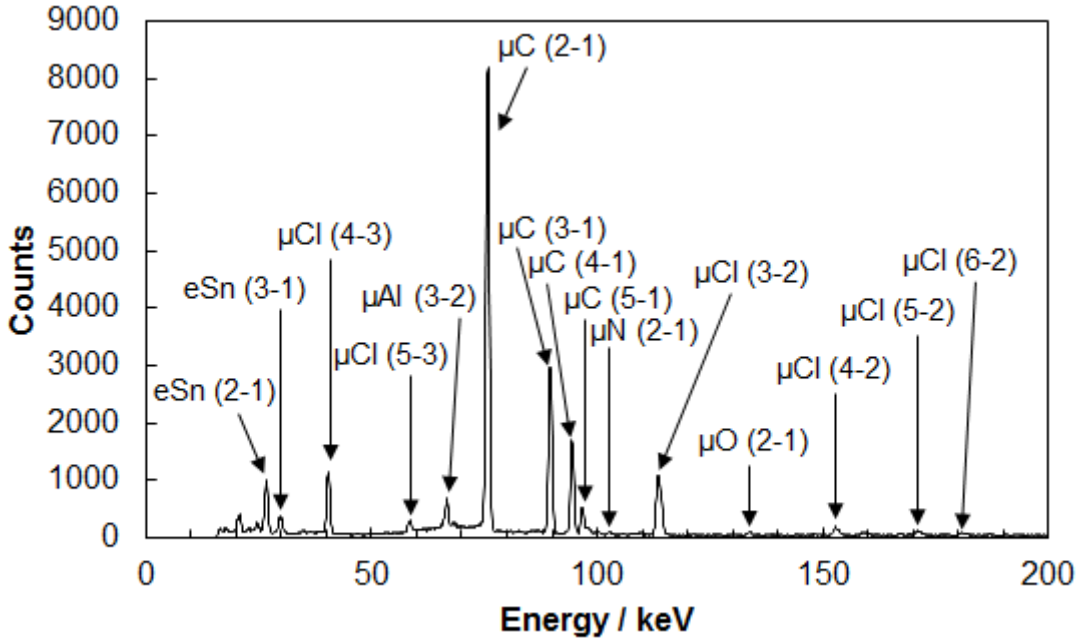

Fig. 3-25 X-ray spectrum of C_6H_6+CCl_4 (15%) sample (0–200 keV).

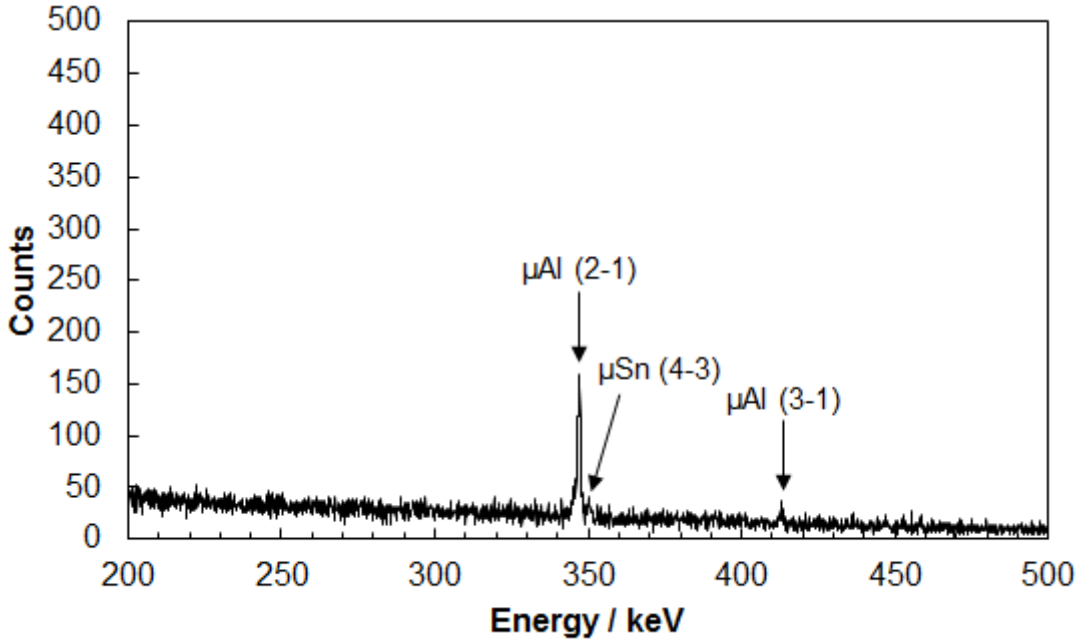

Fig. 3-26 X-ray spectrum of C_6H_6+CCl_4 (15%) sample (200–500 keV).

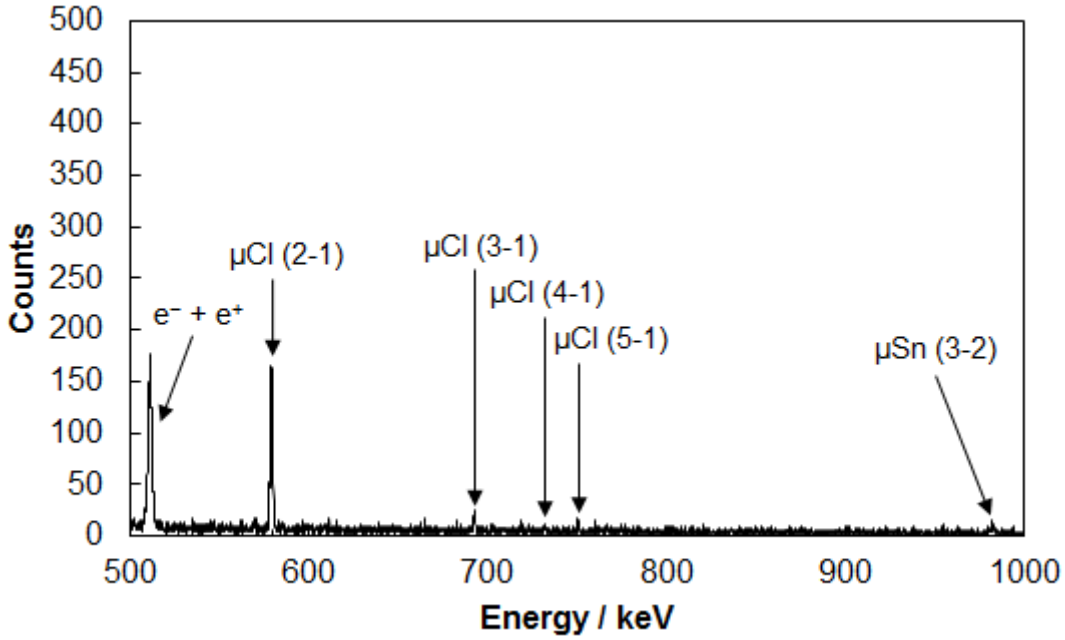

Fig. 3-27 X-ray spectrum of C_6H_6+CCl_4 (15%) sample (500–1000 keV).

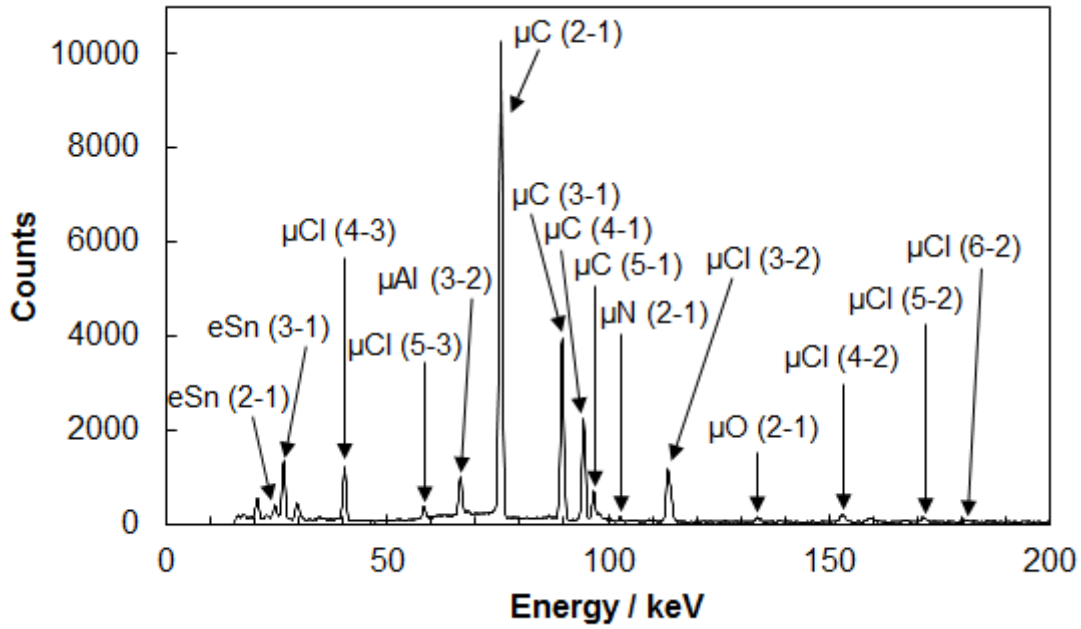

Fig. 3-28 X-ray spectrum of C_6H_{12}+CCl_4 (15%) sample (0–200 keV).

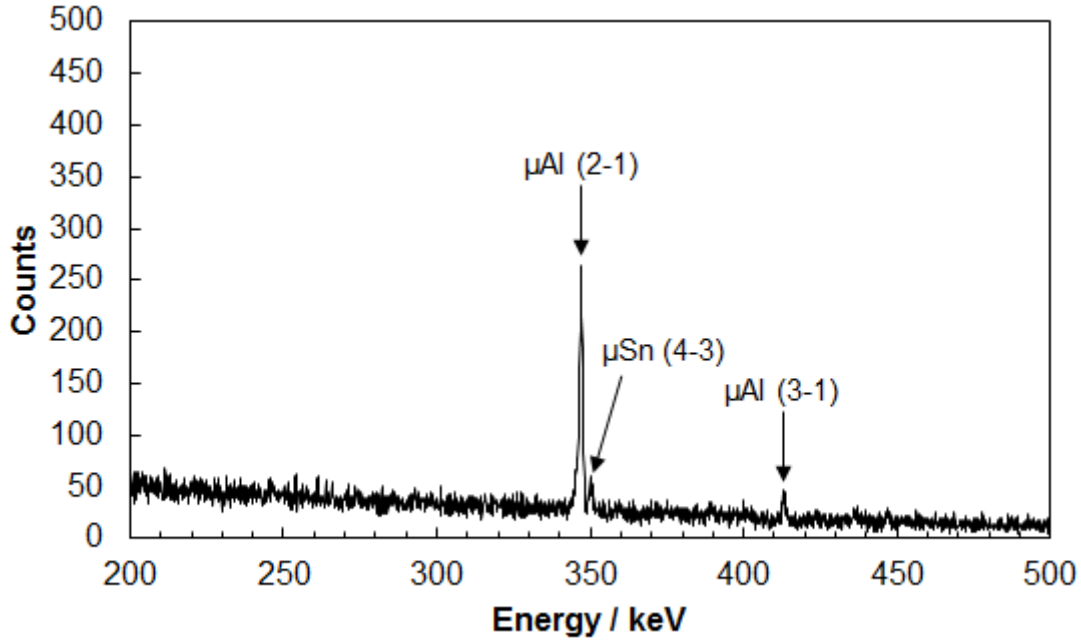

Fig. 3-29 X-ray spectrum of C_6H_{12}+CCl_4 (15%) sample (200–500 keV).

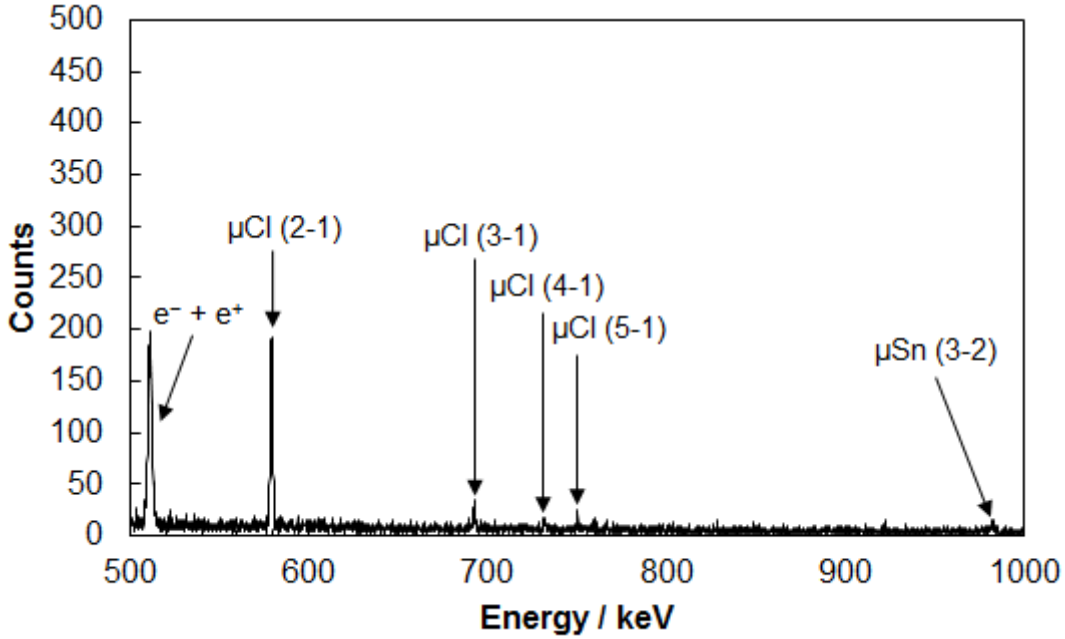

Fig. 3-30 X-ray spectrum of C_6H_{12}+CCl_4 (15%) sample (500–1000 keV).

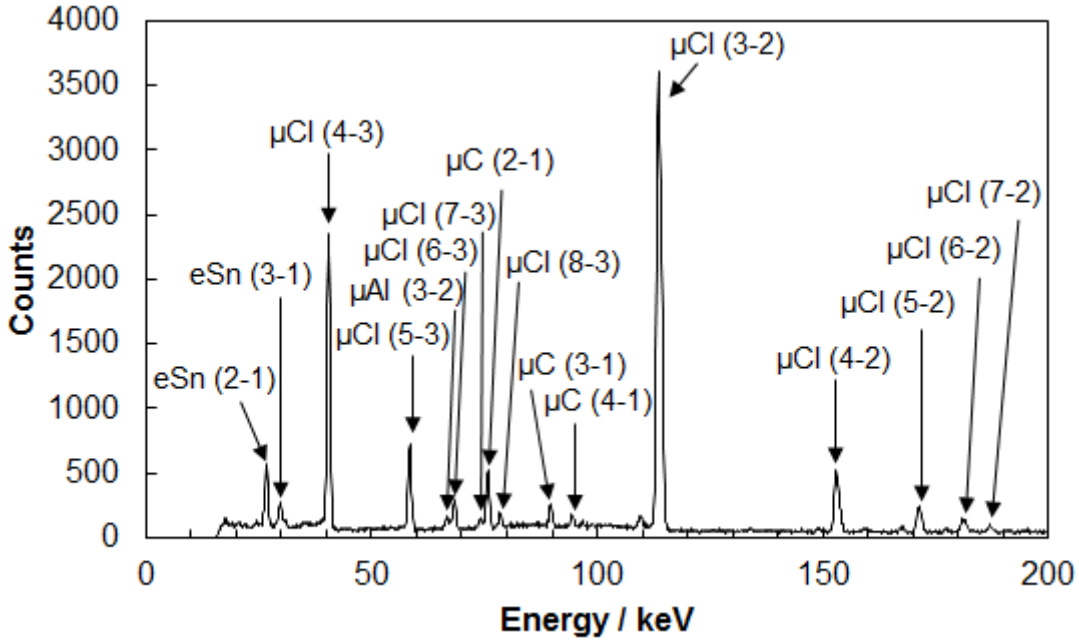

Fig. 3-31 X-ray spectrum of CCl_4 sample (0–200 keV).

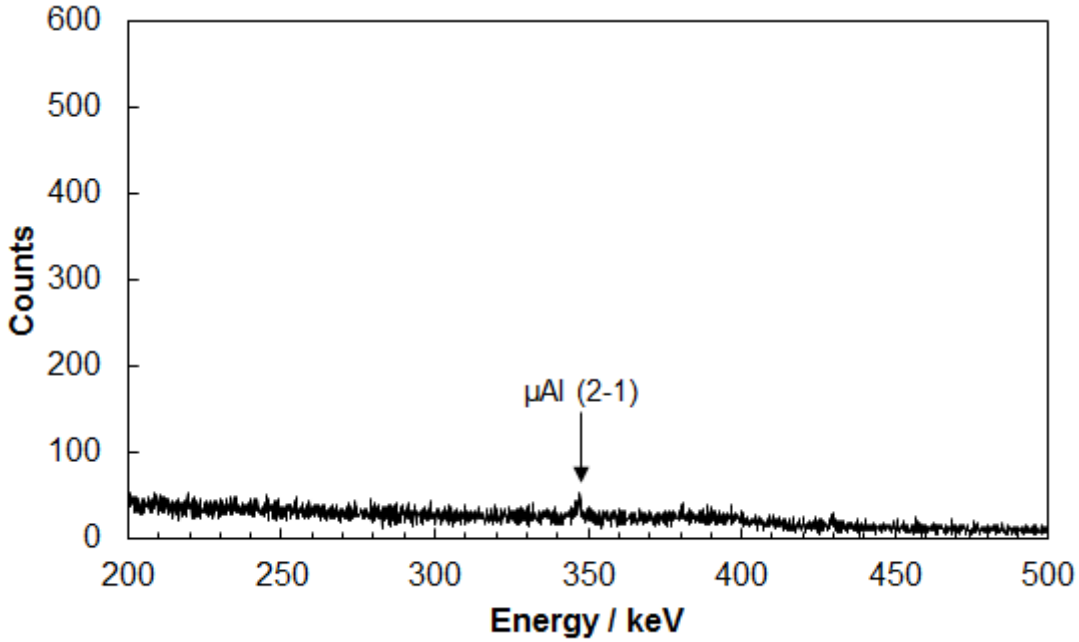

Fig. 3-32 X-ray spectrum of CCl_4 sample (200–500 keV).

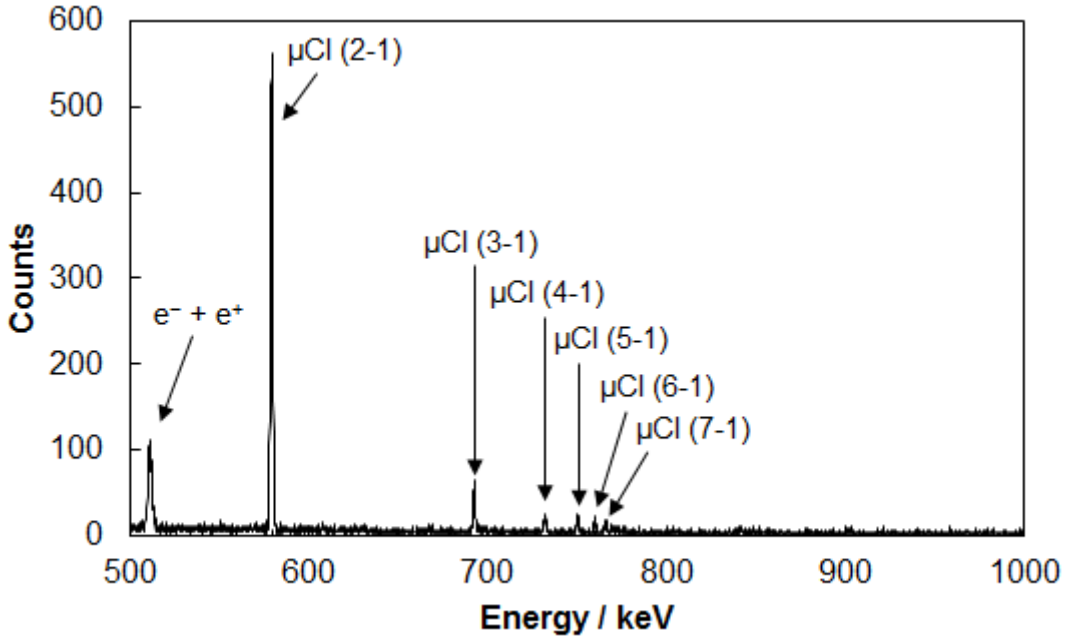

Fig. 3-33 X-ray spectrum of CCl_4 sample (500–1000 keV).

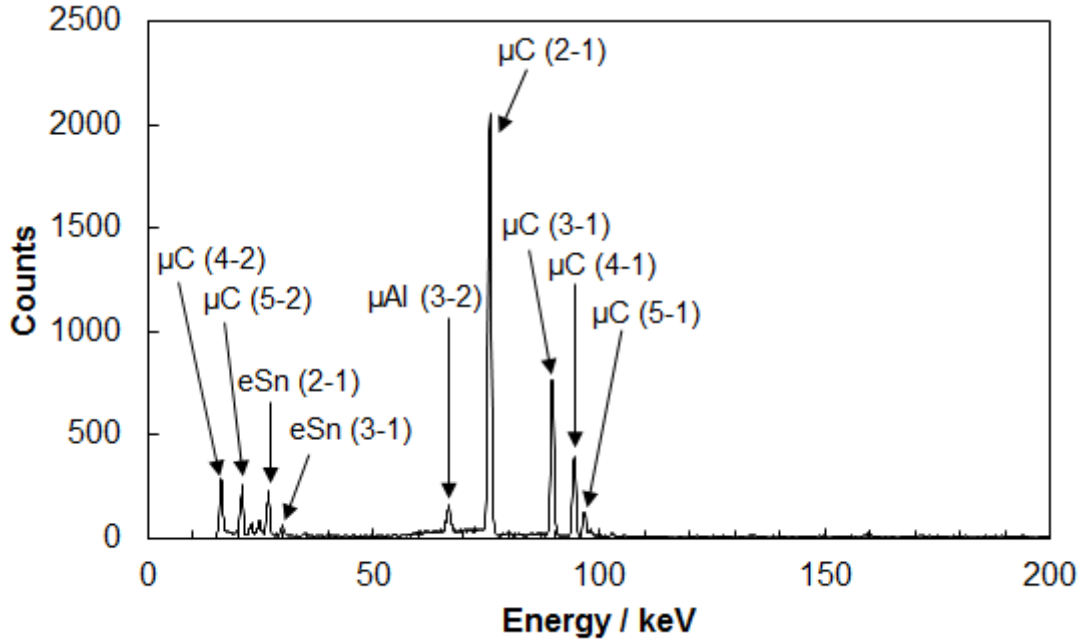

Fig. 3-34 X-ray spectrum of C_6H_6 sample (0–200 keV).

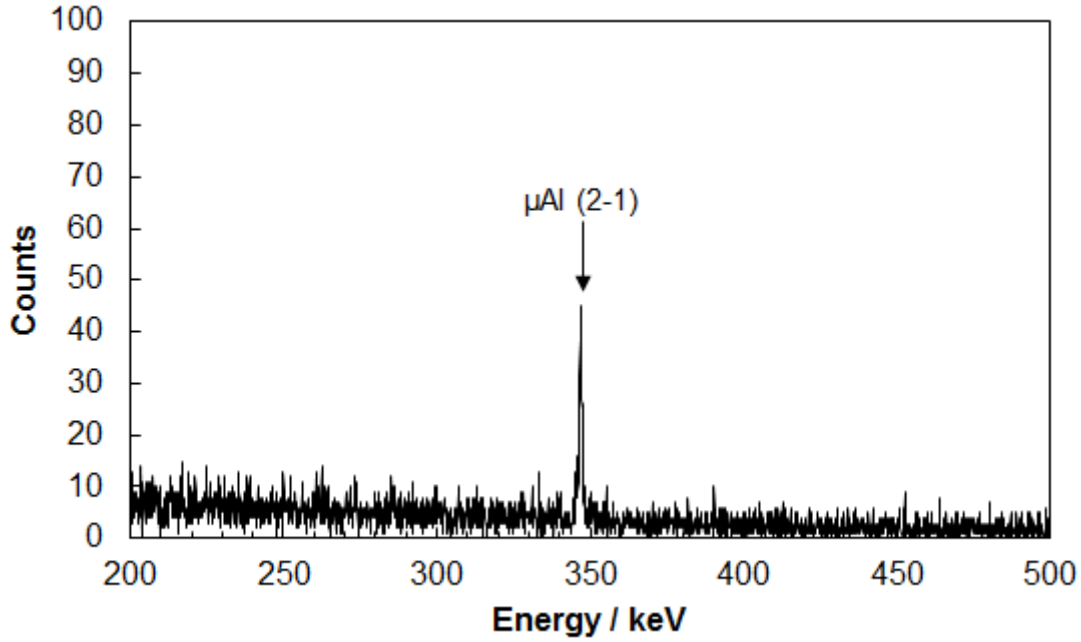

Fig. 3-35 X-ray spectrum of C_6H_6 sample (200–500 keV).

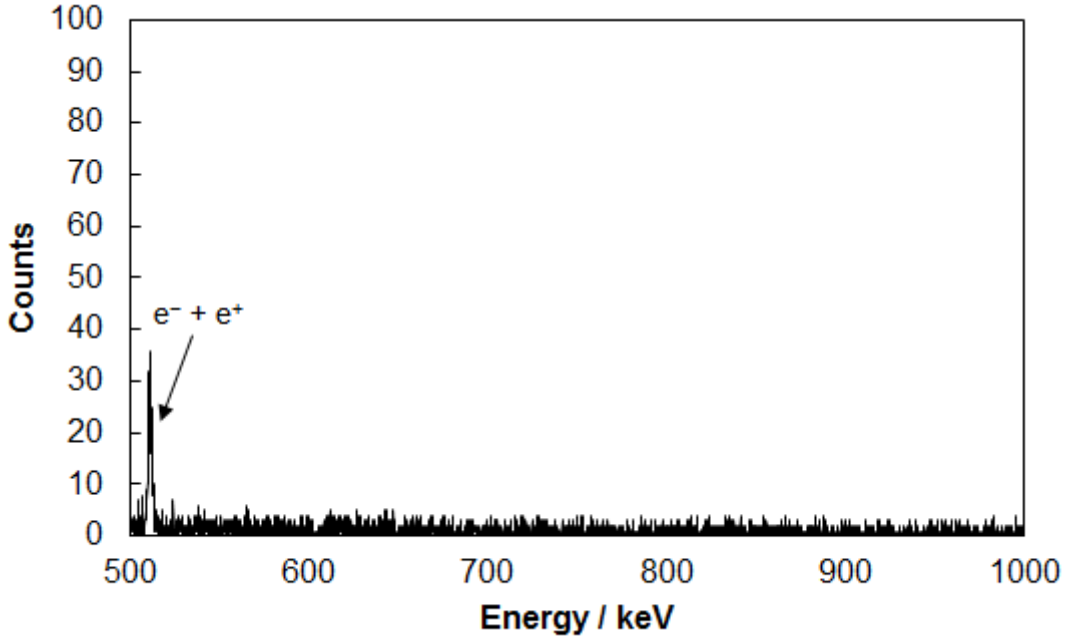

Fig. 3-36 X-ray spectrum of C_6H_6 sample (500–1000 keV).

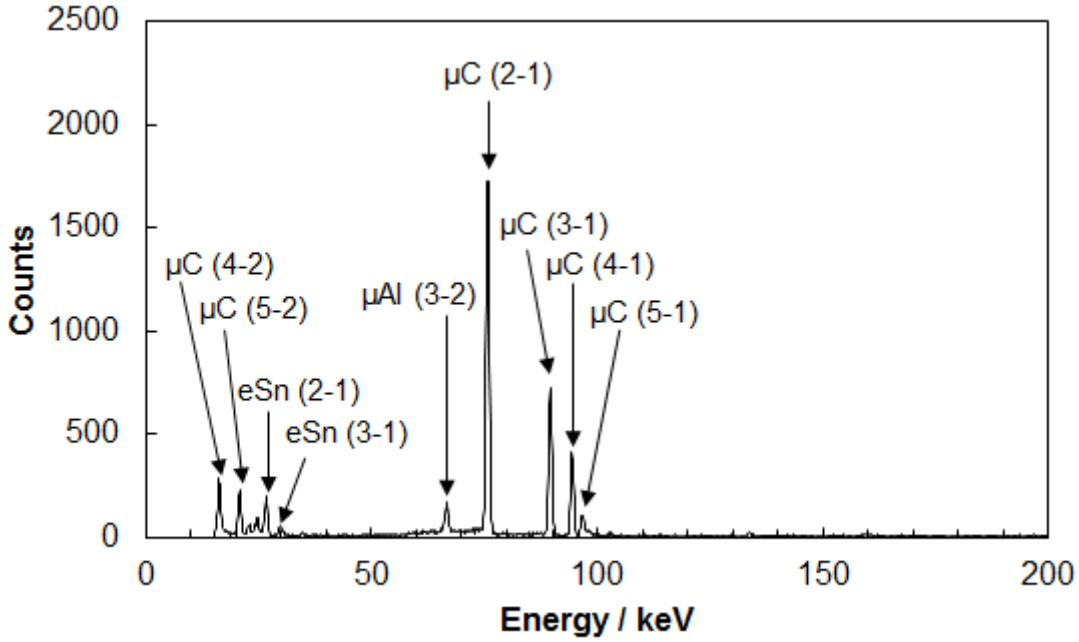

Fig. 3-37 X-ray spectrum of C_6H_{12} sample (0–200 keV).

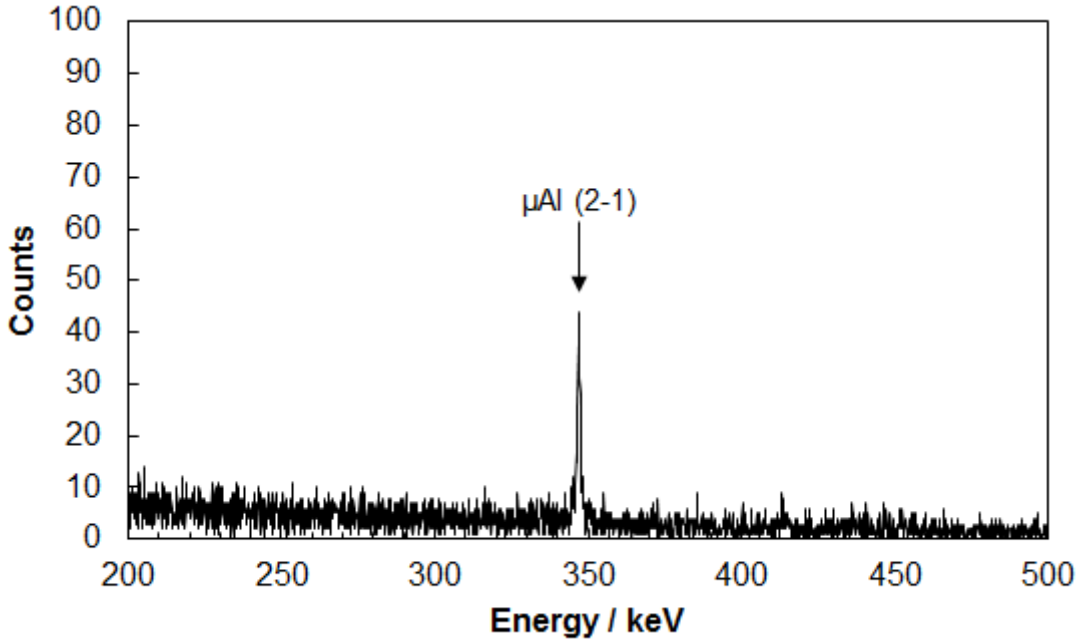

Fig. 3-38 X-ray spectrum of C_6H_{12} sample (200–500 keV).

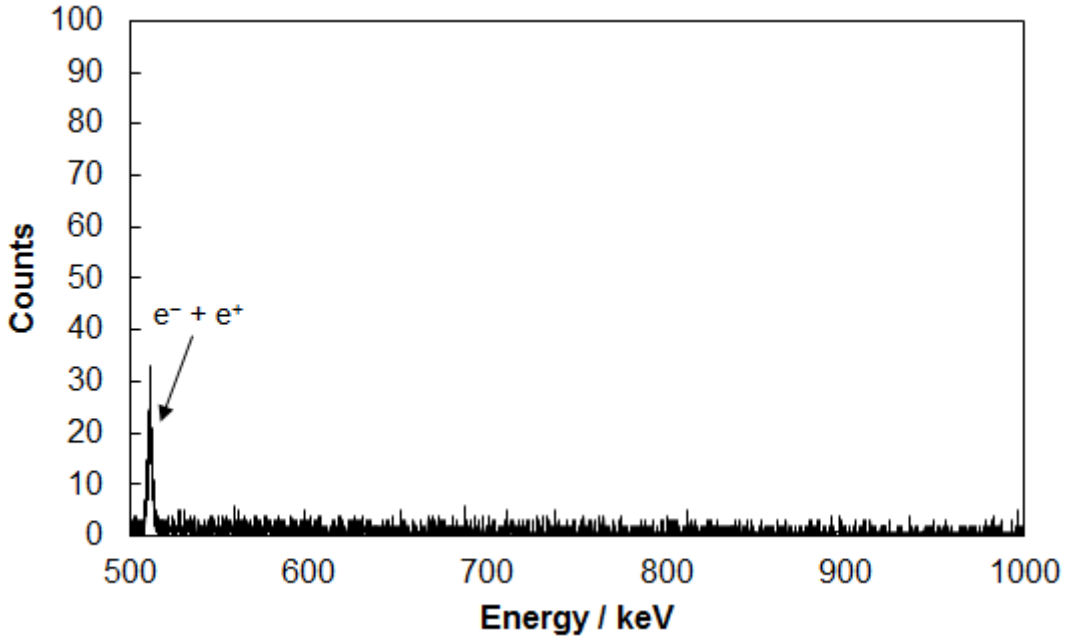

Fig. 3-39 X-ray spectrum of C_6H_{12} sample (500–1000 keV).

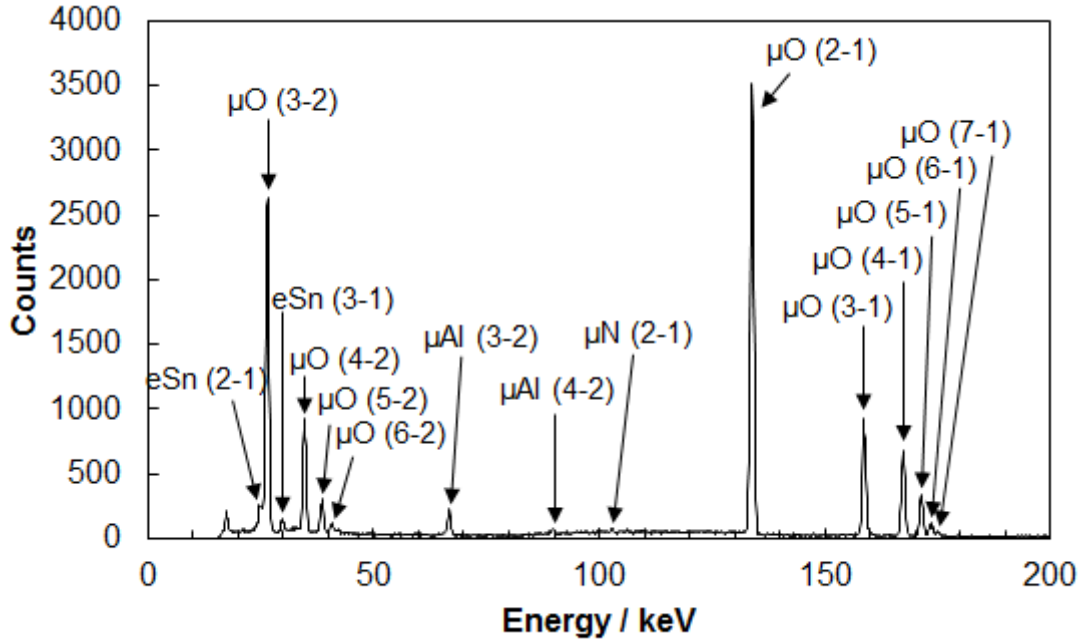

Fig. 3-40 X-ray spectrum of H_2O sample (0–200 keV).

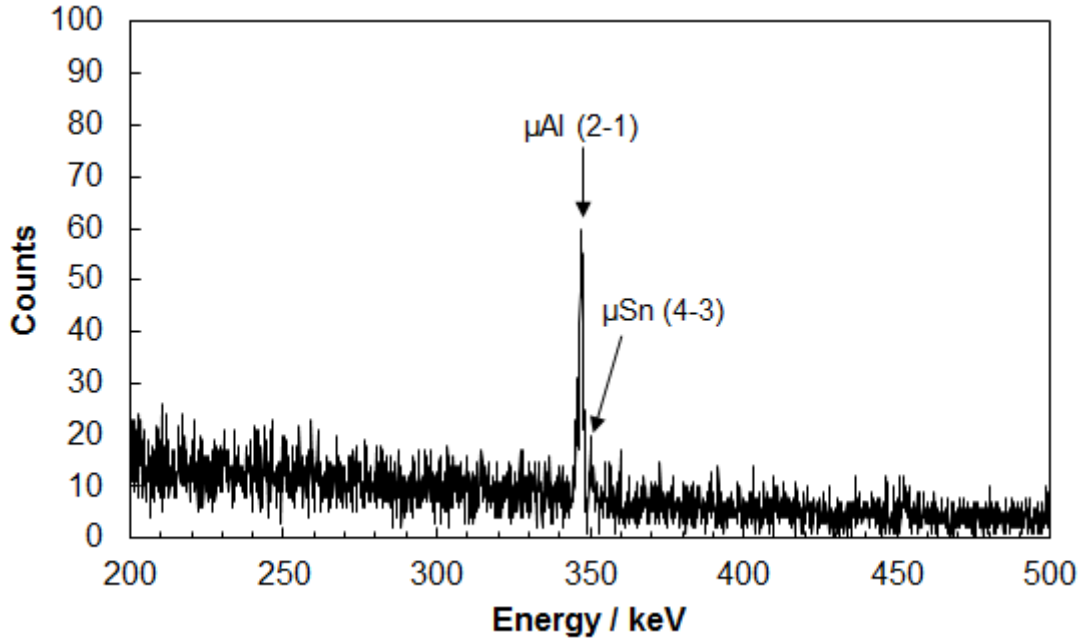

Fig. 3-41 X-ray spectrum of H_2O sample (200–500 keV).

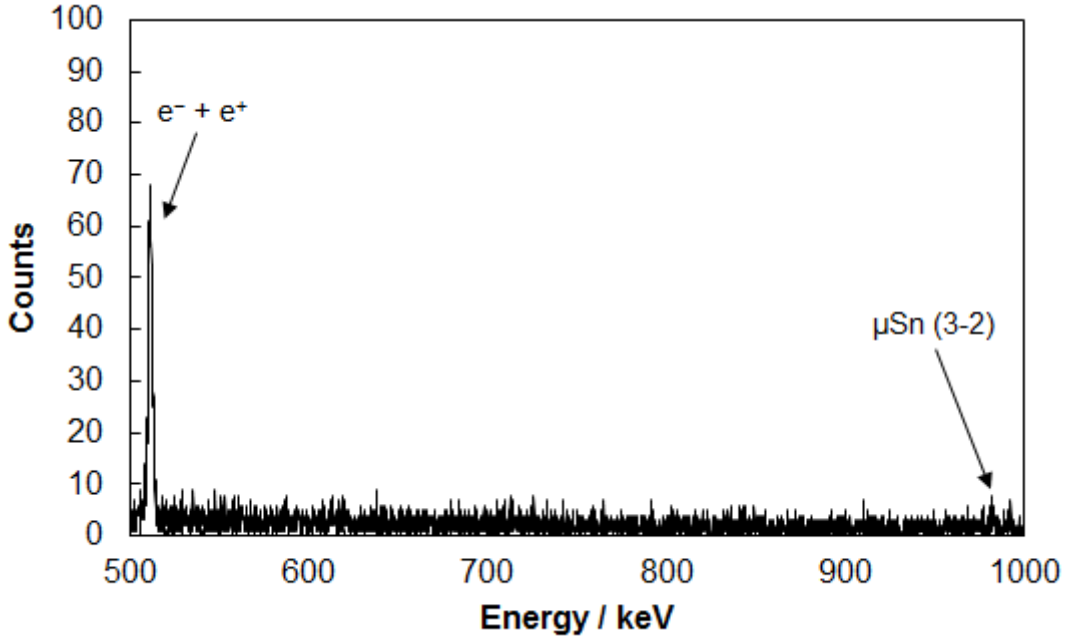

Fig. 3-42 X-ray spectrum of H_2O sample (500–1000 keV).

3.2.2. X-ray Intensity of Each Peak

For each sample, the X-ray intensities of the carbon Lyman series, chlorine Lyman series, aluminum Balmer series were determined. By using the intensity ratio of μAl (3-2) and μAl (4-2) in the H_2O sample not containing carbon atoms, the intensities of μC (3-1) in other samples were corrected.

$$\mu\mathrm{C}\ \ (3-1)_{\mathrm{corr.}} = \mu\mathrm{C}\ \ (3-1) - \mu\mathrm{Al}\ (3\text{-}2) \times \frac{\mu\mathrm{Al}\ (4\text{-}2)\ \ (\mathrm{H_2O}\ \ \mathrm{sample})}{\mu\mathrm{Al}\ (3\text{-}2)\ \ (\mathrm{H_2O}\ \ \mathrm{sample})}$$

The analysis results are shown in Table 3-15 to Table 3-24.

Table 3-15 Muonic X-ray intensities in C_6H_6+CCl_4 (70%) sample.

	Emission rate / s^{-1}	
	Ge-T	**Ge-B**
μC (2-1)	185.2 ± 6.2	148.6 ± 6.7
μC (3-1)	65.4 ± 2.6	55.6 ± 4.1
μC (3-1) corr.	62.6 ± 2.6	51.5 ± 4.2
μC (4-1)	36.9 ± 1.8	29.3 ± 16.7
μC (5-1)	10.8 ± 1.9	10.4 ± 5.0
sum μC Lyman	295.5 ± 7.2	239.7 ± 19.1
μCl (2-1)	566.0 ± 20.2	460.2 ± 15.0
μCl (3-1)	57.2 ± 4.9	49.1 ± 2.8
μCl (4-1)	24.3 ± 3.3	19.5 ± 1.9
μCl (5-1)	25.5 ± 3.7	19.3 ± 2.0
μCl (6-1)	22.2 ± 3.5	16.9 ± 1.9
μCl (7-1)	13.3 ± 2.8	8.7 ± 1.6
sum μCl Lyman	708.4 ± 21.9	573.7 ± 15.7
μAl (3-2)	14.3 ± 1.3	11.8 ± 1.4
μAl (4-2) calc.	2.8 ± 0.3	4.1 ± 0.5

Table 3-16 Muonic X-ray intensities in C_6H_{12}+CCl_4 (70%) sample.

	Emission rate / s^{-1}	
	Ge-T	**Ge-B**
μC (2-1)	188.6 ± 6.3	150.2 ± 6.3
μC (3-1)	67.9 ± 2.7	57.6 ± 5.5
μC (3-1) corr.	64.7 ± 2.7	52.7 ± 5.5
μC (4-1)	39.0 ± 1.8	29.9 ± 4.3
μC (5-1)	13.6 ± 1.7	24.7 ± 18.9
sum μC Lyman	305.9 ± 7.3	257.4 ± 21.1
μCl (2-1)	530.4 ± 19.1	427.3 ± 14.1
μCl (3-1)	56.5 ± 4.8	47.0 ± 2.8
μCl (4-1)	24.8 ± 3.6	19.0 ± 1.8
μCl (5-1)	20.8 ± 3.3	18.6 ± 1.9
μCl (6-1)	21.0 ± 3.2	17.4 ± 1.9
μCl (7-1)	8.6 ± 2.8	9.5 ± 1.6
sum μCl Lyman	662.2 ± 20.7	538.9 ± 14.8
μAl (3-2)	16.8 ± 1.3	14.3 ± 1.9
μAl (4-2) calc.	3.3 ± 0.3	4.9 ± 0.7

Table 3-17 Muonic X-ray intensities in C_6H_6+CCl_4 (30%) sample.

	Emission rate / s^{-1}	
	Ge-T	**Ge-B**
μC (2-1)	350.5 ± 10.8	298.5 ± 9.9
μC (3-1)	128.5 ± 4.2	109.7 ± 4.9
μC (3-1) corr.	123.1 ± 4.3	102.7 ± 5.0
μC (4-1)	70.5 ± 2.5	57.4 ± 16.4
μC (5-1)	21.4 ± 1.5	25.7 ± 7.5
sum μC Lyman	565.4 ± 12.0	484.3 ± 21.2
μCl (2-1)	226.8 ± 8.8	191.0 ± 6.5
μCl (3-1)	28.2 ± 2.7	22.6 ± 1.5
μCl (4-1)	11.9 ± 2.1	10.8 ± 1.2
μCl (5-1)	10.5 ± 2.0	8.8 ± 1.1
μCl (6-1)	10.9 ± 2.1	6.9 ± 1.0
μCl (7-1)	4.1 ± 1.8	4.1 ± 1.0
sum μCl Lyman	292.4 ± 10.0	244.2 ± 7.0
μAl (3-2)	27.8 ± 1.4	20.3 ± 1.7
μAl (4-2) calc.	5.4 ± 0.3	7.0 ± 0.7

Table 3-18 Muonic X-ray intensities in C_6H_{12}+CCl_4 (30%) sample.

	Emission rate / s^{-1}	
	Ge-T	**Ge-B**
μC (2-1)	356.4 ± 11.0	308.0 ± 10.2
μC (3-1)	137.0 ± 4.4	116.7 ± 4.6
μC (3-1) corr.	132.1 ± 4.5	109.5 ± 4.7
μC (4-1)	79.8 ± 2.7	62.5 ± 26.4
μC (5-1)	22.1 ± 1.3	28.5 ± 10.8
sum μC Lyman	590.5 ± 12.2	508.5 ± 30.6
μCl (2-1)	213.1 ± 8.2	171.8 ± 5.8
μCl (3-1)	24.4 ± 2.5	19.2 ± 1.3
μCl (4-1)	10.4 ± 1.8	9.9 ± 1.1
μCl (5-1)	11.5 ± 2.0	8.9 ± 1.1
μCl (6-1)	9.8 ± 2.0	10.6 ± 1.2
μCl (7-1)	5.1 ± 1.5	4.4 ± 0.9
sum μCl Lyman	274.3 ± 9.3	224.9 ± 6.4
μAl (3-2)	25.2 ± 1.2	20.8 ± 1.9
μAl (4-2) calc.	4.9 ± 0.2	7.2 ± 0.7

Table 3-19 Muonic X-ray intensities in C_6H_6+CCl_4 (15%) sample.

	Emission rate / s^{-1}	
	Ge-T	**Ge-B**
μC (2-1)	432.9 ± 13.3	370.5 ± 12.2
μC (3-1)	159.7 ± 5.1	137.3 ± 6.9
μC (3-1) corr.	154.4 ± 5.2	129.7 ± 7.0
μC (4-1)	86.8 ± 2.9	73.2 ± 38.2
μC (5-1)	26.2 ± 1.5	30.2 ± 14.8
sum μC Lyman	700.3 ± 14.6	603.6 ± 43.3
μCl (2-1)	117.4 ± 5.3	98.0 ± 3.7
μCl (3-1)	13.1 ± 1.9	10.8 ± 1.1
μCl (4-1)	4.2 ± 1.4	5.7 ± 0.9
μCl (5-1)	8.1 ± 1.7	3.9 ± 0.8
μCl (6-1)	2.4 ± 1.3	4.0 ± 0.9
μCl (7-1)	n.d.	n.d.
sum μCl Lyman	145.2 ± 6.2	122.4 ± 4.1
μAl (3-2)	27.3 ± 1.3	22.0 ± 2.8
μAl (4-2) calc.	5.3 ± 0.3	7.6 ± 1.0

Table 3-20 Muonic X-ray intensities in C_6H_{12}+CCl_4 (15%) sample.

	Emission rate / s^{-1}	
	Ge-T	**Ge-B**
μC (2-1)	376.5 ± 11.5	331.7 ± 10.7
μC (3-1)	148.4 ± 4.7	130.6 ± 5.3
μC (3-1) corr.	142.4 ± 4.8	122.1 ± 5.5
μC (4-1)	83.2 ± 2.7	68.2 ± 9.8
μC (5-1)	23.9 ± 1.2	33.1 ± 4.7
sum μC Lyman	626.0 ± 12.8	555.2 ± 16.2
μCl (2-1)	96.8 ± 4.2	78.5 ± 2.9
μCl (3-1)	10.8 ± 1.6	10.2 ± 0.9
μCl (4-1)	5.6 ± 1.4	5.2 ± 0.8
μCl (5-1)	4.3 ± 1.2	4.7 ± 0.8
μCl (6-1)	5.3 ± 1.5	3.6 ± 0.7
μCl (7-1)	n.d.	n.d.
sum μCl Lyman	122.7 ± 5.1	102.2 ± 3.3
μAl (3-2)	31.0 ± 1.3	24.6 ± 4.0
μAl (4-2) calc.	6.0 ± 0.2	8.5 ± 1.4

Table 3-21 Muonic X-ray intensities in CCl_4 sample.

	Emission rate / s^{-1}	
	Ge-T	**Ge-B**
μC (2-1)	49.9 ± 2.3	33.9 ± 2.8
μC (3-1)	17.0 ± 1.3	14.7 ± 1.7
μC (3-1) corr.	14.4 ± 1.4	11.9 ± 1.7
μC (4-1)	9.8 ± 1.2	7.3 ± 0.9
μC (5-1)	3.1 ± 1.7	n.d.
sum μC Lyman	77.3 ± 3.4	53.1 ± 3.4
μCl (2-1)	787.0 ± 27.2	634.7 ± 20.4
μCl (3-1)	75.2 ± 5.9	64.7 ± 3.5
μCl (4-1)	33.5 ± 4.2	28.9 ± 2.4
μCl (5-1)	35.4 ± 4.2	27.1 ± 2.3
μCl (6-1)	26.2 ± 4.0	24.0 ± 2.2
μCl (7-1)	27.3 ± 5.0	13.4 ± 1.9
sum μCl Lyman	984.6 ± 29.2	792.7 ± 21.2
μAl (3-2)	13.4 ± 1.4	8.1 ± 0.7
μAl (4-2) calc.	2.6 ± 0.3	2.8 ± 0.3

Table 3-22 Muonic X-ray intensities in C_6H_6 sample.

	Emission rate / s^{-1}	
	Ge-T	**Ge-B**
μC (2-1)	448.2 ± 14.7	255.7 ± 8.4
μC (3-1)	173.0 ± 6.4	100.4 ± 3.7
μC (3-1) corr.	166.8 ± 6.5	94.2 ± 3.7
μC (4-1)	93.5 ± 3.9	53.3 ± 2.2
μC (5-1)	27.0 ± 2.4	15.5 ± 1.4
sum μC Lyman	735.6 ± 16.7	418.7 ± 9.6
μAl (3-2)	31.6 ± 2.4	18.0 ± 1.4
μAl (4-2) calc.	6.1 ± 0.5	6.2 ± 0.5

Table 3-23 Muonic X-ray intensities in C_6H_{12} sample.

	Emission rate / s^{-1}	
	Ge-T	**Ge-B**
μC (2-1)	420.6 ± 14.0	238.9 ± 7.9
μC (3-1)	174.4 ± 6.5	100.1 ± 3.7
μC (3-1) corr.	167.0 ± 6.7	92.7 ± 3.8
μC (4-1)	98.1 ± 4.2	55.9 ± 2.4
μC (5-1)	29.1 ± 2.9	16.5 ± 1.6
sum μC Lyman	714.9 ± 16.2	403.9 ± 9.3
μAl (3-2)	38.0 ± 2.6	21.7 ± 1.5
μAl (4-2) calc.	7.4 ± 0.5	7.5 ± 0.6

Table 3-24 Muonic X-ray intensities in H_2O sample.

	Emission rate / s^{-1}	
	Ge-T	**Ge-B**
μAl (3-2)	22.8 ± 1.3	13.7 ± 0.4
μAl (4-2)	4.4 ± 0.8	4.7 ± 0.1
μAl (4-2) / (3-2)	0.19 ± 0.04	0.34 ± 0.01

3.2.3. X-ray Structure

The values obtained by normalizing the X-ray intensities of each transition of carbon with the intensity of μC (2-1) and the values obtained by normalizing the X-ray intensities of each transition of chlorine with the intensity of μCl (2-1) are shown in Table 3-25 to Table 3-33 and summarized in Fig. 3-43 to Fig. 3-46. The spectra measured with the Ge-B detector are poor in resolution on the low energy side, and problems such as difficulty in separating adjacent peaks such as μCl (7-3), μC (2-1), μCl (8-3), so the error is large.

When comparing the values of μC (3-1) / (2-1) between samples, the value in the CCl_4 sample was lower than the value in the other samples. This is consistent with the fact that the CCl_4 sample does not contain hydrogen atoms and no muon transfer takes place. In other samples, the value of μC (3-1) / (2-1) tended to increase as the concentration of carbon tetrachloride was lower, although it was within the error range. This is consistent with the fact that the lower the concentration of carbon tetrachloride is, the smaller the muon transfer to the chlorine atom decreases and the muon transfer to the carbon atom increases. Comparing with the same carbon tetrachloride concentration, although it is within the error range, the value of μC (3-1) / (2-1) tended to be slightly higher in the samples of cyclohexane than in the samples of benzene. This is consistent with the fact that the total amount of muon transfer in the samples of cyclohexane are larger than that in the samples of benzene because the number of hydrogen atoms of cyclohexane molecules is larger than that of benzene molecules.

Table 3-25 Muonic carbon X-ray structure normalized by μC (2-1) intensity and muonic chlorine X-ray structure normalized by μCl (2-1) intensity C_6H_6+CCl_4 (70%) sample.

	Ge-T	Ge-B
μC (3-1) / (2-1)	0.338 ± 0.018	0.347 ± 0.032
μC (4-1) / (2-1)	0.199 ± 0.012	0.197 ± 0.113
μC (5-1) / (2-1)	0.058 ± 0.010	0.070 ± 0.034
μCl (3-1) / (2-1)	0.101 ± 0.009	0.107 ± 0.007
μCl (4-1) / (2-1)	0.043 ± 0.006	0.042 ± 0.004
μCl (5-1) / (2-1)	0.045 ± 0.007	0.042 ± 0.004
μCl (6-1) / (2-1)	0.039 ± 0.006	0.037 ± 0.004
μCl (7-1) / (2-1)	0.023 ± 0.005	0.019 ± 0.004

Table 3-26 Muonic carbon X-ray structure normalized by μC (2-1) intensity and muonic chlorine X-ray structure normalized by μCl (2-1) intensity C_6H_{12}+CCl_4 (70%) sample.

	Ge-T	Ge-B
μC (3-1) / (2-1)	0.343 ± 0.018	0.351 ± 0.040
μC (4-1) / (2-1)	0.207 ± 0.012	0.199 ± 0.030
μC (5-1) / (2-1)	0.072 ± 0.009	0.164 ± 0.126
μCl (3-1) / (2-1)	0.106 ± 0.010	0.110 ± 0.007
μCl (4-1) / (2-1)	0.047 ± 0.007	0.044 ± 0.005
μCl (5-1) / (2-1)	0.039 ± 0.006	0.044 ± 0.005
μCl (6-1) / (2-1)	0.040 ± 0.006	0.041 ± 0.005
μCl (7-1) / (2-1)	0.016 ± 0.005	0.022 ± 0.004

Table 3-27 Muonic carbon X-ray structure normalized by μC (2-1) intensity and muonic chlorine X-ray structure normalized by μCl (2-1) intensity C_6H_6+CCl_4 (30%) sample.

	Ge-T	Ge-B
μC (3-1) / (2-1)	0.351 ± 0.016	0.344 ± 0.020
μC (4-1) / (2-1)	0.201 ± 0.009	0.192 ± 0.055
μC (5-1) / (2-1)	0.061 ± 0.005	0.086 ± 0.025
μCl (3-1) / (2-1)	0.124 ± 0.013	0.118 ± 0.009
μCl (4-1) / (2-1)	0.053 ± 0.009	0.057 ± 0.007
μCl (5-1) / (2-1)	0.046 ± 0.009	0.046 ± 0.006
μCl (6-1) / (2-1)	0.048 ± 0.010	0.036 ± 0.005
μCl (7-1) / (2-1)	0.018 ± 0.008	0.022 ± 0.005

Table 3-28 Muonic carbon X-ray structure normalized by μC (2-1) intensity and muonic chlorine X-ray structure normalized by μCl (2-1) intensity C_6H_{12}+CCl_4 (30%) sample.

	Ge-T	Ge-B
μC (3-1) / (2-1)	0.371 ± 0.017	0.356 ± 0.019
μC (4-1) / (2-1)	0.224 ± 0.010	0.203 ± 0.086
μC (5-1) / (2-1)	0.062 ± 0.004	0.093 ± 0.035
μCl (3-1) / (2-1)	0.114 ± 0.012	0.112 ± 0.009
μCl (4-1) / (2-1)	0.049 ± 0.009	0.058 ± 0.007
μCl (5-1) / (2-1)	0.054 ± 0.009	0.052 ± 0.006
μCl (6-1) / (2-1)	0.046 ± 0.010	0.061 ± 0.007
μCl (7-1) / (2-1)	0.024 ± 0.007	0.026 ± 0.005

Table 3-29 Muonic carbon X-ray structure normalized by μC (2-1) intensity and muonic chlorine X-ray structure normalized by μCl (2-1) intensity C_6H_6+CCl_4 (15%) sample.

	Ge-T	Ge-B
μC (3-1) / (2-1)	0.357 ± 0.016	0.350 ± 0.022
μC (4-1) / (2-1)	0.200 ± 0.009	0.197 ± 0.103
μC (5-1) / (2-1)	0.061 ± 0.004	0.081 ± 0.040
μCl (3-1) / (2-1)	0.111 ± 0.017	0.110 ± 0.012
μCl (4-1) / (2-1)	0.036 ± 0.012	0.058 ± 0.009
μCl (5-1) / (2-1)	0.069 ± 0.015	0.040 ± 0.009
μCl (6-1) / (2-1)	0.021 ± 0.011	0.041 ± 0.010
μCl (7-1) / (2-1)	—	—

Table 3-30 Muonic carbon X-ray structure normalized by μC (2-1) intensity and muonic chlorine X-ray structure normalized by μCl (2-1) intensity C_6H_{12}+CCl_4 (15%) sample.

	Ge-T	Ge-B
μC (3-1) / (2-1)	0.378 ± 0.017	0.368 ± 0.020
μC (4-1) / (2-1)	0.221 ± 0.010	0.206 ± 0.030
μC (5-1) / (2-1)	0.063 ± 0.004	0.100 ± 0.014
μCl (3-1) / (2-1)	0.112 ± 0.017	0.130 ± 0.013
μCl (4-1) / (2-1)	0.057 ± 0.014	0.066 ± 0.010
μCl (5-1) / (2-1)	0.044 ± 0.012	0.060 ± 0.010
μCl (6-1) / (2-1)	0.055 ± 0.015	0.046 ± 0.009
μCl (7-1) / (2-1)	—	—

Table 3-31 Muonic carbon X-ray structure normalized by μC (2-1) intensity and muonic chlorine X-ray structure normalized by μCl (2-1) intensity CCl_4 sample.

	Ge-T	Ge-B
μC (3-1) / (2-1)	0.289 ± 0.032	0.351 ± 0.058
μC (4-1) / (2-1)	0.197 ± 0.026	0.214 ± 0.032
μC (5-1) / (2-1)	0.061 ± 0.034	—
μCl (3-1) / (2-1)	0.095 ± 0.008	0.102 ± 0.006
μCl (4-1) / (2-1)	0.043 ± 0.006	0.046 ± 0.004
μCl (5-1) / (2-1)	0.045 ± 0.006	0.043 ± 0.004
μCl (6-1) / (2-1)	0.033 ± 0.005	0.038 ± 0.004
μCl (7-1) / (2-1)	0.035 ± 0.006	0.021 ± 0.003

Table 3-32 Muonic carbon X-ray structure normalized by μC (2-1) intensity and muonic chlorine X-ray structure normalized by μCl (2-1) intensity C_6H_6 sample.

	Ge-T	Ge-B
μC (3-1) / (2-1)	0.372 ± 0.019	0.368 ± 0.019
μC (4-1) / (2-1)	0.209 ± 0.011	0.208 ± 0.011
μC (5-1) / (2-1)	0.060 ± 0.006	0.060 ± 0.006

Table 3-33 Muonic carbon X-ray structure normalized by μC (2-1) intensity and muonic chlorine X-ray structure normalized by μCl (2-1) intensity C_6H_{12} sample.

	Ge-T	Ge-B
μC (3-1) / (2-1)	0.397 ± 0.021	0.388 ± 0.020
μC (4-1) / (2-1)	0.233 ± 0.013	0.234 ± 0.013
μC (5-1) / (2-1)	0.069 ± 0.007	0.069 ± 0.007

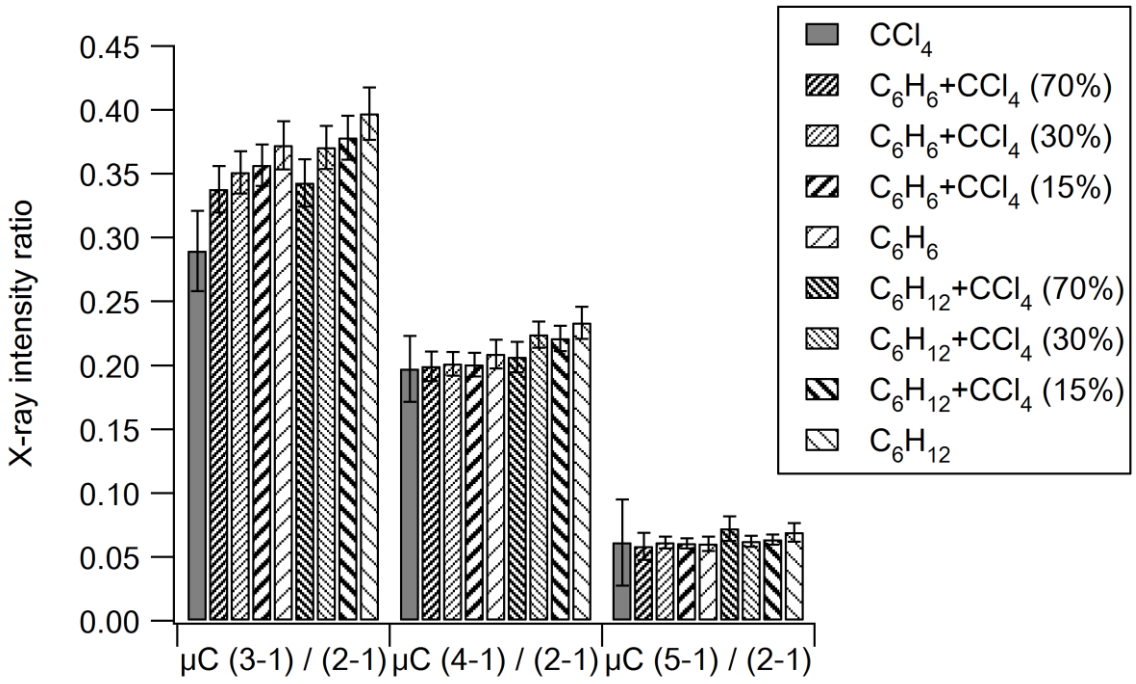

Fig. 3-43 Muonic carbon X-ray structure normalized by μC (2-1) intensity measured by Ge-T detector.

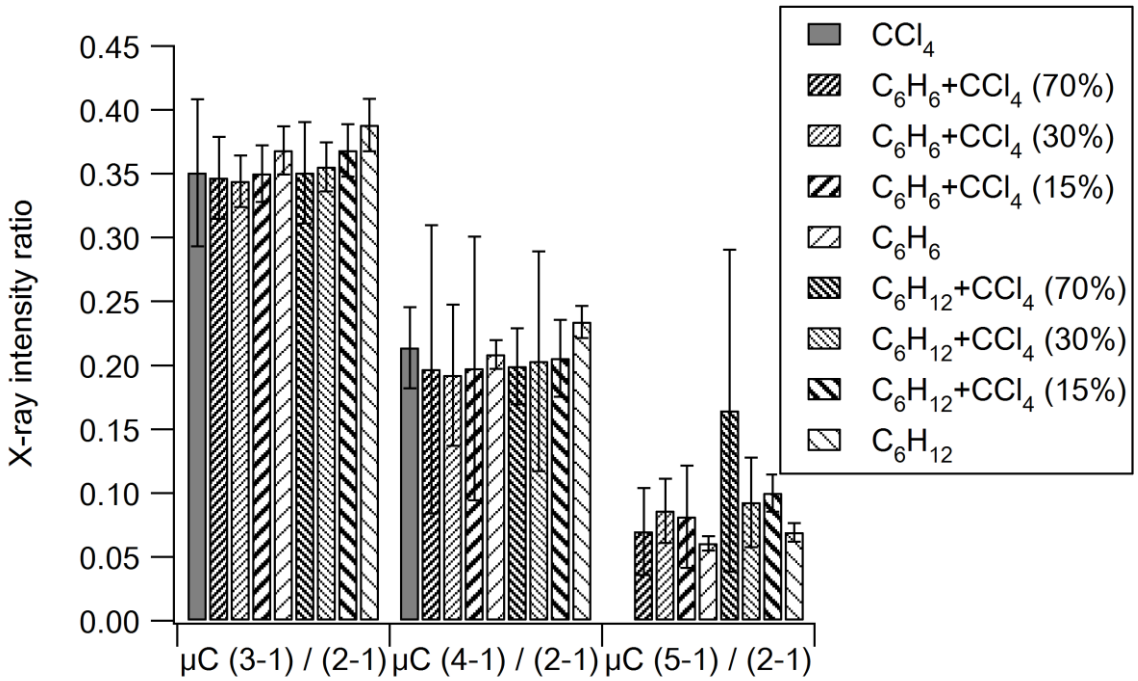

Fig. 3-44 Muonic carbon X-ray structure normalized by μC (2-1) intensity measured by Ge-B detector.

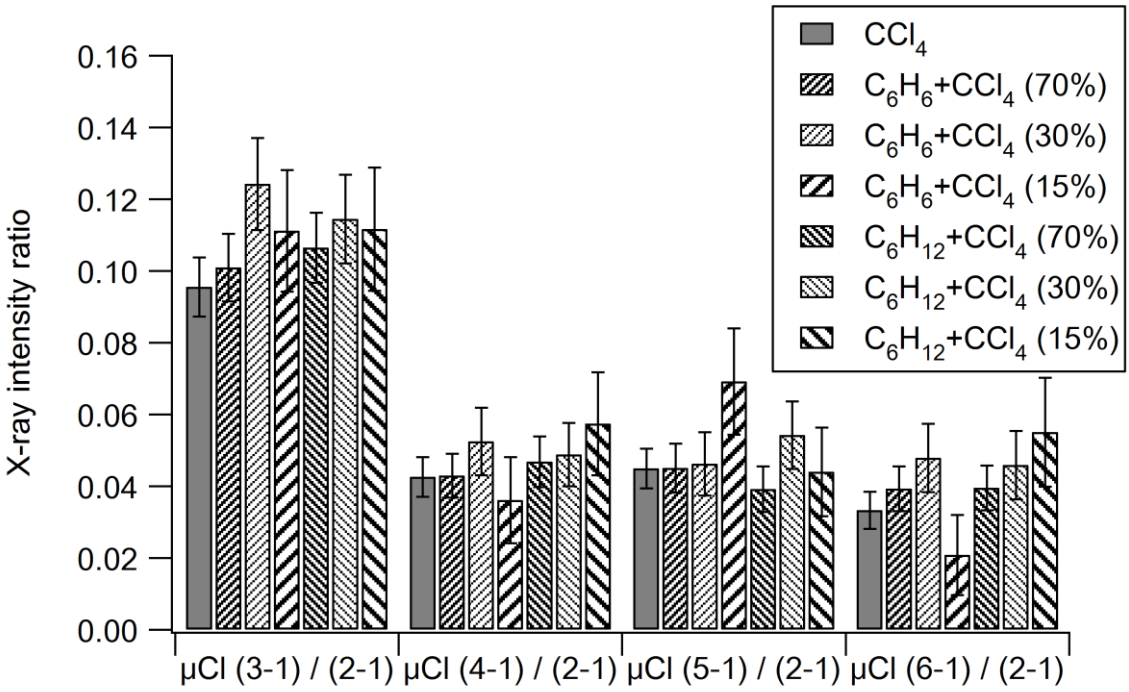

Fig. 3-45 Muonic chlorine X-ray structure normalized by μCl (2-1) intensity measured by Ge-T detector.

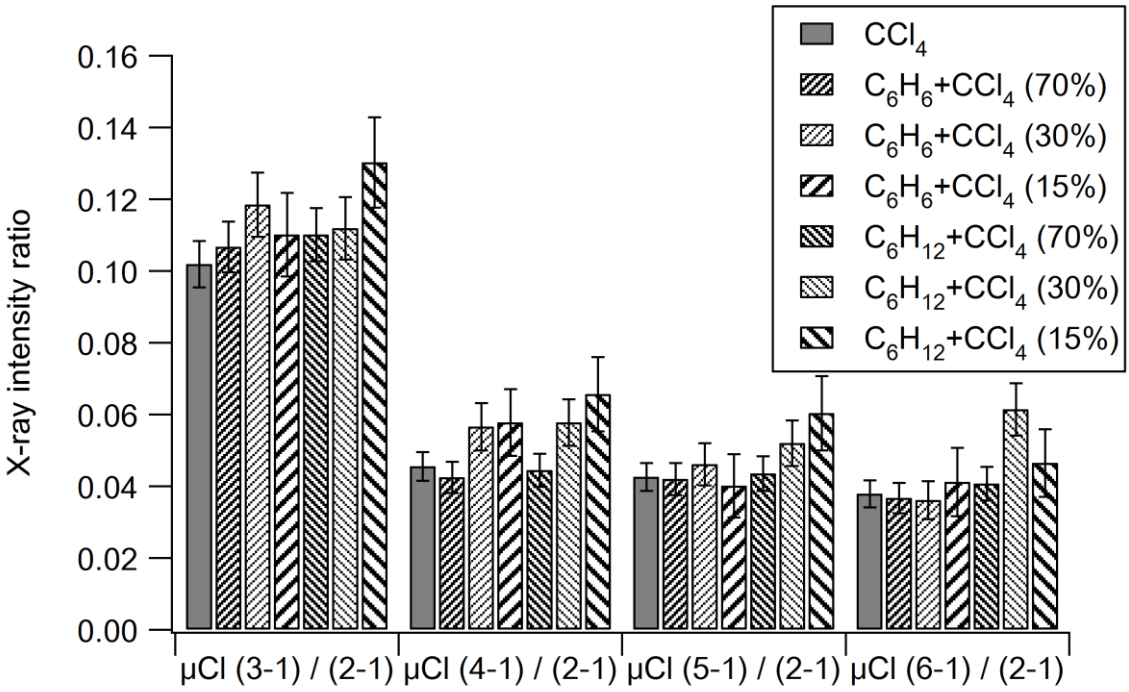

Fig. 3-46 Muonic chlorine X-ray structure normalized by μCl (2-1) intensity measured by Ge-B detector.

3.2.4. X-ray Intensity Ratio

The ratios of the X-ray intensity of the carbon Lyman series to the X-ray intensity of the chlorine Lyman series are shown in Table 3-34. These corresponds the ratio of the number of muon captures to carbon atoms to the number of muon captures to chlorine atoms in each sample. When comparing the samples with the same carbon tetrachloride concentration, the values of the samples of cyclohexane were larger at all concentrations than the values of the samples of benzene samples.

Table 3-34 Muonic X-ray intensity ratio of carbon to chlorine.

	μC Lyman / μCl Lyman		
	Ge-T	**Ge-B**	**Average**
C_6H_6+CCl_4 (70%) sample	0.417 ± 0.016	0.418 ± 0.035	0.417 ± 0.015
C_6H_{12}+CCl_4 (70%) sample	0.462 ± 0.018	0.478 ± 0.041	0.465 ± 0.017
C_6H_6+CCl_4 (30%) sample	1.93 ± 0.08	1.98 ± 0.10	1.95 ± 0.062
C_6H_{12}+CCl_4 (30%) sample	2.15 ± 0.09	2.26 ± 0.15	2.18 ± 0.074
C_6H_6+CCl_4 (15%) sample	4.82 ± 0.23	4.93 ± 0.39	4.85 ± 0.197
C_6H_{12}+CCl_4 (15%) sample	5.10 ± 0.24	5.43 ± 0.24	5.27 ± 0.167
CCl_4 sample	0.078 ± 0.004	0.067 ± 0.005	0.073 ± 0.003

4. Discussion

4.1. Discussion I: Experiment of Gas System

4.1.1. Muon Transfer Rate

Since the X-ray of the delayed spectrum is derived from the muon transfer, the intensity of the muonic X-ray in the delayed spectrum is proportional to the number of muon captures due to the muon transfer. And the number of muon captures due to muon transfer is proportional to the muon transfer rate and mixing ratio. Therefore, the ratio of the X-ray intensity of carbon to the X-ray intensity of neon corresponds to the ratio of the muon transfer rate to carbon to the muon transfer rate to neon, except for the contribution of the mixing ratio. Since the neon mixing ratios and the muon transfer rates to neon in two samples are the same, the muon transfer rate to carbon can be compared between samples by the ratio of the X-ray intensity of carbon to the X-ray intensity of neon.

Table 4-1 shows the X-ray intensity ratios in the Benzene sample and Cyclohexane sample, and the ratio of the value of Benzene sample to the value of Cyclohexane sample. The values shown in the table are the average values of LEPS and Loax detectors. As shown in the table, the difference in the X-ray intensity ratios between Benzene sample and Cyclohexane sample was within the error range regardless of the X-ray series of neon. That is, the difference in the muon transfer rate between Benzene sample and Cyclohexane sample was within the error range in the precision of this experiment. It is concluded that the large difference in the muon transfer rate as seen in the pion transfer of liquid system was not appeared in the gas system.

Table 4-1 Muonic X-ray intensity ratio of carbon to neon in delayed spectrum of Benzene sample and Cyclohexane sample.

	Benzene sample	**Cyclohexane sample**	**Benzene / Cyclohexane**
μC HC / μNe Balmer	6.4 ± 0.7	5.7 ± 0.5	1.11 ± 0.16
μC HC / μNe Lyman	8.0 ± 1.3	8.8 ± 1.6	0.90 ± 0.22
μC HC / μNe All	3.5 ± 0.4	3.5 ± 0.3	1.02 ± 0.14

4.2. Discussion II: Experiment of Liquid System

4.2.1. Muon Capture Ratio

When the muon is captured by atoms, it finally de-excites to the 1s orbital. Therefore, the sum of the X-ray intensities of the Lyman series, which is the series leading to the 1s orbital, is proportional to the number of captured in each element. As a result, the ratio of the X-ray intensity of the Lyman series of carbon and chlorine corresponds the ratio of the number of muon captures to carbon atoms and chlorine atoms. The results show that the values of samples of cyclohexane were larger at all carbon tetrachloride concentrations than the values of samples of benzene. This indicates that the muon is more likely to be captured on the carbon atom of cyclohexane than the carbon atom of benzene. However, since this value is the sum of muon direct capture and capture by muon transfer, it is necessary to analyze in order to obtain information on the muon transfer rate.

4.2.2. Analysis of Muon Transfer Rate using the Model

4.2.2.1. Model Overview

To analyze the muon transfer rate from the capture ratio results, the following model was set up. Considering two steps in which the muon is first captured by the molecule and then captured by each atom in the molecule, the capture probability to carbon atoms and chlorine atoms (W_C and W_{Cl}, respectively) are expressed as follows.

$$\mathrm{W_C} = W'_C + W'_H \times P_{ex} \times \frac{\Lambda_C C_C}{\Lambda_C C_C + \Lambda_{Cl} C_{Cl}} + W'_H \times (1 - P_{ex})$$

$$\mathrm{W_{Cl}} = W'_{Cl} + W'_H \times P_{ex} \times \frac{\Lambda_{Cl} C_{Cl}}{\Lambda_C C_C + \Lambda_{Cl} C_{Cl}}$$

$$\mathrm{W'_C} = \frac{K_{HC}(1-C)}{K_{HC}(1-C) + K_{CCl4} C} \times (1 - K_H) + \frac{K_{CCl4} C}{K_{HC}(1-C) + K_{CCl4} C} \times (1 - \mathrm{K_{Cl}})$$

$$\mathrm{W'_{Cl}} = \frac{K_{CCl4} C}{K_{HC}(1-C) + K_{CCl4} C} \times \mathrm{K_{Cl}}$$

$$\mathrm{W'_H} = \frac{K_{HC}(1-C)}{K_{HC}(1-C) + K_{CCl4} C} \times K_H$$

where

K_{HC}: capture ratio to hydrocarbon molecule,

K_{CCl4}: capture ratio to carbon tetrachloride molecule,

C: number of carbon tetrachloride molecules / total number of molecules

(= concentration of carbon tetrachloride),

K_H: capture ratio to hydrogen atoms when captured by hydrocarbon molecules,

K_{Cl}: capture ratio to chlorine atom when captured by carbon tetrachloride molecule,

Λ_Z: transfer rate to Z atom,

C_Z: number of Z atoms per 1 cm^3,

P_{ex}: probability that external transfer occurs

W'_C, W'_{Cl} and W'_H are direct capture probability to each atom. The first term of W_C and W_{Cl} is contribution of direct capture, the second term of W_C and W_{Cl} is contribution of external transfer, the third term of W_C is contribution of internal transfer. Fig. 4-1 shows a scheme of the model equation. The term indicated by each number in the figure represents the probability of each step of muon capture. W_C is the sum of the probabilities of each step reaching C, and W_{Cl} is the sum of the probabilities of each step reaching Cl.

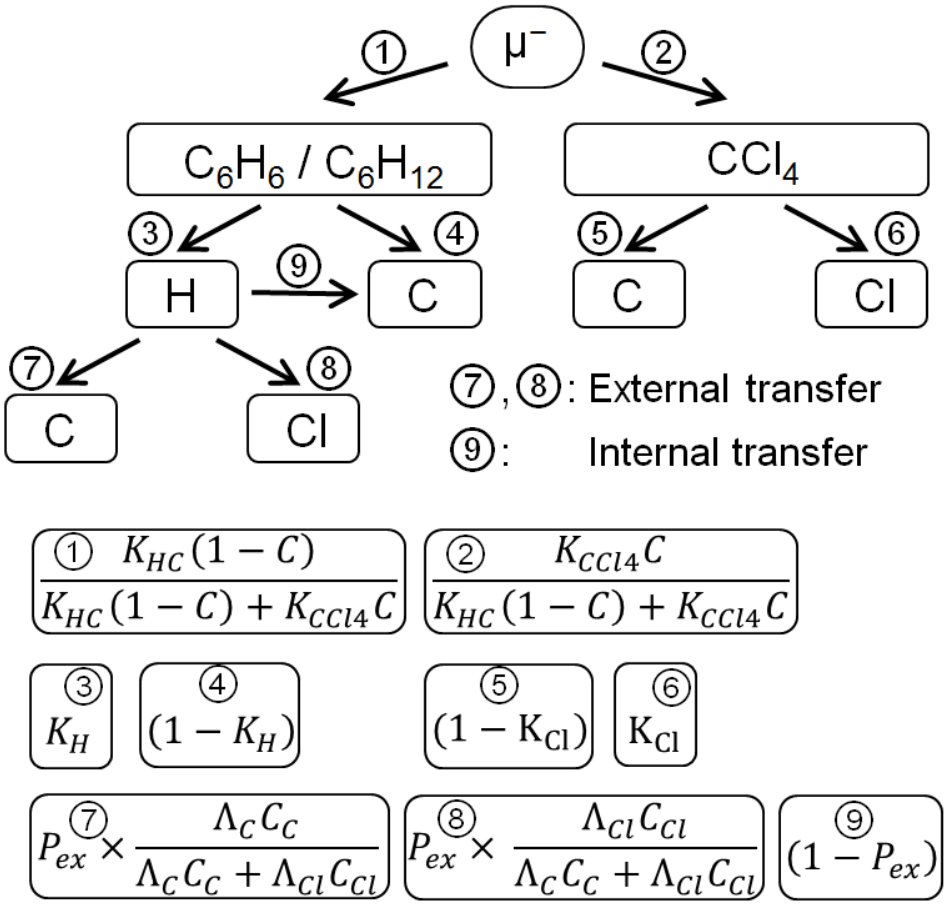

Fig. 4-1 Scheme of the model equation. The term indicated by each number represents the probability of each step of muon capture.

4.2.2.2. Values Used for Analysis

For the analysis, the values shown in Table 4-2 were used. The capture ratio to hydrocarbon molecules and carbon tetrachloride molecules, and the capture ratio to hydrogen atoms when captured by a hydrocarbon molecule cannot be obtained from this experiment. Therefore, the experimantal values of the pion experiment and the values by large mesomolecular (LMM) model were used.[27,28] This assumes that the initial process of capture is equal between muon and pion. The capture ratio to chlorine atoms when captured by a carbon tetrachloride molecule was obtained from the capture ratio of chlorine and carbon in the CCl_4 sample of this study.

In LMM model, the capture ratio to hydrogen atoms when captured by a hydrocarbon

molecule is expressed by the following equation.[27,28]

$$K_H = \frac{\nu(1+\sigma)}{(N+\nu)(1-\sigma)Z_{eff}}$$

Here, N is sum of the core electrons relevant to capture process in the molecule, ν is sum of the valence electrons in the molecule, Z_{eff} is sum of the relevant core and valence electrons of one carbon atom in the molecule, and σ is ionicity parameter that is zero in covalent bonds. In benzene, N = 18, ν = 12 and Z_{eff} = 4, and in cyclohexane, N = 18, ν = 24 and Z_{eff} = 4.[27,28] As a result, K_H becomes the values shown in Table 4-2.

Table 4-2 Parameters used for the analysis.

	C_6H_6	**C_6H_{12}**	**Note**
K_{HC} / K_{CCl4}	0.873±0.012	1.149±0.016	Experimental results in the pion experiment[27]
K_H	12 / 120	24 / 144	LMM model[27,28]
K_{Cl}	0.932±0.003		This work

4.2.2.3. Analysis Result

When the value of P_{ex} was fixed at a certain value such as 1.0, 0.9, 0.8, and the values of K_{HC} / K_{CCl4}, K_H, and K_{Cl} were fixed with the values in Table 4-2, then the model equation was fitted to the experimental value of W_C / W_{Cl} using Λ_C as a free parameter. The experimental W_C / W_{Cl} values used are average value of Ge-T and Ge-B detectors shown in Table 3-34. In the model equation, Λ_C is a relative value of Λ_{Cl} because all Λ_C are located in the same fraction as Λ_{Cl}, thus Λ_{Cl} was fixed at 100 here. The results of fittings are shown in Table 4-3.

Table 4-3 Analyzed muon transfer rate to carbon atoms of benzene and cyclohexane. The Λ_C values shown here are relative values to Λ_{Cl} fixed at 100.

P_{ex}	Λ_C (C_6H_6)	Λ_C (C_6H_{12})
1.00	37.2 ± 10.7	30.6 ± 3.9
0.90	31.8 ± 9.7	26.0 ± 3.5
0.80	26.5 ± 8.7	21.4 ± 3.1
0.70	21.4 ± 7.7	17.0 ± 2.8
0.60	16.4 ± 6.8	12.7 ± 2.4
0.50	11.6 ± 5.8	8.5 ± 2.0
0.40	7.0 ± 4.9	4.4 ± 1.7
0.30	2.6 ± 4.0	0.5 ± 1.3
0.20	−1.6 ± 3.0	−3.3 ± 0.9
0.10	−5.9 ± 1.9	−7.1 ± 0.5
0.01	−10.8 ± 0.3	−11.0 ± 0.1

As shown in the table, although within the error range, if the P_{ex} is the same for cyclohexane and benzene, the optimum value of Λ_C for the samples of benzene is larger than that for the samples of cyclohexane regardless of the value of P_{ex}. For example, when $P_{ex} = 1$, Λ_C (C_6H_6) / Λ_C (C_6H_{12}) ≈ 1.22 ± 0.38. In the pion experiment, since the probability α_γ' that pionic hydrogen atoms are released by cutting off the C–H bond is equal within the error range between benzene and cyclohexane,[20] assuming that P_{ex} is the same for benzene and cyclohexane even for muon is plausible. Also, since it is unlikely that Λ_C is a negative value, it can be seen that P_{ex} is at least approximatelly 0.30 or more.

In addition, when fitting both Λ_C and P_{ex} as free parameters,

Λ_C (C_6H_6) = 37±34 P_{ex} (C_6H_6) = 1.0±0.5

Λ_C (C_6H_{12}) = 31±12 P_{ex} (C_6H_{12}) = 1.0±0.2

In this case, since the error of P_{ex} rides on Λ_C, the error of Λ_C becomes very large as compared with the case where P_{ex} is set to a specific value. The values of P_{ex} converges

to the upper limit of 1 in both systems, and P_{ex} is considered to be a value of 0.8 or more from the error range of cyclohexane P_{ex} value.

4.3. Discussion III: Gas System and Liquid System

4.3.1. Transfer Rate in Gas System and Liquid System

The transfer rates in liquid and gas systems are summarized in Table 4-4.

Table 4-4 Summary of the chemical effect on the transfer rate to carbon atoms in the liquid and the gas system.

	Pion transfer in the liquid system[20]	**Muon transfer in the liquid system**	**Muon transfer in the gas system**
Transfer rate to C of C_6H_6 / Transfer rate to C of C_6H_{12}	2.0±0.4	1.22±0.38	1.02±0.14
Probability that the true value in the upper row is smaller than 1	0.6%	28%	44%

In the pion transfer in the liquid system, the transfer rate to carbon atoms of benzene was approximatelly twice the rate to carbon atoms of cyclohexane. In the muon transfer in the liquid system, although the error was large and within the error range, but the optimal value of the transfer rate to carbon atoms of benzene was approximatelly 1.2 times that of cyclohexane. In the muon transfer in the gas system, the difference in the transfer rate was small compared to the liquid system, and there was almost no difference between the samples.

It is considered that the reason for obtaining such a result is due to the difference in the proportion of the excited state of pionic or muonic hydrogen atoms which causing transfer. First, consider the order of the muon transfer rate in liquid and gas systems.

Estimates of muon transfer rates in the liquid and gas systems are shown in Table 4-5. The transfer rate to carbon atoms was calculated using the literature value $(9.5\pm0.5)\times10^{10}$ s^{-1} of the transfer rate to the carbon atoms of the H_2+CH_4 system,[29] and converted into the carbon atom density of the samples in each experiment. The literature values are normalized to atomic density of liquid hydrogen of 4.25×10^{22} cm^{-3}.

Table 4-5 Estimates of muon transfer rates in the liquid and gas systems.

	The liquid system experiment	**The gas system experiment**
Density of carbon atoms	2.70×10^{22} cm^{-3}	2.87×10^{17} cm^{-3}
Muon transfer rate to carbon atoms	6×10^{10} s^{-1}	6×10^{5} s^{-1}
Average time for completion of transfer	2×10^{-11} s	2×10^{-6} s
Proportion of excited muonic hydrogen atoms ($n \geq 3$) when transfer occurs[30]	approx. 70%	0%

In the gas system, the muon transfer rate is on the order of 10^5 s^{-1}, and the average time required for the transfer to be completed is on the order of 10^{-6} s. All muonic hydrogen atoms de-excited to 1s state or 2s state within 10^{-7} s, the majority becomes 1s state at the stage of 10^{-6} s.[30] Therefore, muon transfer in the gas system must be caused by muonic hydrogen atoms in 1s state. On the other hand, in the liquid system, the muon transfer rate is on the order of 10^{10} s^{-1} , and the average time required for the transfer to be completed is on the order of 10^{-11} s. At the stage of 10^{-11} s, the state of the principal quantum number $n \geq 3$ is approximatelly 70%.[30] Therefore, in the liquid system, the muon transfer occurs mainly from the muonic hydrogen atoms in the excited state with the principal quantum number $n \geq 3$. Furthermore, in the case of a pion transfer in a liquid system, since the lifetime of the pionic hydrogen atoms in the 1s state is extremely short ($< 10^{-15}$ s), the pion transfer occurs only from the excited state pionic hydrogen atoms.

In the pion transfer in the liquid system, it is believed that the difference in the pion

transfer rate to the carbon atoms was caused by the difference in steric hindrance around the carbon atoms of benzene and cyclohexane molecules.[20] In benzene molecule, one hydrogen atom is bonded to a carbon atom, whereas in cyclohexane molecule there are two hydrogen atoms bonded to a carbon atom, so the steric hindrance of cyclohexane molecules when muonic or pionic hydrogen atoms approach a carbon atom is larger than that of benzene molecules. Considering the radius of muon hydrogen or pion hydrogen, for example, it in the principal quantum number n = 3 has a radius of approximatelly 9 times it in the 1s state. Therefore, it is considered that the larger the proportion of the excited state is, the more susceptible to steric hindrance. As a result, the difference due to the molecules of the transfer rate to carbon atoms was reduced in the order of the pion transfer in the liquid system where the transfer occurs only from the excited state, the muon transfer in the liquid system where the transfer from the excited state is approximatelly 70%, and the muon transfer in the gas system without the transfer from the excited state.

4.3.2. Mechanism of Steric Hindrance

The steric hindrance for transfer process by hydrogen atoms is considered to be occurred by the following mechanism. The muon in the excited state muonic hydrogen atoms exists at the high energy level. Therefore, if the excited state muonic hydrogen atoms approach another hydrogen atom, muon transfer to more stable level of another hydrogen atom can occur. On the other hand, even if the ground state muonic hydrogen atoms approach another hydrogen atom, muon transfer to another hydrogen atom does not occur. As a result, only the excited state muonic hydrogen atoms are affected by the hydrogen atoms.

In addition, when muon transfer to another hydrogen atom occur, muon moves to the atomic muon orbital of lower energy level than the former orbital. This effectively corresponds to de-excitation of muonic hydrogen atoms. That is, excited state muonic hydrogen atoms de-excite by collision with hydrogen atoms. Considering the binding

energy, excited state muonic hydrogen atoms can transfer muon to higher energy levels of carbon atoms compared with ground state muonic hydrogen atoms. The atomic muon orbital of a higher energy level has larger radius compared to a lower energy level. Therefore, the cross section of the muon transfer from excited state muonic hydrogen atoms to carbon atom is larger than that from ground state. As a result, if the excited state muonic hydrogen atoms collide with hydrogen atom bonding to carbon atom, probability of muon transfer to carbon atoms becomes smaller. This is considered the mechanism of steric hindrance.

In the case of pion transfer, same mechanism is also possible. Additionally, if excited state pionic hydrogen atoms de-excite to the ground state by collision with hydrogen atoms, pion decays immediately due to reaction with hydrogen nucleus, thus pion transfer to carbon atoms does not occur. This means steric hindrance by hydrogen atoms may affects strongly to pion transfer process compared to muon transfer process.

5. Concluding Remarks

In this work, in order to investigate the chemical effect on the muon transfer process, muon irradiation experiment was carried out with two systems of liquid and gas, using benzene and cyclohexane whose chemical effects on pion transfer process were observed.

In the liquid system, the error was large and the difference was within the error range, but the optimum value of the muon transfer rate to the carbon atoms of benzene was approximatelly 1.2 times the optimum value of the muon transfer rate to the carbon atoms of cyclohexane. This was due to the difference in steric hindrance by molecules as in the case of pion transfer in the liquid system. In benzene molecules, there is one hydrogen atom bonded to the carbon atom, whereas cyclohexane molecules have two hydrogen atoms bonded to the carbon atom. That is, cyclohexane molecules have many obstacles which hinder muonic hydrogen atoms approach carbon atoms compared to benzene molecules. Therefore, the muon transfer rate to carbon atoms of cyclohexane became smaller than the muon transfer rate to carbon atoms of benzene.

In the gas system, the difference between the optimum values of the muon transfer rate to the carbon atoms of benzene and cyclohexane was smaller than that of the liquid system, and there was almost no difference between the samples. This was because all transfers in the gas system occurred from the ground state muonic hydrogen atoms, whereas the transfers in the liquid system occurred from the excited state muonic hydrogen atoms. Threfore, muonic hydrogen atoms in the ground state were less susceptible to steric hindrance by molecules because they are smaller in radius than the excited state.

The pion transfers in the liquid system occur only from the pionic hydrogen atoms in the excited state, and approximatelly 70% of the muon transfers in the liquid system occurred from the muonic hydrogen atoms in the excited state, and the muon transfers in the gas system occurred only from the muonic hydrogen atoms in the ground state. The influence of molecular structure in the transfer process was large in the order of pion transfer process in liquid system, muon transfer process in liquid system, and muon

transfer process in gas system. That is, the larger the proportion of the excited state when muonic or pionic hydrogen atoms undergo transfer, the greater the influence from steric hindrance of the molecule and the larger the difference in transfer rate due to the difference in molecules. This indicates that muonic and pionic hydrogen atoms in the excited state play an important role in the chemical effects on the transfer processes in the hydrocarbon molecules.

6. References

(1) Fitch, V. L.; Rainwater, J. *Phys. Rev.* **1953**, *92* (3), 789–800.

(2) Hüfner, J. *Phys. Rep.* **1975**, *21* (1), 1–79.

(3) Pohl, R.; Antognini, A.; Nez, F.; Amaro, F. D.; Biraben, F.; Cardoso, J. M. R.; Covita, D. S.; Dax, A.; Dhawan, S.; Fernandes, L. M. P.; Giesen, A.; Graf, T.; Hänsch, T. W.; Indelicato, P.; Julien, L.; Kao, C.-Y.; Knowles, P.; Le Bigot, E.-O.; Liu, Y.-W.; Lopes, J. A. M.; Ludhova, L.; Monteiro, C. M. B.; Mulhauser, F.; Nebel, T.; Rabinowitz, P.; dos Santos, J. M. F.; Schaller, L. A.; Schuhmann, K.; Schwob, C.; Taqqu, D.; Veloso, J. F. C. A.; Kottmann, F. *Nature* **2010**, *466* (7303), 213–216.

(4) Antognini, A.; Nez, F.; Schuhmann, K.; Amaro, F. D.; Biraben, F.; Cardoso, J. M. R.; Covita, D. S.; Dax, A.; Dhawan, S.; Diepold, M.; Fernandes, L. M. P.; Giesen, A.; Gouvea, A. L.; Graf, T.; Hansch, T. W.; Indelicato, P.; Julien, L.; Kao, C.-Y.; Knowles, P.; Kottmann, F.; Le Bigot, E.-O.; Liu, Y.-W.; Lopes, J. A. M.; Ludhova, L.; Monteiro, C. M. B.; Mulhauser, F.; Nebel, T.; Rabinowitz, P.; dos Santos, J. M. F.; Schaller, L. A.; Schwob, C.; Taqqu, D.; Veloso, J. F. C. A.; Vogelsang, J.; Pohl, R. *Science* **2013**, *339* (6118), 417–420.

(5) Kubo, M. K.; Moriyama, H.; Tsuruoka, Y.; Sakamoto, S.; Koseto, E.; Saito, T.; Nishiyama, K. *J. Radioanal. Nucl. Chem.* **2008**, *278* (3), 777–781.

(6) Ninomiya, K.; Kubo, M. K.; Nagatomo, T.; Higemoto, W.; Ito, T. U.; Kawamura, N.; Strasser, P.; Shimomura, K.; Miyake, Y.; Suzuki, T.; Kobayashi, Y.; Sakamoto, S.; Shinohara, A.; Saito, T. *Anal. Chem.* **2015**, *87* (9), 4597–4600.

(7) Terada, K.; Sato, A.; Ninomiya, K.; Kawashima, Y.; Shimomura, K.; Yoshida, G.; Kawai, Y.; Osawa, T.; Tachibana, S. *Sci. Rep.* **2017**, *7* (1), 15478.

(8) Bleser, E. J.; Anderson, E. W.; Lederman, L. M.; Meyer, S. L.; Rosen, J. L.; Rothberg, J. E.; Wang, I.-T. *Phys. Rev.* **1963**, *132* (6), 2679–2691.

(9) Suzuki, T. A systematic study of muon capture, University of British Columbia, 1980.

(10) Fermi, E.; Teller, E. *Phys. Rev.* **1947**, *72* (5), 399–408.

(11) Baijal, J. S.; Diaz, J. A.; Kaplan, S. N.; Pyle, R. V. *Nuovo Cimento* **1963**, *30* (3), 711–726.

(12) Suzuki, T.; Mikula, R. J.; Garner, D. M.; Fleming, D. G.; Measday, D. F. *Phys. Lett. B* **1980**, *95* (2), 202–206.

(13) Imanishi, N.; Furuya, T.; Fujiwara, I.; Shinohara, A.; Kaji, H.; Iwata, S. *Phys. Rev. A* **1985**, *32* (5), 2584–2588.

(14) Schneuwly, H.; Boschung, M.; Kaeser, K.; Piller, G.; Rüetschi, A.; Schaller, L. A.; Schellenberg, L. *Phys. Rev. A* **1983**, *27* (2), 950–960.

(15) Petrukhin, V. I.; Suvorov, V. M. *Sov. Phys. JETP* **1976**, *43* (4), 595–598.

(16) Daniel, H. *Phys. Rev. Lett.* **1975**, *35* (24), 1649–1651.

(17) Daniel, H. *Z. Phys. A* **1979**, *291* (1), 29–31.

(18) Horváth, D.; Bannikov, A. V.; Kachalkin, A. K.; Lévay, B.; Petrukhin, V. I.; Vasilyev, V. A.; Yutlandov, I. A.; Strakovsky, I. I. *Chem. Phys. Lett.* **1982**, *87* (5), 504–507.

(19) Horváth, D.; Measday, D. F.; Entezami, F.; Hasinoff, M. D.; Noble, A. J.; Stanislaus, S.; Virtue, C. J.; Clough, A. S.; Smith, J. R. H.; Salomon, M.; Aniol, K. A. *Phys. Rev. A* **1991**, *44* (3), 1725–1732.

(20) Shinohara, A.; Muroyama, T.; Miura, T.; Saito, T.; Yokoyama, A.; Furukawa, M. *Hyperfine Interact.* **1997**, *106* (1–4), 301–306.

(21) *J-PARC Annual Report 2008*; Otomo, T., Takada, H., Eds.; 2008.

(22) Strasser, P.; Fujimori, H.; Koseki, K.; Hori, Y.; Matsumoto, H.; Shimomura, K.; Koda, A.; Kawamura, N.; Makimura, S.; Kato, M.; Kobayashi, Y.; Higemoto, W.; Ito, T. U.; Ninomiya, K.; Kojima, K.; Kadono, R.; Nishiyama, K.; Miyake, Y. *Phys. Procedia* **2012**, *30*, 65–68.

(23) Research Center for Nuclear Physics. RCNP Photo Gallery http://www.rcnp.osaka-u.ac.jp/en/local/album/ (accessed Jan 2, 2018).

(24) Matsumoto, Y.; Fukuda, M.; Hatanaka, K.; Ieiri, M.; Kawashima, Y.; Kohno, Y.;

Kuno, Y.; Minakawa, M.; Morinobu, S.; Sakamoto, Y. N. H.; Sato, A.; Takahisa, K.; Ueda, H. In *Proceedings of IPAC2015*; Richmond, 2015; pp 2537–2540.

(25) Ziegler, J. F.; Ziegler, M. D.; Biersack, J. P. *Nucl. Instrum. Methods Phys. Res. B* **2010**, *268* (11–12), 1818–1823.

(26) Hirayama, H.; Namito, Y.; Bielajew, A. F.; Wilderman, S. J.; Nelson, W. R. *The EGS5 Code System*; SLAC-R-730; Stanford, 2005.

(27) Muroyama, T. Yuki ekitai kagobutsu niokeru pai chukanshi suiso genshi no keisei to ten'i katei [Formation and transfer process of pionic hydrogen atoms in lquid organic compounds], Nagoya University, 1997 (in Japanese).

(28) Shinohara, A.; Muroyama, T.; Shintai, J.; Kurachi, J.; Furukawa, M.; Miura, T.; Yoshimura, Y.; Saito, T.; Ohdaira, T.; Imanishi, N. *Phys. Rev. A* **1996**, *53* (1), 130–138.

(29) Jacot-Guillarmod, R.; Mulhauser, F.; Piller, C.; Schaller, L. A.; Schellenberg, L.; Schneuwly, H.; Thalmann, Y.-A.; Tresch, S.; Werthmüller, A.; Adamczak, A. *Phys. Rev. A* **1997**, *55* (5), 3447–3452.

(30) Pisano, V.; Puddu, G.; Quarati, P.; Sulis, L. *Nuovo Cimento A* **1982**, *72* (1), 27–39.

7. Acknowledgments

The work described in this thesis has been carried out under the direction of Professor Atsushi Shinohara of Osaka University. I would like to express my deepest gratitude to him for his valuable guidance, helpful suggestions, kind encouragement, and constant support throughout this study.

I also wish to express my sincere gratitude to Dr. Kazuhiko Ninomiya of Osaka University for his valuable direction, helpful discussion and kind advice. Without his continuous support, this work would have never been accomplished.

I wish to express acknowledgments to Professor Michio Okada of Osaka University, Professor Mitsutaka Okumura of Osaka University and Professor Kenya Kubo of International Christian University for their worthful suggestions and interest in this thesis.

I would like to deeply express my appreciation to Professor Yasuhiro Miyake and Dr. Naritoshi Kawamura of High Energy Accelerator Research Organization (KEK) for their advice and cooperation in the experiments at J-PARC. I would also like to express my deep appreciation to Professor Taichi Miura of KEK and Dr. Wataru Higemoto of Japan Atomic Energy Agency for their support at J-PARC. I am deeply grateful to Dr. Motonobu Tampo and Mr. Koji Hamada of KEK for their help at J-PARC. I also wish to express my sincere appreciation to Professor Kentaro Terada, Dr. Akira Sato, Dr. Yoshitaka Kawashima and Dr. Dai Tomono of Osaka University for their support on the experiments at RCNP.

I wish to express my heartfelt gratitude to Dr. Go Yoshida of KEK for his encouragement, discussion and cooperation throughout this research. I also wish to express my sincere gratitude to Mr. Kazuya Fujihara of KEK for his discussion and cooperation in this study.

I would like to express my appreciation to Professor Takashi Yoshimura, Dr. Yoshitaka Kasamatsu, Dr. Naruto Takahashi, Dr. Koujirou Nagata and Dr. Zijian Zhang of Osaka University for their valuable discussion, support and encouragement. I wish to show my sincere thanks to the members of our research group in the Radiochemistry

Laboratory of Osaka University: Mr. Akihiro Nanbu, Mr. Takuto Kudo, Mr. Ryosuke Yasui (now at the University of Tokyo) and Mr. Michihiro Kitanaka (now at the University of Tokyo) for their useful discussion and support. I wish to thank secretaries of the Radiochemistry Laboratory, Ms. Kanako Kawase and Ms. Noriko Narahara, for their support. I would also like to offer my thanks to many students who spent time together at the Radiochemistry Laboratory, for their encouragement and discussion.

Last but not least, I thank my parents, Kiyoshi Inagaki and Tomoko Inagaki, for their support, understanding and encouragement.

February 2018

Makoto Inagaki

8. List of Publications

Main Publications

[1] Muon transfer rates from muonic hydrogen atoms to gaseous benzene and cyclohexane

M. Inagaki, K. Ninomiya, G. Yoshida, W. Higemoto, N. Kawamura, Y. Miyake, T. Miura, and A. Shinohara

J. Nucl. Radiochem. Sci., vol. 18, p. 5, 2018.

[2] Muonic Atom Formation by Muon Transfer Process in C_6H_6 or C_6H_{12} and CCl_4 Mixtures

M. Inagaki, K. Ninomiya, K. Fujihara, G. Yoshida, Y. Kasamatsu, M. K. Kubo, W. Higemoto, N. Kawamura, T. Nagatomo, Y. Miyake, T. Miura, and A. Shinohara

JPS Conf. Proc., vol. 8, p. 033004, 2015.

Other Publications

[3] Negative muon induced elemental analysis by muonic X-ray and prompt gamma-ray measurements

K. Ninomiya, M. Inagaki, M. K. Kubo, T. Nagatomo, W. Higemoto, N. Kawamura, P. Strasser, K. Shimomura, Y. Miyake, S. Sakamoto, A. Shinohara, and T. Saito

J. Radioanal. Nucl. Chem., vol. 309, p. 65, 2016.

[4] Chemical Environmental Effects on Muon Transfer Process in Low Pressure Mixture Gases; H_2+CO and H_2+CO_2

G. Yoshida, K. Ninomiya, M. Inagaki, W. Higemoto, N. Kawamura, K. Shimomura, Y. Miyake, T. Miura, M. K. Kubo, and A. Shinohara

RADIOISOTOPES, vol. 65, p. 113, 2016.

[5] Muonic atom formation processes for carbon containing molecules
G. Yoshida, K. Ninomiya, M. Inagaki, W. Higemoto, T. U. Ito, N. Kawamura, K. Shimomura, Y. Miyake, T. Miura, K. M. Kubo, and A. Shinohara
J. Phys. Conf. Ser., vol. 635, p. 052047, 2015.

[6] Elemental Analysis System with Negative-Muon Beam
T. Osawa, K. Ninomiya, G. Yoshida, M. Inagaki, K. M. Kubo, N. Kawamura, and Y. Miyake
JPS Conf. Proc., vol. 8, p. 025003, 2015.

[7] The Development of a Non-Destructive Analysis System with Negative Muon Beam for Industrial Devices at J-PARC MUSE
M. Tampo, K. Hamada, N. Kawamura, M. Inagaki, T. U. Ito, K. M. Kojima, K. M. Kubo, K. Ninomiya, P. Strasser, G. Yoshida, and Y. Miyake
JPS Conf. Proc., vol. 8, p. 036016, 2015.